(12) INTERNATIONAL APPLICATION PUBLISHED UNDER THE PATENT COOPERATION TREATY (PCT)

(19) World Intellectual Property Organization
International Bureau

(43) International Publication Date
20 December 2018 (20.12.2018)

WIPO | PCT

(10) International Publication Number
WO 2018/232152 A1

(51) International Patent Classification:
G01N 33/574 (2006.01) *C07K 11/02* (2006.01)
C12N 5/074 (2010.01) *C07K 14/705* (2006.01)
C12N 5/09 (2010.01) *A61K 38/00* (2006.01)

(21) International Application Number:
PCT/US2018/037595

(22) International Filing Date:
14 June 2018 (14.06.2018)

(25) Filing Language: English

(26) Publication Language: English

(30) Priority Data:
62/519,734 14 June 2017 (14.06.2017) US

(71) Applicant: **THE REGENTS OF THE UNIVERSITY OF CALIFORNIA** [US/US]; 1111 North Franklin Street, 5th Floor, Oakland, California 94607 (US).

(72) Inventors: **CHERESH, David**; 9500 Gilman Drive, MC 910, La Jolla, California 92093 (US). **WEIS, Sara**; 9500 Gilman Drive, MC 0910, La Jolla, California 92093 (US). **COSSET, Erika**; 9500 Gilman Drive, MC 0910, La Jolla, California 92093 (US).

(74) Agent: **EINHORN, Gregory P.**; 300 South Wacker Drive, Suite 2500, Chicago, Illinois 60606 (US).

(81) Designated States *(unless otherwise indicated, for every kind of national protection available)*: AE, AG, AL, AM, AO, AT, AU, AZ, BA, BB, BG, BH, BN, BR, BW, BY, BZ, CA, CH, CL, CN, CO, CR, CU, CZ, DE, DJ, DK, DM, DO, DZ, EC, EE, EG, ES, FI, GB, GD, GE, GH, GM, GT, HN, HR, HU, ID, IL, IN, IR, IS, JO, JP, KE, KG, KH, KN, KP, KR, KW, KZ, LA, LC, LK, LR, LS, LU, LY, MA, MD, ME, MG, MK, MN, MW, MX, MY, MZ, NA, NG, NI, NO, NZ, OM, PA, PE, PG, PH, PL, PT, QA, RO, RS, RU, RW, SA, SC, SD, SE, SG, SK, SL, SM, ST, SV, SY, TH, TJ, TM, TN, TR, TT, TZ, UA, UG, US, UZ, VC, VN, ZA, ZM, ZW.

WO 2018/232152 A1

(54) Title: METHODS FOR TREATING DRUG RESISTANT CANCERS

FIG. 6

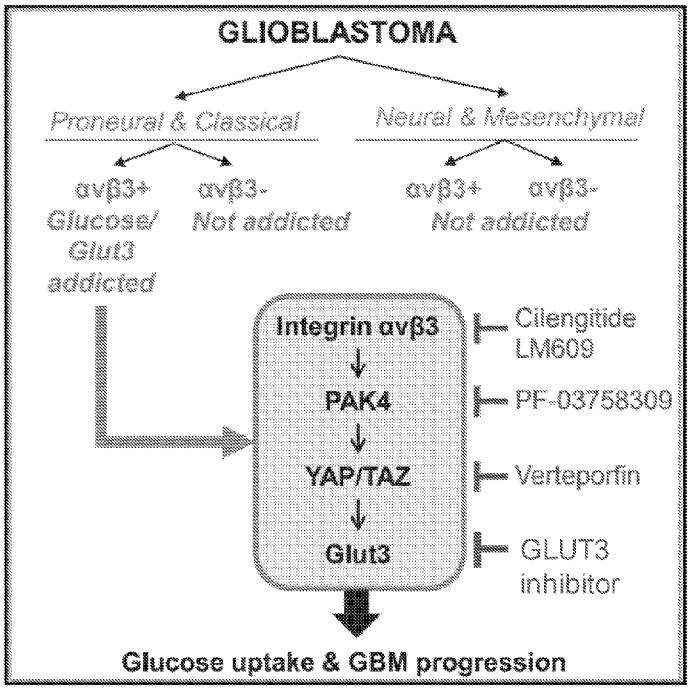

(57) Abstract: Provided are methods for determining whether a glioblastoma (GBM) tumor or GBM cancer cell will be sensitive to a treatment targeting the integrin avb3 (alpha.v.beta.3.) pathway, comprising determining whether the GBM tumor or the GBM cancer cell expresses both avb3+ and Glut3+ along with a specific genetic signature associated with Glut3 addiction, where in alternative embodiments a cell is Glut3 addiction if the GBM tumor or the GBM cancer cell has markers consistent with the Classical or the Proneural molecular subtypes of GBM, or, expresses markers consistent with a Glut3- addicted molecular signature. Also provided herein are methods of treating glioblastoma (GBM) tumors found to be sensitive to agents targeting or inhibiting the integrin avb3 pathway.

[Continued on next page]

(84) Designated States *(unless otherwise indicated, for every kind of regional protection available)*: ARIPO (BW, GH, GM, KE, LR, LS, MW, MZ, NA, RW, SD, SL, ST, SZ, TZ, UG, ZM, ZW), Eurasian (AM, AZ, BY, KG, KZ, RU, TJ, TM), European (AL, AT, BE, BG, CH, CY, CZ, DE, DK, EE, ES, FI, FR, GB, GR, HR, HU, IE, IS, IT, LT, LU, LV, MC, MK, MT, NL, NO, PL, PT, RO, RS, SE, SI, SK, SM, TR), OAPI (BF, BJ, CF, CG, CI, CM, GA, GN, GQ, GW, KM, ML, MR, NE, SN, TD, TG).

Published:

— *with international search report (Art. 21(3))*

METHODS FOR TREATING DRUG RESISTANT CANCERS

RELATED APPLICATIONS

This Patent Convention Treaty (PCT) International Application claims the benefit of priority to U.S. Provisional Application No. 62/519,734, filed June 14, 2017. The aforementioned application is expressly incorporated herein by reference in its entirety and for all purposes.

GOVERNMENT RIGHTS

This invention was made with government support under grant number NCI-CA45726, awarded by the National Institutes of Health (NIH). The government has certain rights in the invention.

TECHNICAL FIELD

This invention generally relates to oncology. In alternative embodiments, provided are methods for determining whether a glioblastoma (GBM) tumor or GBM cancer cell will be sensitive to a treatment targeting the integrin avb3 (αvβ3) pathway, comprising determining whether the GBM tumor or the GBM cancer cell expresses both avb3+ and Glut3+ (also called SLC2A3+) along with (and also having) a specific genetic signature associated with Glut3 addiction, where in alternative embodiments a cell is Glut3 addicted if the GBM tumor or the GBM cancer cell has markers consistent with the Classical or the Proneural molecular subtypes of GBM, or, expresses (e.g., expresses mRNA or protein) markers consistent with a Glut3-addicted genetic-molecular signature, e.g., as listed in Figure 11 or Figure 23, wherein if a GBM tumor or the GBM cancer cell expresses both avb3+ and Glut3+ and this genetic/molecular signature is associated with Glut3 addiction, the GBM tumor or the GBM cancer cell will be (can be predicted to be) sensitive to (will be successfully treated by) the treatment targeting the integrin avb3 (αvβ3) pathway. Also provided herein are methods of treating glioblastoma (GBM) tumors found to be sensitive to agents targeting or inhibiting the integrin avb3 (αvβ3) pathway, wherein the sensitivity is determined by methods as provided herein.

BACKGROUND

In glioblastomas (GBMs), expression of αvβ3 (avb3) and its ligand vitronectin are both linked to tumor progression and invasive behavior at the tumor margin in the

brain of patients with GBM (Gladson and Cheresh, 1991). This prompted development of cilengitide, a cyclic peptide antagonist capable of targeting the ligand binding site of a αvβ3. Despite encouraging phase I/II results showing a durable response to cilengitide for some patients (Nabors et al., 2007; Reardon et al., 2008), the phase III CENTRIC and phase II CORE trials failed to meet overall survival endpoints (Stupp et al., 2014). In a follow-up study, immunohistological analysis of tissues obtained during the CORE trial revealed that higher αvβ3 levels were associated with improved survival in patients treated with cilengitide (Weller et al., 2016). Because this was not the case for the CENTRIC trial, it is still not clear how to identify patients who may benefit from this drug.

SUMMARY

In alternative embodiments, provided are methods for: determining whether a glioblastoma (GBM) tumor or GBM cancer cell will be sensitive or responsive to a treatment targeting the integrin avb3 (αvβ3) pathway, comprising determining or having determined whether the GBM tumor or the GBM cancer cell expresses both avb3+ and Glut3+ along with (and also has) a genetic/molecular signature associated with Glut3 addiction, wherein in alternative embodiments a genetic/molecular signature associated with Glut3 addiction comprises the cell having markers consistent with the Classical or Proneural molecular subtypes of GBM, or the cell expresses (e.g., expresses mRNA or protein) markers consistent with a Glut3-addicted genetic-molecular signature, e.g., expresses markers at levels as listed in Figure 11 or Figure 23 (where a Glut3 addicted marker is expressed at high levels, and a Glut3 non-addicted marker is expressed at low levels), wherein if a GBM tumor or the GBM cancer cell expresses both avb3+ and Glut3+ and has a Glut3+ genetic/molecular signature, the GBM tumor or the GBM cancer cell will be (or can be predicted to be) sensitive to (will be successfully treated by) the treatment targeting the integrin avb3 (αvβ3) pathway.

Not all tumors with positive expression of αvβ3 and GLUT3 are sensitive to drugs targeting this pathway: there are two different ways that patients who will be sensitive to drugs targeting the integrin avb3 (αvβ3) pathway can be further divided after the expression of αvβ3/Glut3 is known. For the first way, GBM tumors can be characterized by their "GBM molecular subtype", and only tumors which have markers consistent with the Classical or Proneural subtypes will be sensitive to

blockade of the αvβ3 pathway. Tumors with positive expression of both αvβ3/Glut3 but markers of the Mesenchymal subtype are not expected to be addicted to Glut3 and thus may not be sensitive to αvβ3 blockade. For the second way, provided herein is a list of genes (as illustrated in Figure 11, see also Figure 23) that can be used to predict (or determine) Glut3 addiction and αvβ3 blockade sensitivity independent of determining the GBM molecular subtype, i.e., if a tumor expresses αvβ3 and GLUT3 and expresses markers consistent with a Glut3-addicted gene signature, e.g., where the markers are expressed at levels as listed in Figure 11 or Figure 23, this signature is predictive of sensitivity to drugs targeting the integrin avb3 (αvβ3) pathway (i.e., the cells are "drug-sensitive" if they are sensitive, or responsive to, any drug, small molecule, protein, or any agent that targets the integrin avb3 (αvβ3) pathway). These exemplary decision-making processes are shown in the schematic illustrated in Figure 6. Alternative methods to determine if a cell is Glut3 addicted are described below.

In alternative embodiments, the cancer or tumor cell treatment targets avb3, Glut3, PAK4, or YAP/TAZ. In alternative embodiments, the treatment comprises administration to an individual in need thereof cilengitide (or, 2-[(2*S*,5*R*,8*S*,11*S*)-5-benzyl-11-{3-[(diaminomethylidene)amino]propyl}-7-methyl-3,6,9,12,15-pentaoxo-8-(propan-2-yl)-1,4,7,10,13-pentaazacyclopentadecan-2-yl]acetic acid).

In alternative embodiments, provided are methods for determining whether a tumor or a cancer cell will be sensitive to (or can be killed or induced to senescence by) a treatment targeting the integrin avb3 (αvβ3) pathway, comprising:

(a) determining or having determined whether the tumor or the cancer cell expresses both avb3+ and Glut3+, or determining whether the tumor or the cancer cell is an avb3+/Glut3+ tumor or cancer cell, and

(b) determining or having determined whether the tumor or the cancer cell is Glut-3 addicted,

wherein optionally determining or having determined whether the tumor or the cancer cell is Glut-3 addicted comprises:

(i) determining or having determined whether the tumor or the cancer cell expresses a marker (e.g., an mRNA or a protein) consistent with a Classical or Proneural subtype, e.g., expresses a marker consistent with the Classical or Proneural molecular subtypes of GBM,

wherein optionally the marker consistent with a Classical or Proneural subtype comprises an *EGFR*, *GLI1*, *NES*, *DLL3* or *OLIG2* gene transcript or an EGFR, GLI1, NES, DLL3 or OLIG2 protein, or

(ii) determining or having determined whether the tumor or the cancer cell expresses (e.g., expresses mRNA or protein) consistent with a Glut3 addicted gene/ molecular signature,

wherein optionally gene expression consistent with a Glut3 addicted gene signature comprises gene expression consistent with a high (a Glut3 addicted signature) or low (a Glut3 non-addicted signature) expression of at least one (one or more) of the genes, or 2, 3, 4, 5, 6, 7, 8, 9, 10, 11, 12, 13, 14, 15, 16, 17, 18, 19, 20, 21, 22, 23, 24, 25, 26, 27, 28, 29 or all 30 of the genes, as listed in Figure 11 or Figure 23, optionally one, several or all of the 314 genes in Figure 11, or optionally one, several or all of the 15 genes in Figure 23),

(where the Glut3-addicted gene signature comprises having a Glut3 addicted marker expressed at high levels, and a Glut3 non-addicted marker expressed at low levels),

wherein if a tumor or a cancer cell expresses both avb3+ and Glut3+ and is Glut-3 addicted, the tumor or the cancer cell will be sensitive to (will be substantially sensitive to) or will be successfully treated by (e.g., can be killed or induced to senescence by) the treatment targeting the integrin avb3 (αvβ3) pathway,

wherein optionally the tumor or cancer cell is a glioblastoma (GBM) tumor or cell, a melanoma tumor or melanoma cell or a primitive neuroectodermal tumor (PNET) or PNET cell.

In alternative embodiments, the treatment targeting the integrin avb3 (αvβ3) pathway targets avb3, Glut3, PAK4, or YAP/TAZ.

In alternative embodiments, the treatment comprises administering or having administered to an individual in need thereof cilengitide (or, 2-[(2*S*,5*R*,8*S*,11*S*)-5-benzyl-11-{3-[(diaminomethylidene)amino]propyl}-7-methyl-3,6,9,12,15-pentaoxo-8-(propan-2-yl)-1,4,7,10,13-pentaazacyclopentadecan-2-yl]acetic acid).

In alternative embodiments, the determining or having determined if the tumor or the cancer cell expresses both avb3+ and Glut3+ comprises determining if the tumor or the cancer cell expresses both an avb3+ and a Glut3+ protein, or both an

avb3+ and a Glut3+ message (mRNA, transcript), or both an avb3+ and a Glut3+ protein and message,

and optionally the determining or having determined if the tumor or the cancer cell expresses both an avb3+ and a Glut3+ protein is by a method comprising use of antibodies that specifically bind to a protein of the integrin avb3 pathway, optionally comprising an avb3, Glut3, PAK4, or YAP/TAZ binding antibody (an antibody that specifically binds avb3, Glut3, PAK4, or YAP/TAZ),

and optionally the determining or having determined if the tumor or the cancer cell expresses both an avb3+ and a Glut3+ message (mRNA, transcript) is by a method comprising use of a polymerase chain reaction (PCR) (optionally comprising use of primers capable of amplifying an avb3+ and a Glut3+ message); or, gene expression profiling, an array, or a probe hybridization to a message, optionally a Northern blot (optionally comprising use of primers capable of specifically hybridizing to) an avb3+ and a Glut3+ message).

In alternative embodiments, the determining or having determined if the tumor or the cancer cell expresses a marker consistent with a Classical or Proneural subtype or expresses markers at levels consistent with the Glut3-addicted gene signature, e.g., as listed in Figure 11 or Figure 23, comprises determining or having determined if the tumor or the cancer cell expresses an mRNA and/or a protein consistent with a Classical or a Proneural subtype, or expresses an mRNA or protein markers consistent with the Glut3-addicted gene signature, e.g., expressed at levels as listed in Figure 11 or Figure 23,

and optionally the determining or having determined if the tumor or the cancer cell expresses a protein consistent with a Classical or a Proneural subtype, or has a Glut3-addicted gene signature, e.g., is a high or a low expressed protein from a gene as listed in Figure 11 or Figure 23, is by a method comprising use of antibodies that specifically bind to a protein consistent with a Classical or a Proneural subtype, or a protein from a gene associated with Glut3 addiction, e.g., as listed in Figure 11 or Figure 23,

and optionally the determining or having determined if the tumor or the cancer cell expresses a message (mRNA, transcript) consistent with a Classical or a Proneural subtype, or expresses markers consistent with the Glut3-addicted gene signature, e.g., as listed in Figure 11 or Figure 23, is by a method comprising use of a polymerase chain reaction (PCR) (optionally comprising use of primers capable of

amplifying a message (mRNA, transcript) consistent with a Classical or a Proneural subtype, or markers consistent with the Glut3-addicted gene signature, e.g., as listed in Figure 11 or Figure 23); or, by gene expression profiling, optionally by using an array, or optionally by using a probe hybridization to a message of interest, optionally a Northern blot (optionally comprising use of primers capable of specifically hybridizing to) a message (mRNA, transcript) consistent with a Classical or a Proneural subtype, or markers consistent with the Glut3-addicted gene signature, e.g., as listed in Figure 11 or Figure 23.

In alternative embodiments, the determining or having determined if the tumor or the cancer cell expresses both avb3+ and Glut3+ comprises taking or isolating a cell or a sample of cells, optionally cancer cells or tumors cells, from a patient, optionally a patient tentatively diagnosed or definitely diagnosed with the tumor or cancer, optionally GBM, and determining if the cell or sample of cells expresses both avb3+ and Glut3+ and is Glut-3 addicted.

In alternative embodiments, provided are methods for treating or ameliorating, or killing, or inducing into senescence, a tumor or a cancer cell in a patient or *ex vivo*, wherein optionally the tumor or cancer cell is a glioblastoma (GBM) tumor or a GBM cancer cell, or a melanoma or a primitive neuroectodermal tumor (PNET), or treating or ameliorating a tumor or cancer, optionally GBM, a melanoma or a primitive neuroectodermal tumor (PNET), in an individual in need thereof, comprising:

(a) determining or having determined whether the tumor or cancer, optionally a glioblastoma (GBM) tumor or a GBM cancer cell, will be sensitive to a treatment targeting the integrin avb3 (αvβ3) pathway using a method as provided herein, and

(b) if the method of step (a) determines, or has had determined, that the tumor or cancer, optionally a glioblastoma (GBM) tumor or a GBM cancer cell, will be sensitive to a treatment targeting the integrin avb3 (αvβ3) pathway, administering or having administered the treatment targeting the integrin avb3 (αvβ3) pathway to an individual in need thereof, or,

administering or having administered the treatment to the tumor or cancer cell, optionally to a glioblastoma (GBM) tumor or GBM cancer cell, if the tumor or cancer cell is derived from or isolated from the individual in need thereof, or if the tumor or cancer cell is determined to be sensitive to a treatment targeting the integrin avb3 (αvβ3) pathway using a method as provided herein (e.g., if the glioblastoma (GBM)

tumor or the GBM cancer cell is found to express both avb3+ and Glut3+ and is Glut-3 addicted).

In alternative embodiments, the treatment targets avb3, Glut3, PAK4, or YAP/TAZ, or the treatment comprises administering or having administered to an individual in need thereof cilengitide (or, 2-[(2*S*,5*R*,8*S*,11*S*)-5-benzyl-11-{3-[(diaminomethylidene)amino]propyl}-7-methyl-3,6,9,12,15-pentaoxo-8-(propan-2-yl)-1,4,7,10,13-pentaazacyclopentadecan-2-yl]acetic acid).

The details of one or more exemplary embodiments are set forth in the accompanying drawings and the description below. Other features, objects, and advantages of the invention will be apparent from the description and drawings, and from the claims. All publications, patents, patent applications cited herein are hereby expressly incorporated by reference for all purposes.

BRIEF DESCRIPTION OF THE DRAWINGS

The drawings set forth herein are illustrative of embodiments as provided herein and are not meant to limit the scope of the invention as encompassed by the claims.

FIG. 1A-D illustrate β3 levels correlate with poor survival in GBM and expression of genes involved in glucose metabolism:

FIG. 1A graphically illustrates data of a hierarchical cluster that stratifies patients into two groups according to median survival, and by correlating gene expression with GBM patient survival, identifies a $\beta3^{high}$ subset of samples within the shorter-survival group;

FIG. 1B graphically illustrates data showing the probability of survival of GBM patients as a function of days in GBM populations which express high and low levels of β3;

FIG. 1C and FIG. 8A-C illustrate tables showing genes involved in glucose metabolism (*ALDOC*, *PFKM* and *GLUT3*); and

FIG. 1D graphically illustrates data from a Kaplan-Meier analysis indicating that poor survival correlates with high expression of *GLUT3* and low expression of *ALDOC* and *PFKM*,

as discussed in detail in Example 1, below.

FIG. 2A-O: The impact of integrin αvβ3 on GBM is attributed to its regulation of Glut3 expression:

FIG. 2A illustrates images of immunoblots, and graphically illustrates data, showing the expression of indicated proteins for U87MG, LN229 and LN18 GBM cells infected by shRNA Control (Ctrl) or shβ3, graph shows the fold change of protein expression determined by densitometry analysis;

FIG. 2B graphically illustrates data of mRNA expression, which was determined by qPCR in U87MG, LN229 and LN18 infected by shRNA Control (shCtrl) or shβ3;

FIG. 2C graphically illustrates data showing the relative glucose uptake in U87MG, LN229 and LN18 cells with β3 knockdown compared to control (shCtrl);

FIG. 2D graphically illustrates data where the bars represent the relative lactate production in U87MG and LN229 cells with β3 knockdown compared to control (shCtrl);

FIG. 2E graphically illustrates data showing the effect of β3 and Glut3 knockdown on anchorage-independent growth of U87MG under high (4.5 g/l) or low (0.4 or 0.8 g/L) glucose conditions;

FIG. 2F graphically illustrates data showing the effect of β3 and Glut3 knockdown on tumorsphere formation of U87MG under low glucose conditions (0.4 g/L);

FIG. 2G graphically illustrates flow cytometry data, which was used to quantify $\beta3^+$ versus $\beta3^-$ as well as $Glut3^+$ versus $Glut3^-$ in a growth competition assay under low glucose conditions (0.4 g/L);

FIG. 2H graphically illustrates data showing the effect of β3 and Glut3 knockdown on tumor growth *in vivo*: U87MG shCtrl and U87MG β3 and Glut3 shRNA. (n=15 mice per group);

FIG. 2I graphically illustrates data showing the fold change of β-galactosidase positive cells versus the total cell number, Inverted microscopy images of acidic senescence-associated β-galactosidase staining in U87MG shCtrl and U87MG β3 and Glut3 shRNA (n=5 fields counted per group);

FIG. 2J graphically illustrates data of a cell-cycle analysis showing the percentage of cells in G0/G1, S, and G2/M in U87MG cells with β3 and Glut3 knockdown;

FIG. 2K illustrates images show acidic senescence-associated β-galactosidase staining, a marker of senescence, in mice implanted with U87MG shCtrl, shβ3, shGlut3, or shβ3 with ectopic expression of Glut3;

FIG. 2L graphically illustrates data of a flow cytometry analysis used to quantify U87MG shCtrl (GFP-) versus U87MG shβ3-Glut3+ (GFP+) in a growth competition assay;

FIG. 2M graphically illustrates data showing the effect of ectopic expression of Glut3 on U87MG β3 shRNA on anchorage-independence growth;

FIG. 2N graphically illustrates data showing the fold change of β-galactosidase positive cells versus the total cell number; inverted microscopy images of acidic senescence-associated β-galactosidase staining in U87MG β3 shRNA overexpressing Glut3 compare to U87MG shCtrl (n=5 fields counted per group); and,

FIG. 2O graphically illustrates data showing the effect of ectopic expression of Glut3 on tumor growth *in vivo*: U87MG shCtrl and U87MG β3 and Glut3 shRNA. (n=15 mice per group);

as discussed in detail in Example 1, below.

FIG. 3A-J: β3 modulates Glut3 expression through PAK4-YAP/TAZ axis:

FIG. 3A graphically illustrates data of a Kaplan-Meier analysis of a Freije dataset for TAZ expression (n=42 for β3 low and n=43 for β3 high; P = 0.03);

FIG. 3B illustrates immunoblots showing the effect of β3 knockdown on protein expression of YAP and β3; bars represent the fold change of protein expression determined by densitometry analysis;

FIG. 3C graphically illustrates data showing the effect of β3 knockdown on mRNA expression of YAP and TAZ determined by qRT-PCR, displayed as fold change for gene expression normalized to sh-control in U87MG (n=3), LN229 (n=3) and U251 (n=2);

FIG. 3D illustrates immunoblots showing the effect of YAP/TAZ knockdown on Glut3 protein expression, and the graph shows the fold increase determined by densitometry analysis. U87MG (n=3), LN229 (n=3) and U251 (n=2);

FIG. 3E graphically illustrates data showing the effect of YAP/TAZ knockdown on mRNA expression for Glut3, YAP and TAZ determined by qRT-PCR, displayed as fold change of gene expression normalized to sh-control;

FIG. 3F graphically illustrates data showing acidic senescence-associated β-galactosidase staining in U87MG shCtrl versus YAP/TAZ shRNA;

FIG. 3G graphically illustrates data showing the effect of ectopic expression of YAP on U87MG β3 shRNA on anchorage-independent growth;

FIG. 3H graphically illustrates data showing the fold change of protein expression in U87MG (n=2) and LN229 (n=2) determined by densitometry analysis;

FIG. 3I graphically illustrates data showing acidic senescence-associated β-galactosidase staining in U87MG shCtrl and PAK4 siRNA (n=3); and

FIG. 3J graphically illustrates data of a Cell-cycle analysis showing the percentage of cells in G0/G1, S, and G2/M in U87MG cells with PAK4 siRNA (n=3);

as discussed in detail in Example 1, below.

FIG. 4A-E: Integrin αvβ3 is required for Glut3 expression in patient-derived gliomaspheres that show heterogeneity in Glut3 "addiction":

FIG. 4A illustrates representative immunoblots showing expression of β3, Glut3, and TAZ in GSCs with a schematic representing the decision tree for selecting GSCs based on β3/Glut3 expression (n=2);

FIG. 4B illustrates immunoblots (upper image) showing the effect of β3 knockdown on expression of indicated proteins in Ge479 (n=3), and a graph (lower image) showing data representing the fold change of protein expression relative to sh-control determined by densitometry analysis;

FIG. 4C graphically illustrates data showing the effect of glucose concentration on cell viability measured by CELLTITER-GLO™ (CellTiter-Glo) in GSCs (n=3-5);

FIG. 4D graphically illustrates data showing the effect of Glut3 knockdown on cell viability measured by CELLTITER-GLO™ in GSCs (n=3-4); and,

FIG. 4E graphically illustrates data showing the expression of glycolytic, pentose phosphate and mitochondrial oxidative phosphorylation (OXPHOS) related genes, which were determined by qRT-PCR after β3 or Glut3 knockdown in Ge479, Bars show the fold change of gene expression normalized to sh-control;

as discussed in detail in Example 1, below.

FIG. 5 A-I: The mesenchymal subtype of GBM is enriched for genes involved in glycolytic pathway and sensitive to αvβ3 antagonists, YAP and PAK4 inhibitors:

FIG. 5A graphically illustrates data showing an enrichment analysis of glycolytic genes for the Freije dataset;

FIG. 5B graphically illustrates a Kaplan-Meier analysis of Freije dataset for PGK1 expression;

FIG. 5C graphically illustrates an enrichment analysis for β3, Glut3 (also found in figure 5A), YAP and TAZ;

FIG. 5D graphically illustrates the effect of LM609 (αvβ3 function blocking antibody) and cilengitide (cyclic peptide antagonist of αv integrins including αvβ3 and αvβ5) on cell viability measured by CELLTITER-GLO™ in GSCs;

FIG. 5E graphically illustrates the effect of YAP inhibitor (verteporfin) or PAK4 inhibitor (PF-03758309, CAS no. 898044-15-0) on cell viability measured by CELLTITER-GLO™ in GSCs;

FIG. 5F schematically illustrates an exemplary model of Glut3 addiction in GBM;

FIG. 5G schematically illustrates data identifying Glut3 addicted vs. Glut3 non-addicted samples using 96 signature genes. mRNA was determined by qRT-PCR (n=2) and Bio-Rad software has been used for analysis;

FIG. 5H graphically illustrates the effect of LM609 (αvβ3 function blocking antibody) and cilengitide (cyclic peptide antagonist of αv integrins including αvβ3 and αvβ5) on cell viability measured by CELLTITER-GLO™ in GSCs (n=3-5); and,

FIG. 5I graphically illustrates the effect of YAP inhibitor (verteporfin) or PAK4 inhibitor (PF-03758309) on cell viability measured by CELLTITER-GLO™ in GSCs (n=3-5);

as discussed in detail in Example 1, below.

FIG. 6 illustrates a schematic depicting an exemplary model of Glut3 addiction in GBM; as discussed in detail in Example 1, below.

FIG. 7 illustrates a table summarizing pValues from Kaplan-Meier curves generated from datasets confirm *ITGB3* as a strong prognostic factor associated with poor GBM patient survival, as discussed in detail in Example 1, below.

FIG. 8A-C and FIG. 11 illustrate tables showing genes involved in glucose metabolism (*ALDOC*, *PFKM* and *GLUT3*), as discussed in detail in Example 1, below.

FIG. 9 illustrates a table summarizing data from Kaplan-Meier curves from the "Lee" and "TCGA" datasets: whereas *ALDOC* and *PFKM* do not consistently correlate with patient outcome, *GLUT3* expression tracks with poor survival for all datasets, as discussed in detail in Example 1, below.

FIG. 10 illustrates a table showing a list of primers used for qRT-PCR, as discussed in detail in Example 1, below.

FIG. 11 illustrates a table showing list of genes defining Glut3 addicted vs non-addicted signature, as discussed in detail in Example 1, below; bioinformatics

software was used to perform differential gene expression analysis on GBM samples from the "Freije" dataset. The Glut3 non-addicted signature includes genes that were expressed at significantly higher levels in Glut3-positive GBM samples from patients with *longer* (i.e., higher than median) survival compared with GBM samples from patients with shorter survival. Similarly, the Glut addicted signature includes genes that were expressed at a significantly higher level in Glut3-positive GBM samples from patients with *shorter* survival.

FIG. 12A-B schematically illustrates data from the analysis of multiple datasets revealing that *ITGB3* (β3) and *GLUT3* as co-expressed genes not only in GBM, but also in other cancer types, as discussed in detail in Example 1, below.

FIG. 13A-H: The impact of integrin αvβ3 on GBM is attributed to its regulation of Glut3 expression:

FIG. 13A graphically illustrates the effect of a β3 knockdown on U87MG, LN229 and LN18 cell viability in high (4.5μg/L) vs low (1μg/L) glucose measured by Alamar blue;

FIG. 13B illustrates a histological analysis of U87MG cells with shCtrl and shGlut3; tumors were stained for haematoxylin and eosin (H&E), β3 and Glut3;

FIG. 13C graphically illustrates a cell cycle analysis showing the percentage of cells in G0/G1, S, and G2/M for U87MG cells with knockdown of Glut1 or Glut;

FIG. 13D illustrates a histological analysis of U87MG with shCtrl or β3 shRNA along with ectopic expression of Glut3 ($Glut3^{+}$), tumors were stained for haematoxylin and eosin (H&E), β3 and Glut3;

FIG. 13E graphically illustrates data showing the fold change of β-galactosidase positive cells versus the total cell number. Inverted microscopy images of acidic senescence-associated β- galactosidase staining in LN229 and LN18 Ctrl, β3 and Glut3 siRNA (n=5 fields counted per group);

FIG. 13F graphically illustrates a cell-cycle analysis showing the percentage of cells in G0/G1, S, and G2/M in LN229 and U251 cells with β3 and Glut3 knockdown;

FIG. 13G graphically illustrates a flow cytometry analysis used to quantify γH2AX expression in LN229 cells with β3 and Glut3 knockdown. The graph shows the fold increase of γH2AX expression (n=2); and

FIG. 13H illustrates immunoblots (left image) show expression of β3 and Glut3 in U87MG with shCtrl, shGlut3 or β3 shRNA along with ectopic expression of

Glut3 (Glut3+) (n=3-4), and graphically illustrates (right image) the fold change determined by densitometry analysis;

as discussed in detail in Example 1, below.

FIG. 14A-G: TAZ expression is correlated with poor survival and effect of YAP and PAK4 inhibitors:

FIG. 14A graphically illustrates a Kaplan-Meier analysis of TCGA dataset for WWTR1 (TAZ) expression;

FIG. 14B graphically illustrates data showing the effect of YAP inhibitor, Verteporfin on its target genes (CTGF and CYR61). Expression of CTGF, CYR61 and Glut3 were determined by qRT-PCR in LN229 (n=3) and U87MG (n=2); graph shows the fold change for gene expression normalized to control;

FIG. 14C illustrates immunoblots showing the effect of PAK4 inhibitor, PF-03758309 on the phosphorylation of PAK4 (pPAK4); representative immunoblots show effect of PF-03758309 on expression of indicated proteins in U87MG (n=2);

FIG. 14D graphically illustrates that genetic knockdown of PAK4 reduces expression of Glut3 and YAP, but not integrin β3 for the LN229 and U87MG GBM cell lines;

FIG. 14E illustrates representative immunoblots showing the expression of β3 and YAP in U87MG with shCtrl, shβ3, and shβ3 along with ectopic expression of YAP (YAP+) (n=2);

FIG. 14F illustrates the effect of PAK4 inhibitor PF-03758309 on the phosphorylation of PAK4 (pPAK4): left image illustrates representative immunoblots showing the effect of PF-03758309 on expression of indicated proteins in Ge479 (n=2-3), and right image graphically presents this data; and

FIG. 14G illustrates immunoblots showing the effect of PAK4 knock down on indicated proteins in U87MG (n=2) and LN229 (n=2);

as discussed in detail in Example 1, below.

FIG. 15: GSCs are tumorigenic and multipotent:

FIG. 15A illustrates representative light micrograph images showing H&E staining for Ge518 GSCs-derived tumor in immune-compromised mice (n = 3). GSCs show invasive phenotype (right panel, top) and necrotic foci (right panel, bottom).

FIG. 15B illustrates light micrograph images showing that GSCs are multipotent and can differentiate to form neurons (βIIITubulin) (upper image) and astrocytes (GFAP) (lower image); DAPI was used for nuclear counterstaining;

FIG. 15C graphically illustrates data showing that GSCs express cancer stem cell markers (CD133, Oct4 and Nanog); mRNA expression was determined by qPCR in all GSCs and normalized to housekeeping genes (HKGs);

FIG. 15D-E: shows a histological analysis of brain GBM tissue array (GL805c): FIG. 15D graphically illustrates a bar graph representing β3 and Glut3 expression level detected on tumor cells for 70 specimens, and FIG 15E illustrates light microscopy images of tumors stained for haematoxylin and eosin (H&E), β3 and Glut3;

FIG. 15F graphically illustrates data showing β3, TAZ and YAP mRNA expression, which were determined by qPCR for Ge479 (n=3);

FIG. 15G illustrates representative immunoblots showing expression of indicated proteins when ectopically expressed β3 is GBM6 (n=2);

FIG. 15H graphically illustrates data showing β3 and Glut3 mRNA expression, mRNA was determined by qPCR in all GBM lines; and

FIG. 15I-J: graphically illustrate data showing the effect of β3 (FIG. 15I) and Glut3 (FIG. 15J) knockdown on mRNA expression of ITGB3 (β3) and SLC2A3 (Glut3) determined by qRT-PCR, displayed as fold change for gene expression normalized to siCtrl in Ge518, Ge269 and Ge479 (n=2-4);

as discussed in detail in Example 1, below.

FIG. 16A-F: GSCs classification and enrichment analysis of glycolytic genes:

FIG. 16A graphically illustrates data showing mRNA levels in various neural, proneural, mesenchymal, and classical GSC (Glioblastoma Stem Cell) samples; mRNA was determined by qPCR in all GSCs, several genes (listed in the table of Figure 10) have been tested for each GBM subtypes, and an enrichment score was determined according to gene expression normalized to housekeeping genes;

FIG. 16B graphically illustrates an enrichment analysis of glycolytic genes in mesenchymal and other samples (HK2, ENO1, PFKM, GAPDH and ALDOA); and,

FIG. 16C-F graphically illustrate Kaplan-Meier analyses of Freije dataset for: FIG. 16C graphically illustrates PFKL expression (n = 42 β3 low, n = 43 β3 high; P = 0.041); FIG. 16D graphically illustrates LDHA expression (n = 42 β3 low, n = 43 β3 high; P = 0.006); FIG. 16E graphically illustrates LDHB expression (n = 42 β3 low, n = 43 β3 high; P = 0.03) and FIG. 16F graphically illustrates GAPDH expression (n = 42 β3 low, n = 43 β3 high; P = 0.008);

as discussed in detail in Example 1, below.

FIG. 17A-B: FIG. 17A illustrates a schematic depicting a Mayo Clinic sample request, where samples were requested based on their Glut3 addicted vs. non-addicted signature (also depicted in Figure 18), and then analyzed for cell viability in presence of cilengitide and LM609; and, FIG. 17B graphically illustrating the effect of LM609 (αvβ3 function blocking antibody) and cilengitide (cyclic peptide antagonist of αv integrins including αvβ3 and αvβ5) on Mayo Clinic GSCs cell viability measured by CELLTITER-GLO™ (CellTiter-Glo) in GSCs (n=3-5, except n=2 for GBM150 and GBM85), as discussed in detail in Example 1, below.

FIG. 18 illustrates a table showing Glut3 addicted vs non-addicted signature for Mayo Clinic GSCs extracted from Next Generation Sequencing (NGS) data. M = Mesenchymal, C = Classical, P = Proneural and N = Neural, as discussed in detail in Example 1, below.

FIG. 19 illustrates the relative normalized expression of various mRNAs (as indicated in the Figure) in Glut3 addicted and Glut3 non-addicted samples, as determined by qRT-PCR (n=2), and Bio-Rad software has been used for analysis, as discussed in detail in Example 1, below.

FIG. 20A-B: FIG. 20A graphically illustrates the effect of LM609 (αvβ3 function blocking antibody) and cilengitide (cyclic peptide antagonist of αv integrins including αvβ3 and αvβ5) on cell viability of Ge479 knockdown for β3, PAK4 and YAP/TAZ measured by CELLTITER-GLO™ in GSCs (n=3-5); FIG. 20B graphically illustrates the effect of LM609 (αvβ3 function blocking antibody) and cilengitide (cyclic peptide antagonist of αv integrins including αvβ3 and αvβ5) on cell viability of GBM6 with ectopic expression of β3 measured by CELLTITER-GLO™ in GSCs (n=3-5), as discussed in detail in Example 1, below.

FIG. 21 graphically illustrates data showing the effect of Cilengitide on tumor growth, where mice bearing orthotopic Ge518 (Glut3 non-addicted) and Ge479 (Glut3 addicted) brain tumors were treated with vehicle or cilengitide (25mg kg-1; 8 mice per group), as discussed in detail in Example 1, below.

FIG 22 illustrates images of histological analysis of Ge518 and Ge479 xenografts. Ge518 (n=2-3 mice) and Ge479 (n=3-4 mice) tumors were stained for haematoxylin and eosin (H&E), β3 (brown), Glut3 (blue) and CD31 (brown), as discussed in detail in Example 1, below.

FIG 23 illustrates a three-step process to determine GBM tumor Glut3 addiction status: a tumor is predicted to be Glut3-addicted if there is evidence of 1)

high dual expression of ITGB3 (integrin β3) and SLC2A3 (Glut3), 2) high expression of markers associated with the addiction signature, and 3) low expression of markers associated with the non-addiction signature. Bioinformatics software is used to make the determination of high vs. low expression for each gene among the samples being compared. This is a relative value based on the expression levels among the datasets analyzed. For the 5 PDX models compared in Figure 18, THBS1 expression ranges from 0 to 45, where the units represent normalized FPKM (fragments per kilobase per million mapped reads). In contrast, expression levels of BCAN range from 1 to 743. It is therefore useful to compare a sample with unknown status to multiple benchmark samples with known Glut3 addiction (or non-addiction) to determine the high/low threshold values for each gene.

Like reference symbols in the various drawings indicate like elements.

Reference will now be made in detail to various exemplary embodiments, examples of which are illustrated in the accompanying drawings. The following detailed description is provided to give the reader a better understanding of certain details of aspects and embodiments as provided herein, and should not be interpreted as a limitation on the scope of the invention.

DETAILED DESCRIPTION

In alternative embodiments, provided are methods for treating cancers, e.g., glioblastoma (GBM) tumors or GBM cancer cells, which is sensitive to a treatment targeting the integrin avb3 (αvβ3) pathway, wherein ascertaining whether the cancer or tumor cell is sensitive to treatment targeting the integrin avb3 (αvβ3) pathway is determined by using a method as provided herein. In alternative embodiments, provided are methods for determining whether a glioblastoma (GBM) tumor or GBM cancer cell will be sensitive to a treatment targeting the integrin avb3 (αvβ3) pathway, comprising determining whether the GBM tumor or the GBM cancer cell expresses both avb3+ and Glut3+ along with (and) a genetic signature associated with Glut3 addiction, e.g., in one embodiment, the GBM tumor or the GBM cancer cell is an avb3+/Glut3+ tumor or cancer cell and it has markers consistent with the Classical or Proneural molecular subtypes of GBM or expresses (e.g., expresses mRNA or protein) at least one (one or more) one of the genes consistent with a Glut3 addicted gene/molecular signature, e.g., as listed in Figure 11 or Figure 23, wherein if a GBM

tumor or the GBM cancer cell expresses both avb3+ and Glut3+ and has a molecular signature associated with Glut3 addiction, the GBM tumor or the GBM cancer cell will be sensitive to (will be successfully treated by) the treatment targeting the integrin avb3 (αvβ3) pathway.

In alternative embodiments, embodiments provided herein solve the problem of why certain glioblastoma (GBM) tumors are either sensitive or resistant to agents targeting or inhibiting the integrin avb3 (αvβ3) pathway, including avb3, Glut3, PAK4, or YAP/TAZ. This invention for the first time found that expression of integrin avb3 or GLUT3 is not sufficient to predict sensitivity to these agents. Instead, we found that subsets of avb3+/Glut3+ tumors are sensitive to agents targeting or inhibiting the integrin avb3 (αvβ3) pathway, and that these subsets of avb3+/Glut3+ tumors fall within the Classical and Proneural molecular subtypes previously described for GBM. Therefore, provided herein are methods for determining whether a GBM tumor may be a good or bad candidate for therapeutic strategies targeting or inhibiting the integrin avb3 pathway, including avb3, Glut3, PAK4, or YAP/TAZ. We estimate this "sensitive" population to represent about 10% of GBM tumors. Also provided herein are methods of treating glioblastoma (GBM) tumors found to be sensitive to agents targeting or inhibiting the integrin avb3 (αvβ3) pathway, wherein the sensitivity is determined by methods as provided herein.

Methods as provided herein for the first time find and describe that integrin αvβ3 regulates Glut3 (SLC2A3) expression and thus allows cells to evade senescence. In one embodiment, we found and defined a subpopulation of αvβ3-positive GBM tumors that are particularly sensitive to cilengitide (or, 2-[(2*S*,5*R*,8*S*,11*S*)-5-benzyl-11-{3-[(diaminomethylidene)amino] propyl}-7-methyl-3,6,9,12,15-pentaoxo-8-(propan-2-yl)-1,4,7,10,13-pentaazacyclopentadecan-2-yl]acetic acid) or other agents targeting this axis (i.e., the integrin avb3 pathway). Interestingly, αvβ3 expression is not sufficient to predict sensitivity, as only a subset of αvβ3-expressing GBM tumors are addicted to Glut3. This subset (GBM tumors are addicted to Glut3) includes tumors within the Classical or Proneural GBM molecular subtypes, or tumors which express markers consistent with the Glut3-addicted gene/ molecular signature, e.g., as listed in Figure 11 or Figure 23. These findings may explain why the integrin antagonist cilengitide had a benefit for some patients, but not others, in recently completed clinical trials in which the drug was given to patients from an unselected population.

In alternative embodiments, embodiments provided herein solve the problem, and unmet need, to predict which patients will or will not be responsive to treatments for GBM. Despite gene expression analysis to compare individual GBM tumors, to date no targeted therapies have shown efficacy. We have discovered that the addiction of certain GBM cells to Glut3 can be used to predict drug sensitivity. This addiction is a unique type of biomarker, and one which would typically be tested in functional assays. In alternative embodiments, we have compared the gene expression profiles of tumors that are Glut3-addicted versus (vs.) non-addicted (see FIG. 11), and thus we have established a panel of genes that can be used to infer Glut3 addiction, and thus sensitivity to cilengitide and other agents targeting the integrin avb3 pathway, including avb3, Glut3, PAK4, or YAP/TAZ. In alternative embodiments Glut3 addiction is identified using the full panel of 314 signature genes as illustrated in FIG. 11. In alternative embodiments, these include high expression of SEMA6A, ARHGEF7, MAPK81P1, and PAFAH1B1, along with low expression of CNTN1, KDM2A, ZNF395, RASA3, PRSS23, SNX10, ZKSCAN1, CCPG1, SLC36A1, P4HA2, VDR, WAC, LDHA, and LOX.

In alternative embodiments of methods provided herein, a patient is diagnosed with a cancer, e.g., a GBM, and a biopsy is taken (e.g., a blood or a tissue sample) and analyzed for gene expression. Depending on the gene expression profile, a treatment with cilengitide – or any drug, small molecule, polypeptide and the like, targeting the integrin avb3 pathway, including avb3, Glut3, PAK4, or YAP/TAZ, would be recommended (for administration to the patient diagnosed with the cancer or tumor), or not. Methods as provided herein allow this drug, small molecule or other therapeutic that target elements of the integrin avb3 pathway, including avb3, Glut3, PAK4, or YAP/TAZ, to be used on this identified (i.e., drug sensitive) patient population. We estimate about 10% of GBM patients to fall into this category. This embodiment has been validated using established human GBM cell lines and patient-derived GBM stem cells, *in vivo* and *in vitro*, as described in Example 1, below.

Exemplary Methods for Identifying Cells that are Glut-3 Addicted

In alternative embodiments, provided are methods for determining whether a tumor or a cancer cell will be sensitive to (or can be killed or induced to senescence by) a treatment targeting the integrin avb3 ($\alpha v\beta 3$) pathway, comprising: (a) determining or having determined whether the tumor or the cancer cell expresses both

avb3+ and Glut3+, or determining whether the tumor or the cancer cell is a avb3+/Glut3+ tumor or cancer cell, and (b) determining or having determined whether the tumor or the cancer cell is Glut-3 addicted.

In alternative embodiments, determining or having determined whether the tumor or the cancer cell is Glut-3 addicted comprises determining or having determined whether the tumor or the cancer cell expresses a marker (e.g., an mRNA or a protein) consistent with a Classical or Proneural subtype, e.g., expresses a marker consistent with the Classical or Proneural molecular subtypes of GBM, wherein optionally the marker consistent with a Classical or Proneural subtype comprises an *EGFR*, *GLI1*, *NES*, *DLL3* or *OLIG2* gene transcript or an EGFR, GLI1, NES, DLL3 or OLIG2 protein.

In alternative embodiments, determining or having determined whether the tumor or the cancer cell is Glut-3 addicted comprises determining or having determined whether the tumor or the cancer cell expresses (e.g., expresses mRNA or protein) from at least one (one or more) or two or more, or 3, 4, 5, 6, 7 or 8 or more, of the genes as listed in Figure 11 or Figure 23, at levels as indicated in the Figures.

In alternative embodiments, the expression of a single gene is sufficient to make a determination of (to predict) Glut3 addiction; however, in alternative embodiments, the expression levels of approximately 2, 3, 4, 5, 6, 7 or 8 gene is sufficient to make a determination of (to predict) Glut3 addiction – where both high and low expression of selected genes is taken into consideration in making the determination, e.g., as schematically shown in Figure 23.

In alternative embodiments, a minimum of approximately 6 genes is sufficient to make a determination of Glut3 addiction: where in one embodiment, 3 of which can be classified as being expressed at high levels, and 3 of which can be classified as being expressed at low levels, to be sufficient to make a determination of Glut3 addiction. In alternative embodiments, a minimum of approximately 8 genes is sufficient to make a determination of Glut3 addiction: where in one embodiment, 4 of which can be classified as being expressed at high levels, and 4 of which can be classified as being expressed at low levels, to be sufficient to make a determination of Glut3 addiction; in another embodiment, 5 genes classified as being expressed at high levels, and 3 genes classified as being expressed at low levels is sufficient to make a determination of Glut3 addiction; in another embodiment, 3 genes classified as being expressed at high levels, and 5 genes classified as being expressed at low levels is

sufficient to make a determination of Glut3 addiction; and the like. The more genes analyzed, the better confidence the practitioner has in the predictive value of this screen, i.e., of the methods as provided herein.

The "expression level" for any single gene, i.e., whether it is expressed at a "high" or a "low" level" is relative measurement, not an absolute one. The raw value for a single gene is first normalized to multiple housekeeping genes, positive controls, and negative controls. Gene expression can be compared within a single biological sample, or between multiple samples.

In alternative embodiments, determining or having determined whether the tumor or the cancer cell is Glut-3 addicted comprises using a custom array comprising substantially or all or these genes as listed in Figure 11. In alternative embodiments, the array is a 314 gene expression array which is generated by comparing GLUT3 expression with survival from the publicly available Freije dataset: 143 genes on Glut3 non-addicted list (Fig. 11 - left column), where a drug-sensitive tumor should show low expression, and 171 genes on Glut3-addicted list (Fig 11 - right column), where a drug-sensitive tumor should show high expression. Sensitivity to $\alpha v\beta 3$ blockade (i.e., how drug-sensitive the tumor is) will be proportional to how well a given tumor fits this profile. A tumor with the best predicted sensitivity will show very high expression of some (but not all) of the 171 genes on the Glut3-addicted panel and very low expression of some (but not all) of the 143 genes on the Glut3 non-addicted panel.

In alternative embodiments, determining or having determined whether the tumor or the cancer cell is Glut-3 addicted comprises using custom array containing a subset of genes shown in Fig 5G, i.e., a subset of the 19 listed genes. This is a subset of the full list shown in Figure 11, and was validated using patient-derived (Glioblastoma Stem Cell) models with known Glut3 addiction status:

- 15 genes indicated Glut3 non-addiction, for example, in alternative embodiments, a drug-sensitive sensitive tumor will show low expression of 1, 2, 3, 4, 5, 6, 7, 8, 9, 10, 11, 12, 13, 14 or all 15 of the genes: CNTN1, KDM2A, ZNF395, RASA1, PRSS23, SNX10, ZKSCAN1, CCPG1, PLOD2, SLC36A1, P4HA2, VDR, WAC, LDHA and/or LOX; and
- 4 genes indicated Glut3-addiction, for example, in alternative embodiments, a drug-sensitive tumor will show high expression of 1, 2, 3

or all 4 of the genes: SEMA6A, ARHGEF7, MAPK8IP1 and/or PAFAH1B1.

Validation:

Note that for the GBM GSC models shown, the tumors with proven Glut3 addiction (GBM39/GBM79) or non-addiction (GBM518/GBM269) evaluated independently using Glut3 knockdown did not show identical expression profiles. For this reason, in some embodiments, analysis of a single marker may not be sufficient to infer Glut3 addiction, but rather 2, 3, 4, 5, 6, 7 or 8 or more gene levels may need to be analyzed (e.g., as described herein) for a more accurate determination of Glut3 addiction.

In alternative embodiments, determining or having determined whether the tumor or the cancer cell is Glut-3 addicted comprises using a custom array comprising a subset of genes as shown in Figure 18, i.e., a subset of the 53 listed genes. This is a subset of the full list shown in Figure 11, validated using patient-derived xenograft models obtained from the Mayo Clinic;

- 22 genes indicated Glut3 non-addiction, for example, in alternative embodiments, a drug-sensitive tumor will show low expression of 1, 2, 3, 4, 5, 6, 7, 8, 9, 10, 11, 12, 13, 14, 15, 16, 17, 18, 19, 20, 21 or all 22 of the genes: CAV1, CAV2, TAGLN, SERPINE1, THBS1, P4HA2, AHNAK2, DYNLT3, ACTA2, PRSS23, FHL2, TPM1, PLAU, UPP1, NDRG1, LDHA, ANGPTL4, MIR22HG, VMP1, PGK1, TPI1 and/or GSTO1; and
- 30 genes indicated Glut3-addiction, for example, in alternative embodiments, a drug-sensitive tumor will show high expression of 1, 2, 3, 4, 5, 6, 7, 8, 9, 10, 11, 12, 13, 14, 15, 16, 17, 18, 19, 20, 21, 22, 23, 24, 25, 26, 27, 28, 29 or all 30 of the genes: NDRG2, BCAN, OLIG2, DLL3, FHL1, PSAT1, ID4, MAP2, ETV1, ZEB1, CNTN1, MARCKS, TAF9B, PLXNB1, GPSM2, KCNJ10, DHX9, PEA15, PTPN11, HIPK2, ZNF711, MYO6, SEMA6A, POU3F3, GNG4, DGCR2, ARHGEF7, ARHGAP35, PIP4K2B and/or PRKDC.

Validation:

As shown in Fig 18, GBM150 and GBM59 (tumors with independently validated mesenchymal subtype) show high expression of many (but not all) of the Glut3-nonaddicted genes and low expression of many (but not all) of the Glut3-

addicted genes. Cells isolated from these tumors were shown to be largely resistant to both LM609 and cilengitide in Figure 17B.

As shown in Fig 18, GBM14, GBM64, and GBM85 (tumors with independently validated Classical or Proneural subtypes) show low expression of many (but not all) of the Glut3-nonaddicted genes and high expression of many (but not all) of the Glut3-addicted genes. Cells isolated from these tumors were shown to be largely sensitive to both LM609 and cilengitide in Figure 17B.

Note that while the insensitive tumors (GBM150/GBM59) show a similar genetic signature, not all genes show a significant difference in expression compared to the sensitive tumors (GBM14/GBM64/GBM85).

In alternative embodiments, determining or having determined whether the tumor or the cancer cell is Glut-3 addicted comprises using a custom array containing a subset of genes shown in Figure 19, i.e., a subset of the 27 listed genes. This is a subset of the full list shown in Figure 11, validated using patient-derived xenograft models obtained from the Mayo Clinic:

- 19 genes indicated Glut3 non-addiction, for example, in alternative embodiments, a drug-sensitive tumor will show low expression of 1, 2, 3, 4, 5, 6, 7, 8, 9, 10, 11, 12, 13, 14, 15, 16, 17, 18 or all 19 of the genes PAK4, ZNF395, ITGB3, WAC, PRSS23, ANGPTLA4, CCPG1, CAV1, CAV2, LOX, SLC36A1, SERPINE1, PLOD2, AHNAK2, YAP, VDR, PGK1, TPI n2 and/or LDHA; and
- 8 genes indicated Glut3-addiction, for example, in alternative embodiments, a drug-sensitive tumor will show high expression of 1, 2, 3, 4, 5, 6, 7 or all 8 of the genes MAPK8Ip1, Sema6A, ID4, ARHGEF7, ZNF711, NDRG2, BCAN and/or PAFAH1B1.

Validation:

As shown in Fig 18, GBM150 and GBM59 (tumors with independently validated mesenchymal subtype) show high expression of many (but not all) of the Glut3-nonaddicted genes and low expression of many (but not all) of the Glut3-addicted genes. Cells isolated from these tumors were shown to be largely resistant to both LM609 and cilengitide in Figure 17B.

As shown in Fig 18, GBM14, GBM64, and GBM85 (tumors with independently validated Classical or Proneural subtypes) show low expression of many (but not all) of the Glut3-nonaddicted genes and high expression of many (but

not all) of the Glut3-addicted genes. Cells isolated from these tumors were shown to be largely sensitive to both LM609 and cilengitide in Figure 17B.

Note that while the insensitive tumors (GBM150/GBM59) show a similar genetic signature, not all genes show a significant difference in expression compared to the sensitive tumors (GBM14/GBM64/GBM85).

Exemplary Methods for Cell Isolation, Biopsy and Gene Analysis

In alternative embodiments of methods provided herein, after a patient is diagnosed with a cancer or tumor, e.g., a GBM, a melanoma tumor or melanoma cell or a primitive neuroectodermal tumor (PNET) or PNET cell, a biopsy is taken (e.g., a blood, serum or a tissue sample is taken) and analyzed for gene expression. Any biopsy method or technique known in the art can be used, and any method or process for analysis of gene expression or nucleic acid amplification or screening can be used to determine the gene or molecular profile of a cell, and any process or method for the isolation of tumor or cancer cells can be used.

For example, methods for performing a genetic analysis on a DNA target region from a test sample can be performed as described in U.S. Patent App. Nos. 20180163272 A1; 20180163201 A1; 20180142234 A1; 20180119230 A1; 20180119214 A1; 20180155768 A1; 20180137242 A1; and, U.S. Patent Nos. 9,944,978; 9,914,977; 9,650,677; 9,447,411; 9,938,519; 9,932,576.

For example, biopsy methods, or methods for isolating a tumor or cancer cell for analysis, can be performed as described in U.S. Patent App. Nos. 20180161774 A1 (describing a microfluidic device for trapping circulating tumor cells); 20180161021 A1 (describing a biopsy device, comprising a flexible coaxial structure); 20180136210 A1, 20180153529 A1, 20180125466 A1 and 20180116643 A1 (describing biopsy devices); or as described in U.S. Patent Nos. 9,993,230; 9,974,523; 9,968,339.

Exemplary Methods for Treating Cancers

In alternative embodiments, provided are methods for treating or ameliorating, or killing, or inducing into senescence, a tumor or a cancer cell in a patient or *ex vivo*, wherein optionally the tumor or cancer cell is a glioblastoma (GBM) tumor or a GBM cancer cell, or a melanoma or a primitive neuroectodermal tumor (PNET), or treating or ameliorating a tumor or cancer, optionally GBM, a melanoma or a primitive

neuroectodermal tumor (PNET), in an individual in need thereof. Any method or protocol known in the art can be used to practice these methods.

For example, exemplary methods for treating or ameliorating, or killing, or inducing into senescence GBM are described in U.S. Patent Nos. 9,872,857; 9,687,466; 9,662,377; 9,587,239; 9,573,960; 9,421,202; 9,364,532; 9,364,505; 9,283,195; 9,145,462. Exemplary methods for treating or ameliorating, or killing, or inducing into senescence melanomas are described in U.S. Patent Nos. 9,962,348; 9,949,947; 9,937,161; 9,920,121; 9,901,629. Exemplary methods for treating or ameliorating, or killing, or inducing into senescence PNETs are described in U.S. Patent Nos. 7,678,759; 6,667,156; or U.S. Patent App. No. 20130303460 A1.

The invention will be further described with reference to the following examples; however, it is to be understood that the exemplary embodiments provided herein are or the invention are not limited to such examples.

EXAMPLES

EXAMPLE 1: Glut3 addiction is a druggable vulnerability for a molecularly defined subpopulation of glioblastoma (GBM)

This Example and the data presented herein demonstrate that alternative embodiments of methods provided herein are effective in determining whether or not a treatment with cilengitide – or any drug targeting the integrin avb3 pathway, including avb3, Glut3, PAK4, or YAP/TAZ, would be recommended, or not, for treating a GBM.

By analyzing clinical GBM samples and patient-derived glioblastoma-initiating cells, we identified a subpopulation of GBM tumors for which αvβ3 integrin controls Glut3 expression to regulate glucose metabolism, thus allowing cells to avoid senescence. Here, we describe a method to identify those GBM that are particularly sensitive to αvβ3 antagonists, including cilengitide.

While GBM tumors are highly aggressive and therapy-resistant, individual tumors achieve this state via distinct molecular pathways. Here, we define a unique biological subpopulation addicted to an integrin αvβ3-mediated pathway that enhances glucose uptake, making tumors highly sensitive to a variety of agents that disrupt this advantage. Interestingly, αvβ3 expression alone is not sufficient to define this population, as only a subset of αvβ3-expressing GBM tumors are addicted to this

pathway. Our findings may explain why the integrin antagonist cilengitide had a benefit for some patients, but not others, in clinical trials. By revealing a direct link between aberrant integrin expression and altered glucose metabolism, this work identifies a context-dependent druggable vulnerability that can be exploited for GBM therapy.

Results

Integrin β3 mRNA expression correlates with poor survival and expression of genes involved in glucose metabolism

To investigate the clinical relevance of integrin expression in gliomas, we analyzed the correlation between integrin expression and glioma patient survival for the "Freije" dataset (Freije, Cancer Res, 2004). Expression of the integrin β subunit is a rate-limiting determinant of integrin heterodimer formation (Cheresh, 1987), and our analysis reveals *ITGB3* (β3) as the only β subunit whose mRNA expression correlates with poor survival in gliomas (P-value = 0.03) (figure 1A-1B). Because β3 pairs exclusively with the αv subunit in GBM cells, this finding is consistent with our previous report of integrin αvβ3 protein expression in GBM, but not in low grade astroglial-derived tumors (Gladson and Cheresh, 1991). We also generated Kaplan-Meier curves from additional datasets, which confirm *ITGB3* as a strong prognostic factor associated with poor patient survival, as shown in the Table illustrated in FIG. 7. By generating a hierarchical cluster and stratifying patients into two groups according to median survival, we identify a $\beta3^{high}$ subset of samples within the shorter-survival group (FIG. 1A). We reasoned that understanding how integrin β3 contributes to the aggressive phenotype for this subpopulation would enable the design of a targeted therapy approach to exploit the vulnerabilities of this subset.

To consider how high integrin β3 expression may lead to poor survival in GBM, we compared gene expression profiles between $\beta3^{high}$ versus $\beta3^{low}$ samples in GBM patients. We find genes involved in glucose metabolism (*ALDOC*, *PFKM* and *GLUT3*) as one of the main family of genes correlated with β3 expression (figure 1C, supplementary table 2). As for integrin β3, Kaplan-Meier analysis indicates that poor survival correlates with high expression of *GLUT3* (P-value = 0.01) and low expression of *ALDOC* and *PFKM* (FIG. 1D).

To further validate the clinical relevance of this profile, we generated Kaplan-Meier curves from the "Lee" and "TCGA" datasets. Whereas *ALDOC* and *PFKM* do

not consistently correlate with patient outcome, we find that *GLUT3* expression tracks with poor survival for all datasets, see the table illustrated in FIG. 9. Moreover, analysis of multiple datasets reveals *ITGB3* and *GLUT3* as co-expressed genes not only in GBM, but also in other cancer types, as illustrated in FIG. 12A-B.

Targeting β3 strongly inhibits Glut3 expression to decrease cell survival and anchorage-independence

We next considered whether the ability of integrin αvβ3 to promote an aggressive GBM phenotype might be linked to Glut3-mediated cell survival and glucose uptake. For three established GBM cell lines, shRNA-mediated knockdown of integrin β3 strongly inhibits Glut3 expression (FIG. 2A-2B), glucose uptake (FIG. 2C), and lactate production (FIG. 2D). In fact, the effect of β3 knockdown on cell survival is accentuated under low glucose conditions (FIG. 2E and FIG. 13A). Indeed, we observe that knockdown of either β3 or Glut3 decreases anchorage independence (FIG. 2E) and tumorsphere formation (FIG. 2F).

To determine whether highly efficient glucose uptake provides a competitive advantage for $\beta3^+$ cells, we co-cultured $\beta3^+$ (GFP^-) and $\beta3^-$ (GFP^+) cells under standard (4.5g/L) or low (0.4g/L) glucose conditions and monitored their ratio using flow cytometry. Indeed, there are significantly more viable $\beta3^+$ cells present after 1 week of glucose restriction compared with cells for which either β3 or Glut3 had been knocked down (FIG. 2G). More importantly, knockdown of either β3 or Glut3 significantly delays the orthotopic growth of GBM tumors in mice (FIG. 2H and FIG. 13B). Collectively, these results indicate that β3 and Glut3 promote the survival of GBM cells.

We previously reported that knockdown of β3 induced a senescent phenotype in GBM cells (Franovic et al., 2015). Here we show that Glut3 knockdown also induces multiple markers of senescence *in vitro*, including β-galactosidase (SA-β-gal) activity and G0/G1 cell cycle arrest (FIG. 2I-2J). *In vivo*, cells with knockdown of either β3 or Glut3 show SA-β-galactosidase activity within subcutaneous xenografts (FIG. 2K). In contrast, knockdown of the Glut1 or Glut6 glucose transporters does not induce a senescent phenotype (FIG. 13C). We therefore asked whether ectopic expression of Glut3 is sufficient to drive GBM growth in the absence of β3. Indeed, ectopic Glut3 "rescues" the effects of β3 knockdown on 2D and 3D growth and prevents the senescent phenotype *in vitro* and *in vivo* (FIG.2K-2O and FIG. 13D),

suggesting that the regulation of Glut3 expression may largely account for the impact of integrin αvβ3 on GBM progression.

Integrin αvβ3 modulates Glut3 expression through PAK4-YAP/TAZ axis

To understand how integrin αvβ3 regulates Glut3 expression in GBM cells, we considered transcriptional regulators that correlate with β3 expression. We identified "cell signaling" as an important family of genes associated with β3 expression, see FIG. 8C, and found the transcriptional co-activator *WWTR1* (WW domain-containing transcription regulator 1, also known as TAZ) as the top transcription factor in our list of genes, see FIG. 8A-C. Along with its paralog Yes-associated protein (YAP), YAP/TAZ impacts a wide variety of cellular functions, including epithelial-mesenchymal transition, cell growth, organ development, metabolism, and stress responses (Moroishi et al., 2015). Of note, the Kaplan-Meier curves generated from Freije (FIG. 3A) and TCGA (FIG. 14A) datasets reveal that *WWTR1* (TAZ) expression correlates with poor survival (P-values = 0.01 and 0.006 for Freije and TCGA datasets respectively). Moreover, we find that β3 knockdown leads to a marked decrease of YAP/TAZ expression (FIG. 3B-3C). Consistent with previous reports of Glut3 as a YAP-regulated gene (Wang et al., 2015), we find that YAP/TAZ knockdown decreases Glut3 expression (FIG. 3D-3E, FIG. 14B), and this also induces senescence as evidenced by SA-β-galactosidase activity (FIG. 3F). Furthermore, ectopic expression of YAP can rescue colony forming ability in β3-knockdown cells (FIG. 3G and FIG. 14E-G).

Since we recently implicated PAK4 as a mediator of β3 function in GBM cells (Franovic et al., 2015), we considered whether this kinase may also be required for β3-mediated regulation of YAP/TAZ expression. Indeed, inhibition of PAK4 activity using the PAK4 kinase inhibitor PF-03758309 or knockdown of PAK4 expression using shRNA led to a decrease of YAP/TAZ expression (FIG. 3H, FIG. 14C and FIG. 14E-G). Moreover, knockdown of PAK4 (like YAP/TAZ) induced markers of senescence, including SA-β-gal and G0/G1 cell cycle arrest (FIG. 3I-3J). Whereas a critical role for Glut3 in GBM has recently been reported (Flavahan et al., 2013), there have so far been no therapeutic agents capable of targeting its function. By understanding how Glut3 expression is regulated in GBM cells, our new findings highlight multiple strategies to therapeutically target this signaling axis in cells that are addicted to Glut3 for survival.

Integrin αvβ3 is required for Glut3 expression in patient-derived gliomaspheres

To further examine the link between β3 and Glut3 in models that reflect the genetic heterogeneity of human glioblastoma, we derived glioblastoma stem cells (GSCs) from twelve GBM patients and confirmed tumorigenicity, multipotency capacity, and expression of stem cell markers (FIG. 15A-C). For this panel, a third of the GSCs models show high integrin β3 expression (FIG. 4A), and this correlates with positive expression of Glut3 (FIG. 4A). Similarly, histological analysis of a GBM tissue array confirms that only a subset of GBM specimens show high expression of both β3 and Glut3 (FIG. 15D-E). For the β3-positive GSC models on our panel, knockdown of β3 decreases Glut3 expression (FIG. 4B, FIG. 15F and FIG. 15I), while ectopic expression of β3 in the β3-negative GBM6 model induces both Glut3 and YAP expression (FIG. 15G). In contrast to this GSC panel, all of the GBM established cell lines examined show high levels of both αvβ3 and Glut3 (FIG. 2A and FIG. 15H), highlighting the inability of cultured cell lines to accurately reflect the heterogeneity of GBM in this context.

Patient-derived gliomaspheres show heterogeneity in Glut3 "addiction"

In contrast to the established GBM cell lines that are uniformly addicted to both αvβ3 and Glut3, we find that not all of the $\alpha v\beta 3^{+}$/$Glut3^{+}$ patient-derived GSC models are dependent on glucose and/or Glut3 expression for survival. While Ge479 and GBM39 are highly sensitive to glucose deprivation, other patient-derived GSCs show less sensitivity (Ge269 and Ge518) or glucose indifference (Ge738 and GBM6), as demonstrated by their equivalent viability under low or high glucose conditions (FIG. 4C). Importantly, Glut3 knockdown decreases the survival of the glucose-addicted Ge479 GSC model, while Ge269 and Ge518 are only moderately dependent on glucose and not dependent on Glut3 (FIG. 4A-D). For the glucose-addicted Ge479 model, β3 and Glut3 knockdown induces the same pattern of gene expression (increased *ALDOC* and a trend toward increased *HK3*), which is in line with the differential gene expression analysis (FIG. 4E). The apparent dichotomy in αvβ3/Glut3 expression vs. addiction prompted us to consider how the two groups of GSCs models may differ in terms of molecular subtype. Indeed, the Glut3-addicted GSCs models Ge479 and GBM39 express genes consistent with a "Proneural-Classical" GBM subtype (*EGFR*, *GLI1*, *NES*, *DLL3*, *OLIG2*), while the Glut3-independent GCS models Ge269 and Ge518 express markers indicating the

Mesenchymal GBM subtype (*CHI3L1* (YKL40), *LOX*, *CD44*, and *RELB*) (FIG. 16A). Altogether, our results indicate that within the population of GSCs defined by dual high expression of both αvβ3 and Glut3, only a subset of these tumors (i.e. those with Proneural-Classical marker) depend on Glut3 for survival.

The Mesenchymal subtype of GBM is enriched for glycolytic genes, but is insensitive to antagonists of the αvβ3/PAK4/YAP/TAZ pathway

GBM cells avidly take up glucose and are highly metabolically active. This particularity has been exploited clinically by Positron Emission Tomography (PET) combined with an intravenous injection of 18F-fluorodeoxy-glucose (18FDG), a glucose analog. However, not all GBM subtypes avidly take up FDG, suggesting metabolic heterogeneity which is not clearly understood. To investigate how αvβ3 might impact the metabolic landscape of GBM, we performed an enrichment analysis for all genes involved in the glycolytic/gluconeogenesis pathway. For the Mesenchymal subtype of GBM in the Freije dataset, there is a significant enrichment of genes involved in the glycolytic pathway, including *HK3*, *LDHA*, *PFKL*, *PGK1*, *GLUT3*, *GLUT5*, and *GLUT10*, a trend toward enrichment for *HK2*, *ENO1*, *PFKM*, *GAPDH*, and *ALDOA*, and significantly low expression of *ALDOC*, *PFKP*, and *LDHB* (FIG. 5A and FIG. 16B). Kaplan-Meier analysis confirms the clinical relevance for several of these genes (FIG. 5B and FIG. 16C-F). Despite the highly glycolytic expression signature of the Mesenchymal subtype in the Freije dataset and the enrichment of β3, Glut3, YAP, and TAZ (FIG. 5C), we find that Mesenchymal-like GSC models are not addicted to Glut3 (FIG. 4D). It is possible that the abundance of glycolytic genes can compensate for the role of Glut3, thus explaining its non-essential role in tumors of this subtype. Or, the Mesenchymal subtype may depend on metabolic pathways, other than the glycolytic pathway, for survival. Together, these findings suggest that agents targeting the αvβ3/PAK4/YAP/TAZ/Glut3 signaling axis would be most effective for αvβ3/Glut3^{high} tumors that show markers defining a Proneural/Classical, but not Mesenchymal, subtype.

We hypothesized that αvβ3/Glut3^{high}, Glut3-addicted GSCs (GBM39 and Ge479) would be highly sensitive to agents that disrupt the β3-PAK4-YAP/TAZ axis. To test this hypothesis, we evaluated GSC survival in presence of the αv integrin antagonists cilengitide (a cyclic peptide that inhibits αv integrins) or LM609 (a monoclonal antibody specific for integrin αvβ3) (FIG. 5D and FIG. 5H). We found

that sensitivity to any of these agents does not exclusively depend on αvβ3/Glut3 expression, but rather on Glut3/glucose addiction status, which appears to be linked to a Proneural-Classical like subtype. In contrast, GSC with low β3/Glut3 expression (Ge738, GBM6, Ge970.2 and Ge885) consistently showed a moderate enhancement of viability when treated with cilengitide or LM609 (FIG. 5D, FIG. 5H and FIG. 16G). Similar to blockade of αvβ3 directly, inhibitors of YAP or PAK4 reduce *in vitro* viability of the Glut3-addicted Proneural-like Ge479 GSC, but not the Glut3-independent Mesenchymal-like Ge518 model (FIG. 5E and FIG. 5H). Systemic cilengitide treatment prolongs the survival of mice bearing Ge479, but not Ge518, orthotopic tumors (FIG. 5F), further linking Glut3 addiction to a differential selectivity to αvβ3 antagonism *in vivo*.

Finally, we considered how the Glut3 addiction status of a given tumor might be predicted using molecular profiling. To do this, we identified samples from the Freije dataset with high expression of Glut3. For this subset, we asked which genes tracked with Glut3 in terms of patient survival. This generated a list of Glut3/survival-associated genes that we predicted might be useful in the identification of the Glut3 addicted phenotype, see the Table of FIG. 11. To validate this profile, we asked if this profile could differentiate between our Proneural/Classical Glut3-addicted GSC models (GBM39 and Ge479) and our Mesenchymal Glut3-non-addicted GSC models (Ge269 and Ge518). Out of a 115-gene panel, a 19-gene subset (FIG. 5G) allowed us to distinguish between Mesenchymal (LOX, THBS1, and DCN) and Proneural/Classical subtypes (DLL3, OLIG2, CDK17, and MAP2). Therefore, assessing GBM molecular subtype using this gene expression panel could provide a means to identify which αvβ3/Glut3^{high} tumors should be sensitive to inhibitors of αvβ3/PAK4/YAP/TAZ or Glut3 knockdown (FIG. 5F).

To validate our hypothesis and test the ability of our signature to predict sensitivity to αvβ3 antagonists, we analyzed the available gene expression data for 41 models from the Mayo Clinic Brain Tumor Patient-Derived Xenograft National Resource. Based on their expression of genes associated with the Glut3 addicted versus non-addicted signature we generated, we predicted that 8 of the models (approximately 20%) should be sensitive based on their high expression of β3/Glut3 and the Glut3 addicted signature. We therefore obtained 3 models predicted to be addicted, 2 non-addicted, and 2 with β3/Glut3-low to directly test sensitivity to the αvβ3 antagonists cilengitide and LM609 (FIG. 17A-B, FIG. 8A-B, and FIG. 19).

Similar to Ge479 and GBM39, we find sensitivity to integrin blockade for GBM14, 85 and 64, which we predicted to be Glut3 addicted (FIG. 17A-B). Consistently, GBM150 and GBM59 with Glut3 non-addicted signatures are not affected by the integrin antagonists. Like the other GSC with low β3/Glut3 expression, GBM26 and GBM12 show no effect or a moderate enhancement of viability upon cilengitide or LM609 treatment (FIG. 17A-B). Based on gene expression alone, we were able to predict whether a given GBM PDX model would be sensitive or insensitive to αvβ3 blockade for this collection of samples. Our success with a modest sample size suggests promise for expanding this strategy to clinical testing.

Notably, we also find that ectopic expression of β3 in a GCS in a model with low β3/Glut3 (GBM6) it is not sufficient to sensitize the tumor cells to integrin blockade, while β3 knockdown in the Glut3 addicted Ge479 model abolishes their sensitivity (FIG. 20).

More importantly, systemic treatment with the integrin antagonist cilengitide dramatically prolongs the survival of mice bearing Ge479, but not Ge518, orthotopic tumors (FIG. 21 and FIG. 22), further linking Glut3 addiction to a differential selectivity to αvβ3 blockade in vivo. Altogether, our results identify a molecularly defined subset of GBM tumors that are highly sensitive to inhibition of the β3-PAK4-YAP/TAZ axis by virtue of their Glut3 addiction (FIG. 5F and FIG. 6).

Discussion

Previous studies have linked αvβ3 expression to GBM progression (Gladson and Cheresh, 1991). Here, we reveal that integrin αvβ3 expression via activation of PAK4 is required for Glut3 expression in GBM cells, which in some patients leads to Glut3 addiction and sensitivity to αvβ3 antagonists. Although all established GBM cell lines we examined express αvβ3 as a biomarker predicting both Glut3 addiction and sensitivity to inhibitors of αvβ3 integrin, PAK4 or YAP/TAZ, we find this holds true for only a subset of patient-derived gliomasphere models that may more accurately represent the genetic heterogeneity of GBM. Indeed, dual expression of αvβ3/Glut3 drives addiction to this pathway only for Proneural-Classical subtype GBM tumors. In contrast, elements of this pathway are not critical for the growth and viability of patient-derived gliomaspheres that show a gene signature consistent with the Mesenchymal GBM subtype. Thus, our findings provide a possible explanation for the failure of cilengitide to meet its primary survival endpoint in phase III trials,

and we predict patients with αvβ3-positive Proneural-Classical subtype tumors might be the best candidates for this drug.

Integrin αvβ3 as a target for GBM therapy

While a number of integrins contribute to the growth and progression of a wide array of cancers (Desgrosellier and Cheresh, 2010; Desgrosellier et al., 2014; Seguin et al., 2014), we find that only αvβ3 expression is significantly linked to glioblastoma progression. This is consistent with our previous studies showing αvβ3 protein expression on the most advanced form of this disease, and most highly expressed on those cells at the tumor margin (Gladson and Cheresh, 1991). However, despite promising activity in phase I (Nabors et al., 2007) and II (Reardon et al., 2008) trials, the αv integrin antagonist cilengitide failed to produce a significant overall survival benefit in the phase III CENTRIC trial (Stupp et al., 2014), and further clinical development of cilengitide for GBM has been halted (Mason, 2015).

A number of factors may have contributed to the clinical failure of cilengitide, including the stability and pharmacokinetic properties of the drug, its combination with alkylating agents, and use in highly aggressive, drug-resistant cancer (Paolillo et al., 2016). However, we argue it may be important to select a more focused GBM patient population. While higher levels of αvβ3 were associated with a modest survival benefit in the phase II CORE trial, αvβ3 expression did not correlate with outcome for the phase III CENTRIC trial (Weller et al., 2016). These findings, along with our new data, suggest that profiling αvβ3 expression alone is not sufficient to predict sensitivity to this drug. Instead, we have linked cilengitide sensitivity with the ability of αvβ3 to drive Glut3 addiction.

Understanding why certain tumors are addicted to αvβ3, glucose, and Glut3

Using loss/gain-of-function approaches, we have determined that integrin αvβ3 is required for expression of the high affinity glucose transporter, Glut3, in a PAK4 and YAP/TAZ-dependent manner. In turn, Glut3 appears to be a critical mediator of αvβ3 addiction in GBM, as ectopic Glut3 expression can completely rescue the orthotopic tumor growth capacity of β3-knockdown cells by allowing them to avoid senescence. While normal astrocytes do not express Glut3, its expression level correlates to astrocytoma grade (Boado et al., 1994). Previous studies have reported a correlation between glucose level/uptake and poor survival (Patronas et al., 1985), and Flavahan and colleagues reported that brain tumor initiating cells express Glut3, allowing them to outcompete non-tumor cells for glucose within the glucose-

limited tumor environment (Flavahan et al., 2013). Recently, Birsoy and collaborators reported that certain glucose-sensitive cell lines do not increase oxygen consumption upon glucose limitation, and gene expression analysis revealed that these lines have low Glut3 and Glut1 expression (Birsoy et al., 2014). A recent single cell RNA-seq study highlighted the strong heterogeneity in GBM specimens that was not previously well appreciated (Patel et al., 2014); indeed, among all five tumors analyzed, the authors have shown individual cells corresponding to different GBM subtypes. Together, these studies suggest a complicated heterogeneity and metabolic landscape among individual GBM tumors that may not only explain clinical trial failures but also highlight the need to better understand GBM heterogeneity in order to design appropriate therapeutic regimens. Furthermore, the impact of intratumoral heterogeneity for ITGB3 expression on clinical outcomes represents a potential limitation of our study, as tumors with high overall ITGB3 expression may contain a subpopulation of cells with low ITGB3 and GLUT3. Together, these studies suggest a complicated metabolic landscape among individual GBM tumors.

Despite the functional advantages offered by Glut3 expression, we find that only a subpopulation of our patient-derived GSC models actually depend on glucose/Glut3 for their survival. In contrast, all GBM long-cultured cell lines express high level of Glut3 and are addicted to this transporter for survival. As such, long-term culture of established GBM cell lines may somehow enrich for this phenotype, providing a poor reflection of its frequency within the well-appreciated heterogeneity of GBM. The fact that only 15% of our patient-derived GSC models appear to be αvβ3/Glut3 addicted suggests a similar portion of patients might thus be sensitive to αvβ3 antagonists. In this respect, our study reinforces the need to carefully consider whether biomarkers and drug sensitivity established using cell-based models will relate to the heterogeneity of GBM.

Identification of glucose/Glut3 addicted tumors

While we are able to determine glucose/Glut3 addiction status using cell viability assays, we also identify these cells based on a genetic phenotype. Indeed, we find that αvβ3-positive glucose/Glut3 addicted vs. non-addicted tumors can be differentiated in terms of a molecular GBM subtype. Specifically, the glucose/Glut3 addicted tumors represent a subpopulation within the Proneural and Classical subgroups and can be further delineated based on their stem cell behavior. In contrast, a subpopulation of tumors in the Mesenchymal group tend to be positive for

αvβ3/Glut3, yet surprisingly are not addicted to Glut3 and remain insensitive to αvβ3 antagonists. Thus, we estimate that 10-20% of GBM patients may show very significant responses to agents targeting αvβ3/Glut3. Indeed, a number of individual patients showed very significant, durable, yet unexplained responses to cilengitide (Nabors et al., 2007; Reardon et al., 2008). In the Mesenchymal subtype, we found an abundance of glycolytic genes and we found that all Mesenchymal patient-derived cells non-addicted to Glut3. Thus, the role of Glut3 may be negligible when other glycolytic genes are highly-expressed. Or, this subtype might be addicted to another glycolytic gene product, as suggested by Mao and co-workers (Mao P., 2013). At present, it is unclear why certain GBM tumors are, and/or become, addicted to Glut3, while others can circumvent this dependence.

Broader implications for GBM therapeutics

We report that among αvβ3/Glut3-expressing tumors, only a subpopulation is "addicted" to glucose/Glut3. Not only does this phenotype render them particularly sensitive to αvβ3 integrin inhibitors (including αv integrin-targeting cyclic peptide cilengitide or the monoclonal αvβ3 antibody LM609), but we show that such tumors are also sensitive to PAK4 as well as YAP/TAZ inhibitors which suppress αvβ3-mediated Glut3 expression in GBM cells. While the importance of YAP/TAZ in GBM aggressiveness has been reported, our new findings provide some insights in its regulation, signaling, and function within a molecularly defined GBM subpopulation.

Aside from cilengitide, there are a number of αvβ3-targeted strategies in development for GBM, including GLPG0187, a small molecule antagonist of multiple integrins including αvβ3, αvβ5, αvβ6, and α5β1 (Cirkel et al., 2016), as well as approaches that use RGD peptides for αvβ3-targeted delivery of radionuclides (Jin et al., 2017), siRNA (He et al., 2017), and chemotherapy-loaded nanoparticles or nanogels (Chen et al., 2017; Fang et al., 2017). Considering that Glut3 addiction is also a feature of GBM cancer stem cells (Flavahan et al., 2013), targeting this phenotype with an αvβ3 antagonist has the potential to eradicate the most aggressive and drug resistant subpopulation within the tumor.

Figure Legends

Figure 1. β3 levels correlate with poor survival in GBM and expression of genes involved in glucose metabolism:

(A) Hierarchical clustering of integrin β subunit expression correlated to a risk score predicting the patient survival.

(B) Kaplan-Meier analysis of Freije dataset for ITGB3 (β3) expression (n = 42 β3 low, n = 43 β3 high; P-value (p) = 0.03).

(C) Functional annotation clustering (series GSE4412) of gene set enrichment analysis based on $\beta3^{high}$ versus $\beta3^{low}$ expression. Graph shows the percent enrichment for each family of genes.

(D) Kaplan-Meier analysis of Freije dataset for SLC2A3 (Glut3), ALDOC and PFKM expression. SLC2A3 (n=42 Glut3 low, n=43 Glut3 high; P-value=0.01); ALDOC (n=43 ALDOC low, n=42 ALDOC high; P-value=0.022); PFKM (n=43 PFKM low, n=42 PFKM high; P-value=0.0007). See also figure S1, tableS1, S2 and S3.

Figure 2. The impact of integrin αvβ3 on GBM is attributed to its regulation of Glut3 expression:

(A) Immunoblots show expression of indicated proteins for U87MG, LN229 and LN18 GBM cells infected by shRNA Control (Ctrl) or shβ3. Graph shows the fold change of protein expression determined by densitometry analysis.

(B) mRNA was determined by qPCR in U87MG, LN229 and LN18 infected by shRNA Control (shCtrl) or shβ3.

(C) Relative glucose uptake in U87MG, LN229 and LN18 cells with β3 knockdown compared to control (shCtrl).

(D) Bars represent the relative lactate production in U87MG and LN229 cells with β3 knockdown compared to control (shCtrl).

(E) Effect of β3 and Glut3 knockdown on anchorage-independent growth of U87MG under high (4.5 g/l) or low (0.4 or 0.8 g/L) glucose conditions.

(F) Effect of β3 and Glut3 knockdown on tumorsphere formation of U87MG under low glucose conditions (0.4 g/L).

(G) Flow cytometry was used to quantify $\beta3^+$ versus $\beta3^-$ as well as $Glut3^+$ versus $Glut3^-$ in a growth competition assay under low glucose conditions (0.4 g/L).

(H) Effect of β3 and Glut3 knockdown on tumor growth *in vivo*: U87MG shCtrl and U87MG β3 and Glut3 shRNA. (n=15 mice per group).

(I) Graph represents the fold change of β-galactosidase positive cells versus the total cell number. Inverted microscopy images of acidic senescence-associated β-

galactosidase staining in U87MG shCtrl and U87MG β3 and Glut3 shRNA (n=5 fields counted per group).

(J) Cell-cycle analysis showing the percentage of cells in G0/G1, S, and G2/M in U87MG cells with β3 and Glut3 knockdown.

(K) Images show acidic senescence-associated β-galactosidase staining, a marker of senescence, in mice implanted with U87MG shCtrl, shβ3, shGlut3, or shβ3 with ectopic expression of Glut3.

(L) Flow cytometry was used to quantify U87MG shCtrl (GFP-) versus U87MG shβ3-Glut3+ (GFP+) in a growth competition assay.

(M) Effect of ectopic expression of Glut3 on U87MG β3 shRNA on anchorage-independence growth.

(N) Graph represents the fold change of β-galactosidase positive cells versus the total cell number. Inverted microscopy images of acidic senescence-associated β-galactosidase staining in U87MG β3 shRNA overexpressing Glut3 compare to U87MG shCtrl (n=5 fields counted per group).

(O) Effect of ectopic expression of Glut3 on tumor growth *in vivo*: U87MG shCtrl and U87MG β3 and Glut3 shRNA. (n=15 mice per group). This experiment was performed at the same time as the *in vivo* experiment shown in Figure 2H.

Data are represented as mean (n=3-5) ± SEM (*p<0.05, **p<0.01 and ***p<0.001). See also FIG. 13.

Figure 3. β3 modulates Glut3 expression through PAK4-YAP/TAZ axis:

(A) Kaplan-Meier analysis of Freije dataset for TAZ expression (n=42 for β3 low and n=43 for β3 high; P = 0.03).

(B) Immunoblots show the effect of β3 knockdown on protein expression of YAP and β3. Bars represent the fold change of protein expression determined by densitometry analysis. Data are represented as mean (n=3-5) ± SEM (*p<0.05, **p<0.01 and ***p<0.001).

(C) Graph shows the effect of β3 knockdown on mRNA expression of YAP and TAZ determined by qRT-PCR, displayed as fold change for gene expression normalized to sh-control in U87MG (n=3), LN229 (n=3) and U251 (n=2).

(D) Immunoblots show the effect of YAP/TAZ knockdown on Glut3 protein expression, and the graph shows the fold increase determined by densitometry analysis. U87MG (n=3), LN229 (n=3) and U251 (n=2).

(E) Graph shows the effect of YAP/TAZ knockdown on mRNA expression for Glut3, YAP and TAZ determined by qRT-PCR, displayed as fold change of gene expression normalized to sh-control.

(F) Acidic senescence-associated β-galactosidase staining in U87MG shCtrl versus YAP/TAZ shRNA.

(G) Effect of ectopic expression of YAP on U87MG β3 shRNA on anchorage-independent growth.

(H) Graph shows the fold change of protein expression in U87MG (n=2) and LN229 (n=2) determined by densitometry analysis.

(I) Acidic senescence-associated β-galactosidase staining in U87MG shCtrl and PAK4 siRNA (n=3).

(J) Cell-cycle analysis showing the percentage of cells in G0/G1, S, and G2/M in U87MG cells with PAK4 siRNA (n=3).

Data are represented as mean (n=2-5) ± SEM (*$p<0.05$, **$p<0.01$ and ***$p<0.001$). See also FIG. 13.

Figure 4. Integrin αvβ3 is required for Glut3 expression in patient-derived gliomaspheres that show heterogeneity in Glut3 "addiction":

(A) Representative immunoblots show expression of β3, Glut3, and TAZ in GSCs with a schematic representing the decision tree for selecting GSCs based on β3/Glut3 expression (n=2).

(B) Immunoblots show effect of β3 knockdown on expression of indicated proteins in Ge479 (n=3). Graph represents the fold change of protein expression relative to sh-control determined by densitometry analysis.

(C) Effect of glucose concentration on cell viability measured by CELLTITER-GLO™ in GSCs (n=3-5).

(D) Effect of Glut3 knockdown on cell viability measured by CELLTITER-GLO™ in GSCs (n=3-4).

(E) Expression of glycolytic, pentose phosphate and mitochondrial oxidative phosphorylation (OXPHOS) related genes were determined by qRT-PCR after β3 or Glut3 knockdown in Ge479. Bars show the fold change of gene expression normalized to sh-control. See also figure S4.

Figure 5. The mesenchymal subtype of GBM is enriched for genes involved in glycolytic pathway and sensitive to αvβ3 antagonists, YAP and PAK4 inhibitors:

(A) Enrichment analysis of glycolytic genes for the Freije dataset. Compared to other subtypes (Other sub), the Mesenchymal subtype showed high expression of Glut3, HK3, PFKP, PGK1, LDHA, Glut5 and Glut10, and no or low expression of LDHB, PFKP and ALDOC.

(B) Kaplan-Meier analysis of Freije dataset for PGK1 expression (n=42 for β3 low and n=43 for β3 high; P=0.00000007).

(C) Enrichment analysis for β3, Glut3 (also found in figure 5A), YAP and TAZ.

(D) Effect of LM609 (αvβ3 function blocking antibody) and cilengitide (cyclic peptide antagonist of αv integrins including αvβ3 and αvβ5) on cell viability measured by CELLTITER-GLO™ in GSCs.

(E) Effect of YAP inhibitor (Verteporfin) or PAK4 inhibitor (PF-03758309) on cell viability measured by CELLTITER-GLO™ in GSCs.

(F) Illustrates a schematic depicting the proposed model of Glut3 addiction in GBM. In contrast to established GBM cell lines that are uniformly β3/Glut3high and Glut3 addicted, patient-derived GSC models show heterogeneity in expression of β3/Glut3. Importantly, the population of β3/Glut3high GSC models can be further separated into Glut3 addicted vs. Glut3 non-addicted subsets based on a gene signature and/or molecular subtype. Only the β3/Glut3high GSC models with Proneural/Classical subtype markers are sensitive to inhibitors that target elements of the αvβ3/PAK4/YAP pathway.

(G) Schematically illustrates data identifying Glut3 addicted vs. Glut3 non-addicted samples using 96 signature genes. mRNA was determined by qRT-PCR (n=2) and Bio-Rad software has been used for analysis. Only the most significant genes are shown.

(H) Effect of LM609 (αvβ3 function blocking antibody) and cilengitide (cyclic peptide antagonist of αv integrins including αvβ3 and αvβ5) on cell viability measured by CELLTITER-GLO™ in GSCs (n=3-5).

(I) Effect of YAP inhibitor (Verteporfin) or PAK4 inhibitor (PF-03758309) on cell viability measured by CELLTITER-GLO™ in GSCs (n=3-5).

Data are represented as mean (n=3-5) ± SEM (*$p<0.05$, **$p<0.01$ and ***$p<0.001$). See also FIG. 16.

Figure 6. Glut3 addiction has a molecularly defined signature: Glut3 addicted vs Glut3 non-addicted samples were identified using 115 signature genes, and Figure 6 illustrates a schematic depicting an exemplary model of Glut3 addiction in GBM.

Figure 8A-B: Illustrates a table showing a list of genes that are differentially expressed based on $\beta3_{high}$ versus $\beta3_{low}$ expression for the Phillips (FIG. 8A) and Sun (FIG. 8B) datasets. Only the top 120 genes are shown, ranked from 1 to 120. Only genes with $P<0.05$ were considered for analysis.

Figure 11: Illustrates an exemplary list of genes defining Glut3 addicted vs non-addicted signature. Only genes with adjusted p-value<0.01 have been considered for analysis. Genes highlighted in blue have been validated by qRT-PCR. Numbers highlighted in orange indicate genes consistent with GBM subtypes.

Figure 12. β3 and Glut3 expression are correlated in several datasets.

Figure 13. Relative to figure 2.

(A) Effect of β3 knockdown on U87MG, LN229 and LN18 cell viability in high (4.5µg/L) vs low (1µg/L) glucose measured by Alamar blue.

(B) Histological analysis of U87MG cells with shCtrl and shGlut3. Mice bearing U87MG shβ3 do not develop tumors. Tumors were stained for haematoxylin and eosin (H&E), β3 and Glut3.

(C) Cell cycle analysis showing the percentage of cells in G0/G1, S, and G2/M for U87MG cells with knockdown of Glut1 or Glut6.

(D) Histological analysis of U87MG with shCtrl or β3 shRNA along with ectopic expression of Glut3 ($Glut3^+$). Tumors were stained for haematoxylin and eosin (H&E), β3 and Glut3.

(E) Graph represents the fold change of β-galactosidase positive cells versus the total cell number. Inverted microscopy images of acidic senescence-associated β-galactosidase staining in LN229 and LN18 Ctrl, β3 and Glut3 siRNA (n=5 fields counted per group) (n=3).

(F) Cell-cycle analysis showing the percentage of cells in G0/G1, S, and G2/M in LN229 and U251 cells with β3 and Glut3 knockdown (n=3).

(G) Flow cytometry was used to quantify γH2AX expression in LN229 cells with β3 and Glut3 knockdown. The graph shows the fold increase of γH2AX expression (n=2).

(H) Immunoblots show expression of β3 and Glut3 in U87MG with shCtrl, shGlut3 or β3 shRNA along with ectopic expression of Glut3 (Glut3+) (n=3-4). The

graph shows the fold change determined by densitometry analysis. Data are represented as mean (n=3-5) ± SEM (*p<0.05, **p<0.01 and ***p<0.001).

Figure 14. TAZ expression is correlated with poor survival and effect of YAP and PAK4 inhibitors, related to Figure 3.

(A) Kaplan-Meier analysis of TCGA dataset for WWTR1 (TAZ) expression (n = 269 β3 low, n = 2639 β3 high; P = 0.006).

(B) Effect of YAP inhibitor, Verteporfin on its target genes (CTGF and CYR61). Expression of CTGF, CYR61 and Glut3 were determined by qRT-PCR in LN229 (n=3) and U87MG (n=2). Graph shows the fold change for gene expression normalized to control.

(C) Effect of PAK4 inhibitor, PF-03758309 on the phosphorylation of PAK4 (pPAK4). Representative immunoblots show effect of PF-03758309 on expression of indicated proteins in U87MG (n=2).

(D) Graphically illustrates the effect of genetic knockdown of PAK4 on mRNA expression of Glut3, YAP, and integrin β3 for the LN229 and U87MG GBM cell lines. Graph shows the fold change for gene expression normalized to control siRNA.

(E) Representative immunoblots show expression of β3 and YAP in U87MG with shCtrl, shβ3, and shβ3 along with ectopic expression of YAP (YAP+) (n=2).

(F) Effect of PAK4 inhibitor, PF-03758309 on the phosphorylation of PAK4 (pPAK4). Representative immunoblots show effect of PF-03758309 on expression of indicated proteins in Ge479 (n=2-3).

(G) Effect of PAK4 knock down on indicated proteins in U87MG (n=2) and LN229 (n=2).

Figure 15. GSCs are tumorigenic and multipotent, related to Figure 4.

(A) Representative light micrograph showing H&E staining for Ge518 GSCs-derived tumor in immune-compromised mice (n = 3). GSCs show invasive phenotype (right panel, top) and necrotic foci (right panel, bottom).

(B) GSCs are multipotent and can differentiate to form neurons (βIIITubulin) and astrocytes (GFAP). DAPI was used for nuclear counterstaining.

(C) GSCs express cancer stem cell markers (CD133, Oct4 and Nanog). mRNA expression were determined by qPCR in all GSCs and normalized to housekeeping genes (HKGs).

(D-E) Histological analysis of brain GBM tissue array (GL805c). Bar graphs represent β3 and Glut3 expression level detected on tumor cells for 70 specimens (D). Tumors were stained for haematoxylin and eosin (H&E), β3 and Glut3 (E).

(F) β3, TAZ and YAP mRNA were determined by qPCR for Ge479 (n=3).

(G) Representative immunoblots showing expression of indicated proteins when ectopically expressed β3 is GBM6 (n=2).

(H) β3 and Glut3 expression was determined by qPCR in all GBM lines.

(I-J) Graphically illustrate data showing the effect of β3 (FIG. 15I) and Glut3 (FIG. 15J) knockdown on mRNA expression of ITGB3 (β3) and SLC2A3 (Glut3) determined by qRT-PCR, displayed as fold change for gene expression normalized to siCtrl in Ge518, Ge269 and Ge479 (n=2-4).

Figure 16. GSCs classification and enrichment analysis of glycolytic genes, relative to Figure 5 and Figure 10.

(A) mRNA was determined by qPCR in all GSCs. Several genes (listed in table 4) have been tested for each GBM subtypes. An enrichment score has been determined according to gene expression normalized to housekeeping genes.

(B) Enrichment analysis of glycolytic genes (HK2, ENO1, PFKM, GAPDH and ALDOA).

(C-F) Kaplan-Meier analysis of Freije dataset for (B) PFKL expression (n = 42 β3 low, n = 43 β3 high; P = 0.041); (C) LDHA expression (n = 42 β3 low, n = 43 β3 high; P = 0.006); (D) LDHB expression (n = 42 β3 low, n = 43 β3 high; P = 0.03) and (E) GAPDH expression (n = 42 β3 low, n = 43 β3 high; P = 0.008).

Figure 17: (A) Schematic depicting Mayo Clinic sample request. Samples were requested based on their Glut3 addicted vs. non-addicted signature, and then analyzed for cell viability in presence of cilengitide and LM609; and, (B) Effect of LM609 (αvβ3 function blocking antibody) and cilengitide (cyclic peptide antagonist of αv integrins including αvβ3 and αvβ5) on Mayo Clinic GSCs cell viability measured by CELLTITER-GLO™ (CellTiter-Glo) in GSCs (n=3-5, except n=2 for GBM150 and GBM85).

Figure 18: Illustrates a table showing Glut3 addicted vs non-addicted signature for Mayo Clinic GSCs extracted from Next Generation Sequencing (NGS) data. M = Mesenchymal, C = Classical, P = Proneural and N = Neural.

Figure 19: Illustrates the relative normalized expression of various mRNAs (as indicated in the Figure) in Glut3 addicted and Glut3 non-addicted samples, as determined by qRT-PCR (n=2), and Bio-Rad software has been used for analysis.

Figure 20: (A) Effect of LM609 (αvβ3 function blocking antibody) and cilengitide (cyclic peptide antagonist of αv integrins including αvβ3 and αvβ5) on cell viability of Ge479 knockdown for β3, PAK4 and YAP/TAZ measured by CELLTITER-GLO™ in GSCs (n=3-5). For Ge479 parental, the same data are displayed figure 5H; (B) Effect of LM609 (αvβ3 function blocking antibody) and cilengitide (cyclic peptide antagonist of αv integrins including αvβ3 and αvβ5) on cell viability of GBM6 with ectopic expression of β3 measured by CELLTITER-GLO™ in GSCs (n=3-5). For GBM6 parental, the same data are displayed figure 5H.

Figure 21: Graphically illustrates data showing the effect of Cilengitide on tumor growth. Mice bearing orthotopic Ge518 (Glut3 non-addicted) and Ge479 (Glut3 addicted) brain tumors were treated with vehicle or cilengitide (25mg kg-1; 8 mice per group). Data are represented as mean (n=3-5) ± SEM (*$p<0.05$, **$p<0.01$ and ***$p<0.001$).

Figure 22: Illustrates images of histological analysis of Ge518 and Ge479 xenografts. Ge518 (n=2-3 mice) and Ge479 (n=3-4 mice) tumors were stained for haematoxylin and eosin (H&E), β3 (brown), Glut3 (blue) and CD31 (brown). Scale bar, 50μm.

Tables

Figure 7. β3 expression consistently predicts poor survival among several GBM datasets (Freije, Lee and TCGA).

Figure 8C. List of genes differentially expressed based on $\beta3^{high}$ versus $\beta3^{low}$ expression. Only the top 180 genes are showed, ranked from 1 to 180. Only genes with a P-value <0.05 have been considered for analysis.

Figure 9. Correlation between ALDOC, PFKM and Glut3 expression with GBM patient survival among several GBM datasets (Freije, Lee and TCGA).

Figure 10. List of primers used for qRT-PCR.

Figure 11. List of genes defining Glut3 addicted vs non-addicted signature. Only genes with a P-value <0.01 have been considered for analysis.

Material and Methods:

Cell Culture. GBM cell lines were cultured in DMEM supplemented with 10% fetal bovine serum, L-glutamine and antibiotics. All cell lines were routinely tested for mycoplasma. Ge269, 479, 518, 688, 738, 835, 885, 898, 904, 970.2 were gifts from Dr. Valérie Dutoit and Dr. Pierre-Yves Dietrich to Dr E. Cosset and cultured in DMEM/F12 with Glutamax supplemented with B27 supplement and b-FGF, EGF both at 10ng/ml with antibiotics (GSC medium). GBM6 and GBM39 were gifts from Dr. Paul Mischel and cultured in GSC medium.

Chemicals. Verteporfin (YAP inhibitor) was purchased from Sigma and used at the concentration of 0.5-10μM for 24 hours. PF-03758309 (PAK4 inhibitor) was purchased from Chemietek and used at the concentration of 50nM-1000nM for 24 hours.

Isolation and cultivation of gliomaspheres and GBM cells. Isolation of glioblastoma-initiating cells was performed as described (Cosset et al., 2016). Briefly, viable fragments of high-grade human GBM were transferred to a beaker containing 0.25% trypsin in 0.1 mM EDTA (4:1) and slowly stirred at 37°C for 30-60 minutes. Dissociated cells were split and some of them were plated in 75-cm2 tissue culture flasks at 2,500-5,000 cells per cm^2) in DMEM/F-12 medium (1:1) containing N2 and B27 supplements (all from Invitrogen, Carlsbad, CA, http://www.invitrogen.com) supplemented with bFGF and EGF both at 10 ng/ml (Invitrogen). Once established, GSCs were maintained in GSC medium.

Multipotency. GSCs were plated on coverslips coated with poly-L-ornithine and were grown in DMEM complete medium for 2 weeks. Cells were fixed in 4% PFA and incubated overnight with the following antibodies: GFAP (Sigma-Aldrich) and anti-β-Tubulin (Covance). After washing, anti-mouse Alexa565 and anti-rabbit Alexa 488 were used as secondary antibodies. Nuclei were counterstained with DAPI. Image acquisition was done with a Nikon Eclipse C1 Confocal microscope.

Soft agar assay. 4000 cells were seeded in 48-well plates containing 0.3% agar/DMEM medium no glucose with 10% dialyzed FBS on top of a bottom layer of 1% agar. 200μl of additional DMEM medium with 10% dialyzed FBS ± glucose (0-4.5g/L) was added, and cells cultured for 15 days. Colonies were stained with 0.1% crystal violet/20% methanol/PBS and counted.

Cell viability assay. U87MG, LN229, and LN18 cells were seeded at 1K cells per well in black 96-well plates in DMEM medium (no glucose) with 10% dialyzed

FBS ± glucose (0-4.5g/L). Cell viability was determined by Alamar Blue dye (Life Technologies) according to manufacturer's instructions. For GSCs, cells were seeded at 10K cells per well in white 96-well low attachment plates in GSC medium ± glucose (0-4.5g/L). Viable cell numbers were evaluated using a CELLTITER-GLO™ assay kit (Promega). Each condition consisted of, at least, three replicate wells and data were expressed as relative luciferase units or as the percentage of survival of control cells.

Cell transfection (small interfering RNA and plasmids). siRNAs against β3, Glut3, Glut1, Glut6 or PAK4 were transfected using lipofectamine 2000 (Invitrogen), a final concentration of 5nM. Two non-targeting scramble siRNAs (Life Technologies) were used as control. The pcDNAGlut3 plasmid were kindly provided by Dr. Yosuke Maeda (Kumamoto University) and were transfected using Lipofectamine 3000 (Invitrogen). The transfection efficiency was monitored by qRT-PCR and/or immunoblotting. All transfections were performed according to the manufacturer's protocols.

Genetic knockdown and expression constructs. Cells were infected with shRNAs for vector control (shCtrl, Open Biosystems), Glut3 (Santa Cruz Biotechnology), β3 and PAK4 (Open Biosystems) or YAP/TAZ (provided by Dr. K-L Guan) using a lentiviral system. pLENTIβ3 was obtained by subcloning the human β3 cDNA of pENTRβ3 vector in the pLENTI expression vector. pRETROYAP was kindly provided by Dr. K-L Guan. Gene silencing or overexpressing was confirmed by either immunoblot analysis or qPCR analysis.

Tumorsphere formation assay. 1K cells were seeded in low attachment plates in DMEM with Glutamax supplemented with B27 supplement, 20ng/ml of bFGF and EGF, and glucose (0.4-4.5 g/L). The number of tumorspheres was counted after 10-15 days.

Cell cycle and cell synchronization. Cells were synchronized by double-thymidine treatment. Medium was replaced with thymidine-free medium allowing cells to re-enter the cell cycle. After transfection, 100K cells were fixed in cold 70% ethanol, incubated overnight at -20°C, stained using propidium iodide, and subjected to flow cytometry analysis for cell cycle.

SA-β-galactosidase staining. 20K cells were seeded in DMEM complete medium for 5 days and stained with the senescence SA-β-galactosidase staining kit (Cell Signaling) according to the manufacturer's protocol.

Competition mixing assay. Cells co-cultured were seeded at a 1:1 ratio and maintained in DMEM complete medium or low glucose for 7 days. At Day 0 and Day 7, cells were analyzed by flow cytometry for stable expression of GFP or RFP/YFP.

Glucose uptake assay. Cells were seeded in a 6well plates at a density of 300,000 cells per well in DMEM complete medium. On the next day, the cells were washed twice in PBS and incubated in serum-glucose free medium for 2 hours. The medium was then removed, the cells were incubated for 1 hour in DMEM medium with 1g/L of glucose. The uptake was determined by using Glucose Assay Kit (Eton Bioscience) according to the manufacturer's protocol.

Lactate production assay. Cells were seeded in a 6well plates at a density of 300,000 cells per well in DMEM complete medium. On the next day, the cells were washed twice in PBS and incubated in serum-glucose free medium for 2 hours. The medium was then removed, the cells were incubated for 1 hour in DMEM medium with 1g/L of glucose. The uptake was determined by using L-Lactate assay Kit (Eton Bioscience) according to the manufacturer's protocol.

Reverse transcription quantitative PCR (RT-qPCR). Isolation of total RNA and miRNAs were performed by using RNeasy kit from Qiagen according to the manufacturer's instructions. RNA concentration was determined using a spectrometer. 500ng of total RNA was used to synthesize cDNA using a TAKARA kit according to manufacturer's protocol. When not available, primer sequences were designed using Invitrogen primer design and primer3 tools, and are summarized in supplementary Table 4. Real-time PCR was performed using SYBR Green reagent and a Bio-Rad system (Applied Biosystems) according the manufacturer's instructions. Efficacy tests have been performed, and all primers have been validated prior utilization. The relative level of each sample was normalized to, at least, two housekeeping genes (EEF1A1, ALAS1, Cyclophilin A and/or Tuba2). RT-PCR reactions were carried out in technical and biological duplicates or triplicates, and the average cycle threshold (CT) values were determined.

GBM subtyping. GSCs gene expression has been assessed by qRT-PCR. All primers are listed in Supplemental Table 4 according to Proneural, Neural, Classical and Mesenchymal subtypes. Genes involved in the glycolytic, Pentose Phosphate Pathway (PPP) and mitochondrial oxidative phosphorylation (OXPHOS) pathways are listed as well.

Immunoblotting. Proteins were extracted in RIPA buffer and quantified using the Pierce BCA kit (Thermo Fisher). 10-30µg of protein was boiled in NuPage buffer (Thermo Fisher) and loaded onto a denaturing SDS-polyacrylamide gel (10%), transferred to PVDF membranes and blotted with anti-mouse or -rabbit HRP-conjugated secondary antibodies (Bio-Rad). The following antibodies were used for immunoblotting: β3 (Cell Signaling), Glut3 (Santa Cruz Biotechnology), YAP (Santa Cruz) YAP-XP (cell signaling), TAZ (Cell Signaling), PAK4 and pPAK4 (Cell Signaling), and Vinculin and β-actin (Sigma-Aldrich) as loading controls.

Histological analysis (Immunochemistry and Immunofluorescence). For immunohistochemical staining of formalin-fixed paraffin-embedded tissues, antigen retrieval was performed in citrate buffer at pH 6.0 and 95°C for 20 minutes. Sections were blocked then incubated overnight at 4°C in primary antibody integrin αvβ3 (LM609) or β3 (Cell signaling), Glut3 (Santa Cruz Biotechnology), GFAP (cell signaling), βIIITubulin (Sigma-Aldrich), Nestin (Fisher Scientific), CD133 (Miltenyi Biotech) followed by biotin-conjugated anti-rabbit IgG and an avidin-biotin peroxidase detection system with 3,3'-diaminobenzidine substrate (Vector) then counterstained with hematoxylin. A Nikon Eclipse C1 Confocal microscope was used for imaging.

In vivo experiments. All experiments were performed according to the protocol S05018 and approved by the UCSD Institutional Animal Care and Use Committee. The number of mice used for each experiment is indicated in the corresponding figures.

Orthotopic brain tumor xenografts. Intracranial transplantation of U87MG or GSC (Ge518 and Ge479) into 6-8-week-old nu/nu nude immunocompromised mice (Charles River Labs) was performed in accordance with the UCSD Institutional Animal Care and Use Committee. U87MG cells bearing β3, Glut3 shRNA or shβ3 ectopically expressing Glut3 as well as shRNA control (15 mice per group) were orthotopically transplanted following washing and resuspension in PBS. Ge479 and Ge518 were orthotopically transplanted following washing and resuspension in DMEM/F12. Mice were treated with vehicle (PBS) or cilengitide (10mg kg^{-1} or 30mg kg^{-1}; 8 mice per group) five days per week. Briefly, with a stereotaxic frame (Stoelting Co.), a small burr hole was made in the skull 2 mm anterior and 2 mm lateral to the bregma. A 31-gauge Hamilton needle/syringe was inserted 3 mm, and 0.25 µl/minute was dispensed (10^5 tumor cells in 2 µl media). A total of 1 x 10^5 and 3

x 10^5 cells in 2µl was injected respectively for U87MG cells and GSCs respectively. Animals were monitored daily and those exhibiting signs of morbidity and/or development of neurological symptoms were euthanized.

Analysis of microarray data. The files for expression analysis were downloaded from GEO with the accession number GSE4412. Only the data obtained with Affymetrix Human Genome U133A Array (GPL96) was used. The sample description files were downloaded from the supplementary material of the article titled *"Brain tumor initiating cells adapt to restricted nutrition through preferential glucose uptake"* (http://goo.gl/mCnVPA). Microarray data was analyzed with R version 3.3.1 software. Differential expression for β3 and Glut3 was performed with the limma package (version 3.28.21) and GBM subgroup enrichment calculations were performed using hypergeometric probability distribution (R function dhyper). The enrichment significance values were adjusted using the Benjamini-Hochberg method for each gene independently. Panther analysis was used for graphing differential gene expression analysis (Mi et al., 2016). MEM (Multi Experiment Matrix) was used for correlation between Glut3 and β3 expression (Adler et al., 2009). The StDev threshold for Glut3 was set to 0.29. Distance was measured by both Pearson and Spearman's rank correlation distance, and the betaMEM method was used to determine the P-value. Survexpress was used to generate Kaplan-Meier curves of β3, Glut3, ALDOC, PFKM and TAZ from Freije (GSE4412, GPL96, 85 samples), Lee (GSE13041, GPL96, 218 samples) and The Cancer Genoma Atlas (TCGA) (GBM-LGG and GBM, June 2016, 660 and 518 samples respectively) datasets. TCGA dataset has been harvested for generating the hierarchical cluster for all ITGBs and survival months has been used as censor with Cox survival analysis (Aguirre-Gamboa et al., 2013).

Statistics. All statistical analyses were performed using the Student paired t test. We also performed an analysis of variance applying a bivariate analysis. Significant P-values ($p<0.05$) is indicated in the text of the results and/or figure legends. Data are representative of results obtained in the indicated number of independent experiments. For *in vivo* experiments, all statistical analyses were carried out using PRISM™ software (GRAPHPAD™, GraphPad™). Chi-squared tests or *t*-tests were used to calculate statistical significance.

References

Adler, P., et al. (2009). Mining for coexpression across hundreds of datasets using novel rank aggregation and visualization methods. Genome Biol *10*, R139.

Aguirre-Gamboa, et al. (2013). SurvExpress: an online biomarker validation tool and database for cancer gene expression data using survival analysis. PLoS ONE *8*, e74250.

Birsoy, K., et al. (2014). Metabolic determinants of cancer cell sensitivity to glucose limitation and biguanides. Nature *508*, 108-112.

Boado, R. J., et al., (1994). Gene expression of GLUT3 and GLUT1 glucose transporters in human brain tumors. Brain Res Mol Brain Res *27*, 51-57.

Brennan, C. W., *et al.* (2013). The somatic genomic landscape of glioblastoma. Cell *155*, 462-477.

Chen, W., et al, (2017). Cyclo(RGD)-Decorated Reduction-Responsive Nanogels Mediate Targeted Chemotherapy of Integrin Overexpressing Human Glioblastoma In Vivo. Small (Weinheim an der Bergstrasse, Germany) *13*.

Cheresh, D. A. (1987). Human endothelial cells synthesize and express an Arg-Gly-Asp-directed adhesion receptor involved in attachment to fibrinogen and von Willebrand factor. Proc Natl Acad Sci U S A *84*, 6471-6475.

Cirkel, G. A., *et al.* (2016). A dose escalating phase I study of GLPG0187, a broad spectrum integrin receptor antagonist, in adult patients with progressive high-grade glioma and other advanced solid malignancies. Investigational new drugs *34*, 184-192.

Cosset, E., et al. (2016). Human tissue engineering allows the identification of active miRNA regulators of glioblastoma aggressiveness. Biomaterials *107*, 74-87.

Desgrosellier, J. S., and Cheresh, D. A. (2010). Integrins in cancer: biological implications and therapeutic opportunities. Nat Rev Cancer *10*, 9-22.

Desgrosellier, J. S., et al. (2014). Integrin alphavbeta3 drives slug activation and stemness in the pregnant and neoplastic mammary gland. Dev Cell *30*, 295-308.

Fang, Y., Jiang, et al. (2017). Targeted glioma chemotherapy by cyclic RGD peptide-functionalized reversibly core-crosslinked multifunctional poly(ethylene glycol)-b-poly(epsilon-caprolactone) micelles. Acta biomaterialia *50*, 396-406.

Flavahan, W. A., *et al.* (2013). Brain tumor initiating cells adapt to restricted nutrition through preferential glucose uptake. Nat Neurosci *16*, 1373-1382.

Franovic, A., et al (2015). Glioblastomas require integrin alphavbeta3/PAK4 signaling to escape senescence. Cancer Res *75*, 4466-4473.

Freije, W. A., et al (2004). Gene expression profiling of gliomas strongly predicts survival. Cancer Res *64*, 6503-6510.

Gladson, C. L., et al. (1991). Glioblastoma expression of vitronectin and the alpha v beta 3 integrin. Adhesion mechanism for transformed glial cells. J Clin Invest *88*, 1924-1932.

He, S., et al. (2017). A tumor-targeting cRGD-EGFR siRNA conjugate and its anti-tumor effect on glioblastoma in vitro and in vivo. Drug delivery *24*, 471-481.

Jin, Z. H., *et al.* (2017). 67Cu-Radiolabeling of a multimeric RGD peptide for alphaVbeta3 integrin-targeted radionuclide therapy: stability, therapeutic efficacy, and safety studies in mice. Nuclear medicine communications *38*, 347-355.

Lathia, J. D., et al. (2015). Cancer stem cells in glioblastoma. Genes Dev *29*, 1203-1217.

Mason, W. P. (2015). End of the road: confounding results of the CORE trial terminate the arduous journey of cilengitide for glioblastoma. Neuro-oncology *17*, 634-635.

Mi, H., et al. (2016). PANTHER version 10: expanded protein families and functions, and analysis tools. Nucleic Acids Research *44*, D336-D342.

Moroishi, T., Hansen, C. G., and Guan, K.-L. (2015). The emerging roles of YAP and TAZ in cancer. Nat Rev Cancer *15*, 73-79.

Nabors, L. B., *et al.* (2007). Phase I and correlative biology study of cilengitide in patients with recurrent malignant glioma. J Clin Oncol *25*, 1651-1657.

Noushmehr, H., *et al.* (2010). Identification of a CpG island methylator phenotype that defines a distinct subgroup of glioma. Cancer Cell *17*, 510-522.

Nutt, C. L., *et al.* (2003). Gene expression-based classification of malignant gliomas correlates better with survival than histological classification. Cancer Res *63*, 1602-1607.

Paolillo, M., Serra, M., and Schinelli, S. (2016). Integrins in glioblastoma: Still an attractive target? Pharmacol Res *113*, 55-61.

Patronas, N. J., et al. (1985). Prediction of survival in glioma patients by means of positron emission tomography. J Neurosurg *62*, 816-822.

Phillips, H. S., *et al.* (2006). Molecular subclasses of high-grade glioma predict prognosis, delineate a pattern of disease progression, and resemble stages in neurogenesis. Cancer Cell *9*, 157-173.

Reardon, D. A., *et al.* (2008). Randomized phase II study of cilengitide, an integrin-targeting arginine-glycine-aspartic acid peptide, in recurrent glioblastoma multiforme. J Clin Oncol *26*, 5610-5617.

Seguin, L., *et al.* (2014). An integrin beta(3)-KRAS-RalB complex drives tumour stemness and resistance to EGFR inhibition. Nat Cell Biol *16*, 457-468.

Stupp, R., *et al.* (2014). Cilengitide combined with standard treatment for patients with newly diagnosed glioblastoma with methylated MGMT promoter (CENTRIC EORTC 26071-22072 study). The lancet oncology *15*, 1100-1108.

Stupp, R., *et al.* (2005). Radiotherapy plus Concomitant and Adjuvant Temozolomide for Glioblastoma. New England Journal of Medicine *352*, 987-996.

Verhaak, R. G., *et al.* (2010). Integrated genomic analysis identifies clinically relevant subtypes of glioblastoma characterized by abnormalities in PDGFRA, IDH1, EGFR, and NF1. Cancer Cell *17*, 98-110.

Wang, W., et al. (2015). AMPK modulates Hippo pathway activity to regulate energy homeostasis. Nat Cell Biol *17*, 490-499.

Weis, S. M., and Cheresh, D. A. (2011). Tumor angiogenesis: molecular pathways and therapeutic targets. Nature Medicine *17*, 1359-1370.

Weller, M., *et al.* (2016). Cilengitide in newly diagnosed glioblastoma: biomarker expression and outcome. Oncotarget *advance online*.

A number of exemplary embodiments have been described. Nevertheless, it will be understood that various modifications may be made without departing from the spirit and scope of the invention. Accordingly, other embodiments are within the scope of the following claims.

WHAT IS CLAIMED IS:

1. A method for determining whether a tumor or a cancer cell will be sensitive to (or can be killed or induced to senescence by) a treatment targeting the integrin avb3 (αvβ3) pathway, comprising:

(a) determining or having determined whether the tumor or the cancer cell expresses both avb3+ and Glut3+, or determining whether the tumor or the cancer cell is a avb3+/Glut3+ tumor or cancer cell, and

(b) determining or having determined whether the tumor or the cancer cell is Glut-3 addicted,

wherein optionally determining or having determined whether the tumor or the cancer cell is Glut-3 addicted comprises:

(i) determining or having determined whether the tumor or the cancer cell expresses a marker (e.g., an mRNA or a protein) consistent with a Classical or Proneural subtype, e.g., expresses a marker consistent with the Classical or Proneural molecular subtypes of GBM,

wherein optionally the marker consistent with a Classical or Proneural subtype comprises an *EGFR*, *GLI1*, *NES*, *DLL3* or *OLIG2* gene transcript or an EGFR, GLI1, NES, DLL3 or OLIG2 protein, or

(ii) determining or having determined whether the tumor or the cancer cell expresses (e.g., expresses mRNA or protein) consistent with a Glut3 addicted gene signature,

wherein optionally gene expression consistent with a Glut3 addicted gene signature comprises gene expression consistent with a high (a Glut3 addicted signature) or low (a Glut3 non-addicted signature) expression of at least one (one or more) of the genes, or 2, 3, 4, 5, 6, 7, 8, 9, 10, 11, 12, 13, 14, 15, 16, 17, 18, 19, 20, 21, 22, 23, 24, 25, 26, 27, 28, 29 or all 30 of the genes, as listed in Figure 11 or Figure 23, or optionally all of the genes listed in Figure 11 or Figure 23,

wherein if a tumor or a cancer cell expresses both avb3+ and Glut3+ and is Glut-3 addicted, the tumor or the cancer cell will be sensitive to (will be substantially sensitive to) or will be successfully treated by (e.g., can be killed or induced to senescence by) the treatment targeting the integrin avb3 (αvβ3) pathway,

wherein optionally the tumor or cancer cell is a glioblastoma (GBM) tumor or cell, a melanoma tumor or melanoma cell or a primitive neuroectodermal tumor (PNET) or PNET cell.

2. The method of claim 1, wherein the treatment targeting the integrin avb3 (αvβ3) pathway targets avb3, Glut3, PAK4, or YAP/TAZ.

3. The method of claim 2, wherein the treatment comprises administering or having administered to an individual in need thereof cilengitide (or, 2-[(2*S*,5*R*,8*S*,11*S*)-5-benzyl-11-{3-[(diaminomethylidene)amino]propyl}-7-methyl-3,6,9,12,15-pentaoxo-8-(propan-2-yl)-1,4,7,10,13-pentaazacyclopentadecan-2-yl]acetic acid).

4. The method of any of the preceding claims, wherein the determining or having determined if the tumor or the cancer cell expresses both avb3+ and Glut3+ comprises determining if the tumor or the cancer cell expresses both an avb3+ and a Glut3+ protein, or both an avb3+ and a Glut3+ message (mRNA, transcript), or both an avb3+ and a Glut3+ protein and message,

and optionally the determining or having determined if the tumor or the cancer cell expresses both an avb3+ and a Glut3+ protein is by a method comprising use of antibodies that specifically bind to a protein of the integrin avb3 pathway, optionally comprising an avb3, Glut3, PAK4, or YAP/TAZ binding antibody (an antibody that specifically binds avb3, Glut3, PAK4, or YAP/TAZ),

and optionally the determining or having determined if the tumor or the cancer cell expresses both an avb3+ and a Glut3+ message (mRNA, transcript) is by a method comprising use of a polymerase chain reaction (PCR) (optionally comprising use of primers capable of amplifying an avb3+ and a Glut3+ message); or, gene expression profiling, an array, or a probe hybridization to a message, optionally a Northern blot (optionally comprising use of primers capable of specifically hybridizing to) an avb3+ and a Glut3+ message).

5. The method of any of the preceding claims, wherein the determining or having determined if the tumor or the cancer cell expresses a marker consistent with a Classical or Proneural subtype or has a Glut3 addicted gene/molecular signature,

optionally expressing at least one of the genes at levels as listed in Figure 11 or Figure 23, comprises determining or having determined if the tumor or the cancer cell expresses an mRNA and/or a protein consistent with a Classical or a Proneural subtype, or has a Glut3 addicted gene/molecular signature, optionally expressing an mRNA or protein from a gene as listed in Figure 11 or Figure 23,

and optionally the determining or having determined if the tumor or the cancer cell expresses a protein consistent with a Classical or a Proneural subtype, or has a Glut3 addicted gene/molecular signature, optionally expressing a protein from a gene as listed in Figure 11 or Figure 23, is by a method comprising use of antibodies that specifically bind to a protein consistent with a Classical or a Proneural subtype, or a protein from a gene as listed in Figure 11 or Figure 23,

and optionally the determining or having determined if the tumor or the cancer cell expresses a message (mRNA, transcript) consistent with a Classical or a Proneural subtype, or has a Glut3 addicted gene/molecular signature, optionally expressing an mRNA from a gene as listed in Figure 11 or Figure 23, is by a method comprising use of a polymerase chain reaction (PCR) (optionally comprising use of primers capable of amplifying a message (mRNA, transcript) consistent with a Classical or a Proneural subtype, or has a Glut3 addicted gene/molecular signature, optionally an mRNA from a gene as listed in Figure 11 or Figure 23); or, by gene expression profiling, optionally by using an array, or optionally by using a probe hybridization to a message of interest, optionally a Northern blot (optionally comprising use of primers capable of specifically hybridizing to) a message (mRNA, transcript) consistent with a Classical or a Proneural subtype, or optionally an mRNA from a gene as listed in Figure 11 or Figure 23.

6. The method of any of the preceding claims, wherein the determining or having determined if the tumor or the cancer cell expresses both avb3+ and Glut3+ comprises taking or isolating a cell or a sample of cells, optionally cancer cells or tumors cells, from a patient, optionally a patient tentatively diagnosed or definitely diagnosed with the tumor or cancer, optionally GBM, and determining if the cell or sample of cells expresses both avb3+ and Glut3+ and is Glut-3 addicted.

7. A method for treating or ameliorating, or killing, or inducing into senescence, a tumor or a cancer cell in a patient or *ex vivo*, wherein optionally the

tumor or cancer cell is a glioblastoma (GBM) tumor or a GBM cancer cell, or a melanoma or a primitive neuroectodermal tumor (PNET), or treating or ameliorating a tumor or cancer, optionally GBM, a melanoma or a primitive neuroectodermal tumor (PNET), in an individual in need thereof, comprising:

(a) determining or having determined whether the tumor or cancer, optionally a glioblastoma (GBM) tumor or a GBM cancer cell, will be sensitive to a treatment targeting the integrin avb3 (αvβ3) pathway using a method of claim 1, and

(b) if the method of step (a) determines, or has had determined, that the tumor or cancer, optionally a glioblastoma (GBM) tumor or a GBM cancer cell, will be sensitive to a treatment targeting the integrin avb3 (αvβ3) pathway, administering or having administered the treatment targeting the integrin avb3 (αvβ3) pathway to an individual in need thereof, or,

administering or having administered the treatment to the tumor or cancer cell, optionally to a glioblastoma (GBM) tumor or GBM cancer cell, if the tumor or cancer cell is derived from or isolated from the individual in need thereof, or if the tumor or cancer cell is determined to be sensitive to a treatment targeting the integrin avb3 (αvβ3) pathway using a method of claim 1 (e.g., if the glioblastoma (GBM) tumor or the GBM cancer cell is found to express both avb3+ and Glut3+ and is Glut-3 addicted).

8. The method of claim 7, wherein the treatment targets avb3, Glut3, PAK4, or YAP/TAZ.

9. The method of claim 7, wherein the treatment comprises administering or having administered to an individual in need thereof cilengitide (or, 2-[(2*S*,5*R*,8*S*,11*S*)-5-benzyl-11-{3-[(diaminomethylidene)amino]propyl}-7-methyl-3,6,9,12,15-pentaoxo-8-(propan-2-yl)-1,4,7,10,13-pentaazacyclopentadecan-2-yl]acetic acid).

.

FIG. 1A

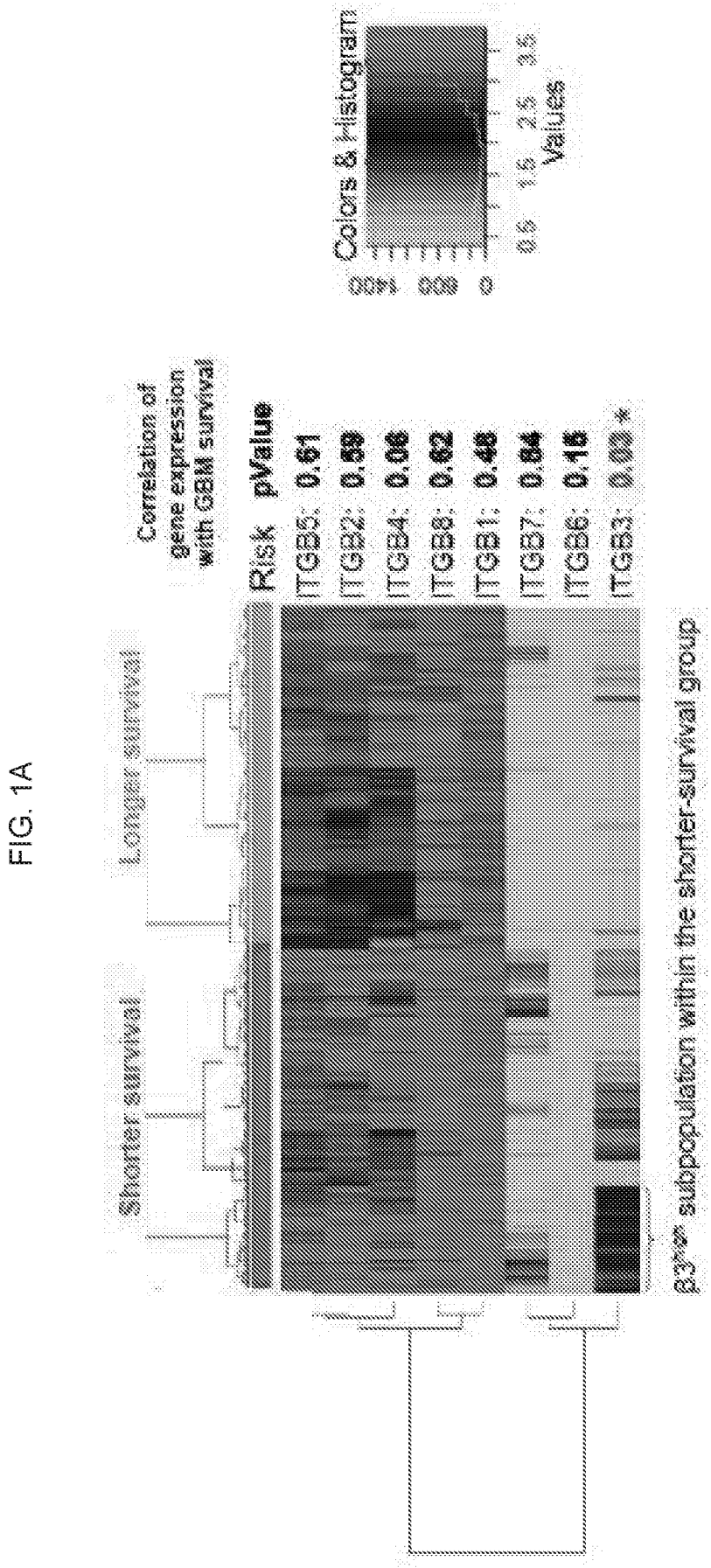
Colors & Histogram
0.5
1.5
2.5
3.5
Values
Shorter survival
Longer survival
Correlation of gene expression with GBM survival
Risk
pValue
ITGB5: 0.61
ITGB2: 0.59
ITGB4: 0.06
ITGB8: 0.62
ITGB1: 0.48
ITGB7: 0.84
ITGB6: 0.16
ITGB3: 0.03 *
β3+ subpopulation within the shorter-survival group

FIG. 1B-D

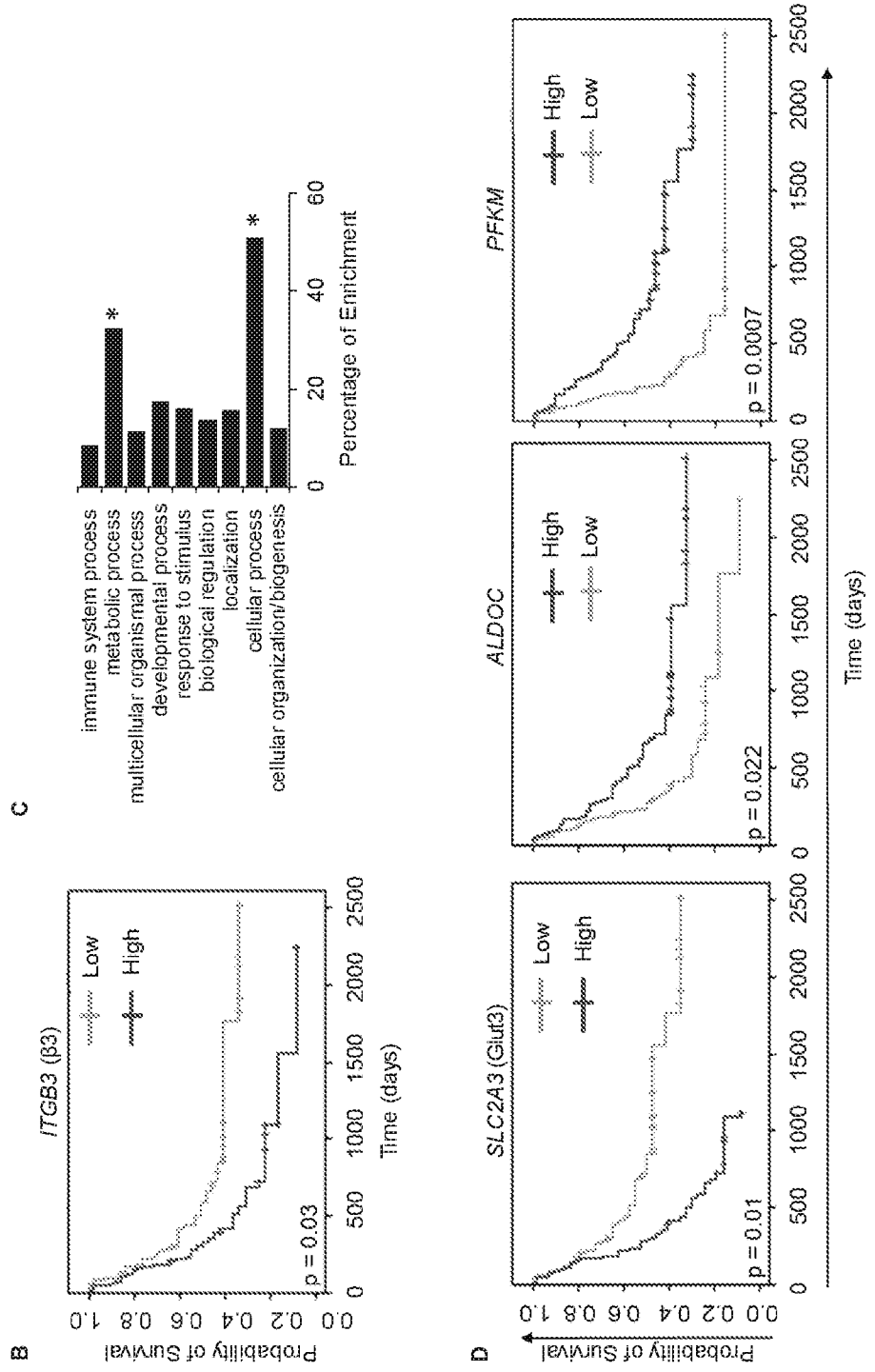
B
ITGB3 (β3)
Low
High
p = 0.03
Probability of Survival
0.0 0.2 0.4 0.6 0.8 1.0
0 500 1000 1500 2000 2500
Time (days)
C
immune system process
metabolic process
multicellular organismal process
developmental process
response to stimulus
biological regulation
localization
cellular process
cellular organization/biogenesis
*
*
0 20 40 60
Percentage of Enrichment
D
SLC2A3 (Glut3)
ALDOC
PFKM
Low
High
p = 0.01
p = 0.022
p = 0.0007
Probability of Survival
0.0 0.2 0.4 0.6 0.8 1.0
0 500 1000 1500 2000 2500
Time (days)

FIG. 2A-H

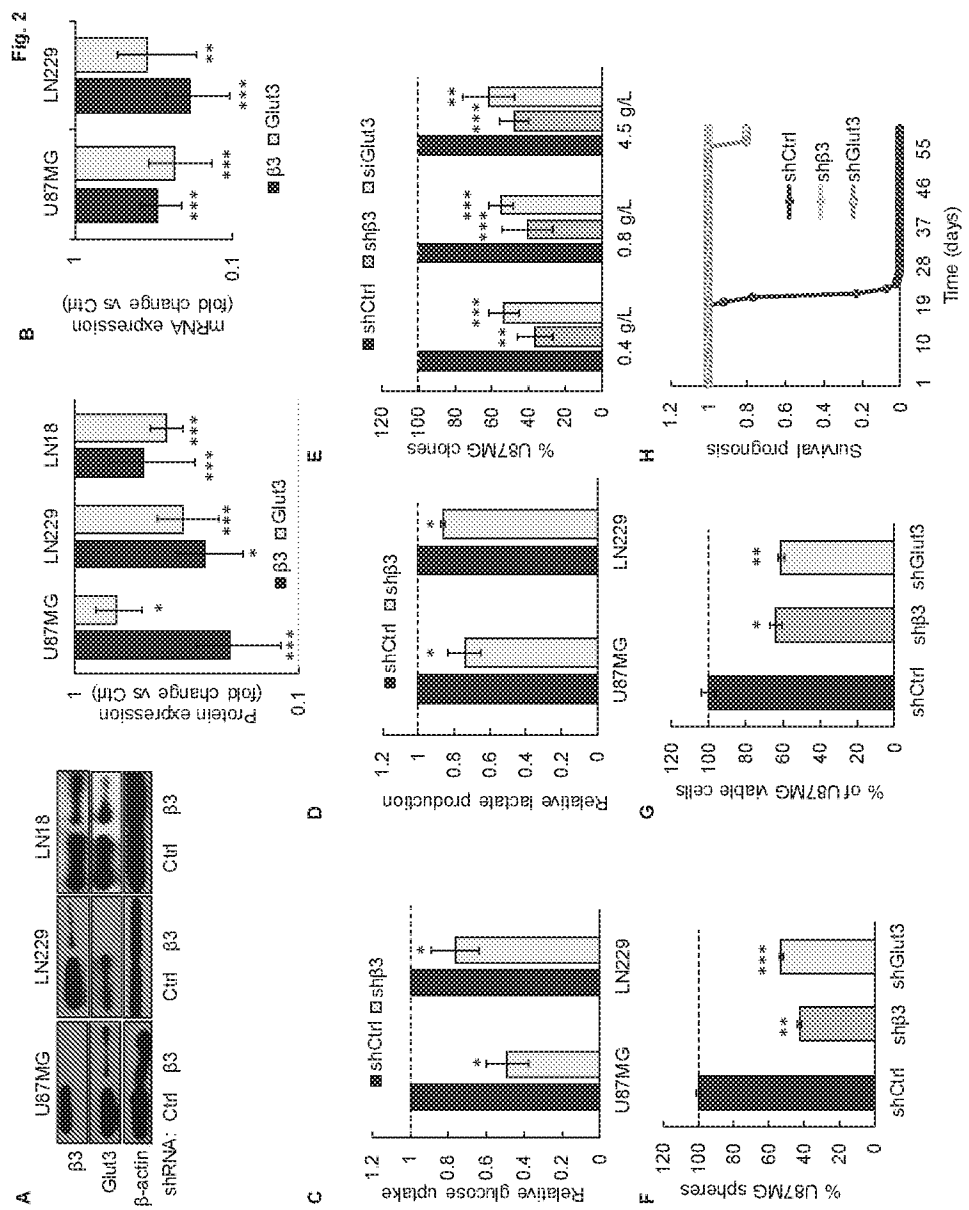
Fig. 2
A
β3
Glut3
β-actin
shRNA: Ctrl β3 Ctrl β3 Ctrl β3
U87MG LN229 LN18
B
mRNA expression (fold change vs Ctrl)
U87MG LN229 LN18
β3 Glut3
C
Relative glucose uptake
shCtrl shβ3
U87MG LN229
D
Relative lactate production
shCtrl shβ3
U87MG LN229
E
Protein expression (fold change vs Ctrl)
U87MG LN229 LN18
β3 Glut3
F
% U87MG spheres
shCtrl shβ3 shGlut3
G
% of U87MG viable cells
shCtrl shβ3 shGlut3
H
Survival prognosis
shCtrl
shβ3
shGlut3
Time (days)
% U87MG clones
shCtrl shβ3 siGlut3
0.4 g/L 0.8 g/L 4.5 g/L

FIG. 2I-O

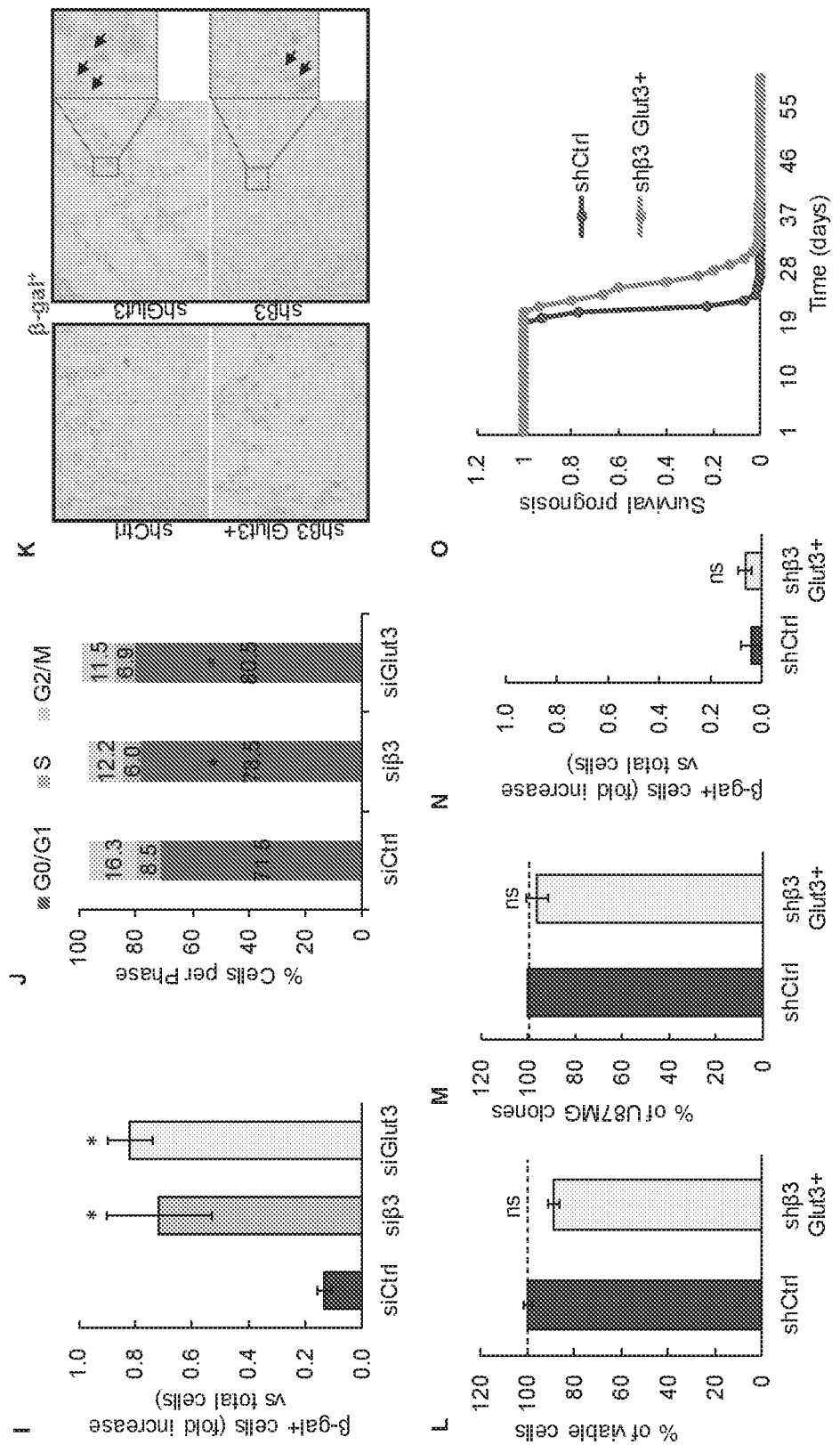
I
β-gal+ cells (fold increase vs total cells)
siCtrl
siβ3
siGlut3
J
% Cells per Phase
G0/G1
S
G2/M
16.3
8.5
12.2
6.8
11.5
6.6
siCtrl
siβ3
siGlut3
K
β-gal+
shβ3 Glut3+
shCtrl
shβ3
shGlut3
L
% of viable cells
ns
shCtrl
shβ3 Glut3+
M
% of U87MG clones
ns
shCtrl
shβ3 Glut3+
N
β-gal+ cells (fold increase vs total cells)
ns
shCtrl
shβ3 Glut3+
O
Survival prognosis
shCtrl
shβ3 Glut3+
Time (days)

FIG. 3A-G

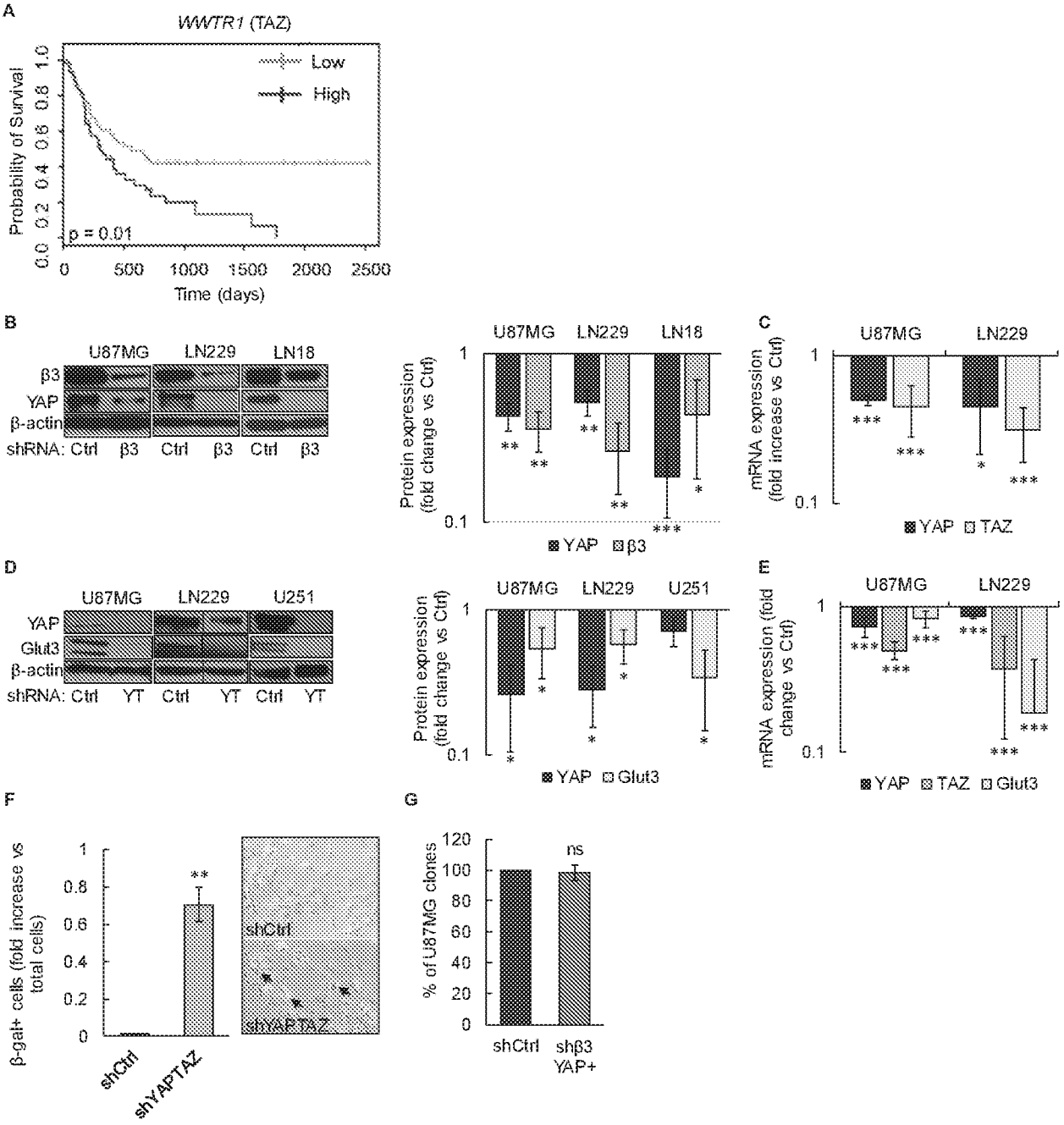
A
WWTR1 (TAZ)
Low
High
Probability of Survival
p = 0.01
Time (days)
B
U87MG LN229 LN18
β3
YAP
β-actin
shRNA: Ctrl β3 Ctrl β3 Ctrl β3
Protein expression (fold change vs Ctrl)
YAP β3
C
mRNA expression (fold increase vs Ctrl)
YAP TAZ
D
U87MG LN229 U251
YAP
Glut3
β-actin
shRNA: Ctrl YT Ctrl YT Ctrl YT
YAP Glut3
E
YAP TAZ Glut3
F
β-gal+ cells (fold increase vs total cells)
shCtrl
shYAPTAZ
G
% of U87MG clones
ns
shCtrl
shβ3 YAP+

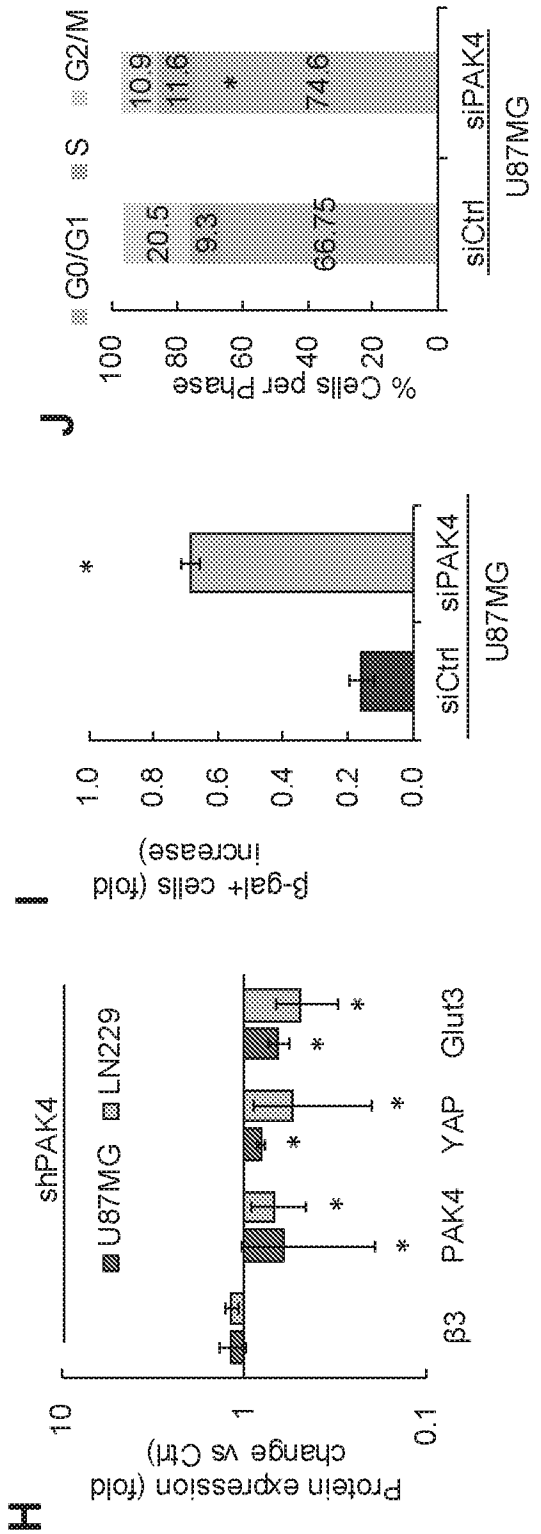
H
Protein expression (fold change vs Ctrl)
10
1
0.1
shPAK4
U87MG
LN229
β3
PAK4
YAP
Glut3
I
β-gal+ cells (fold increase)
1.0
0.8
0.6
0.4
0.2
0.0
siCtrl
siPAK4
U87MG
J
% Cells per Phase
100
80
60
40
20
0
G0/G1
S
G2/M
20.5
9.3
66.75
10.9
11.6
74.6
siCtrl
siPAK4
U87MG

FIG. 3H-J

FIG. 4A-D

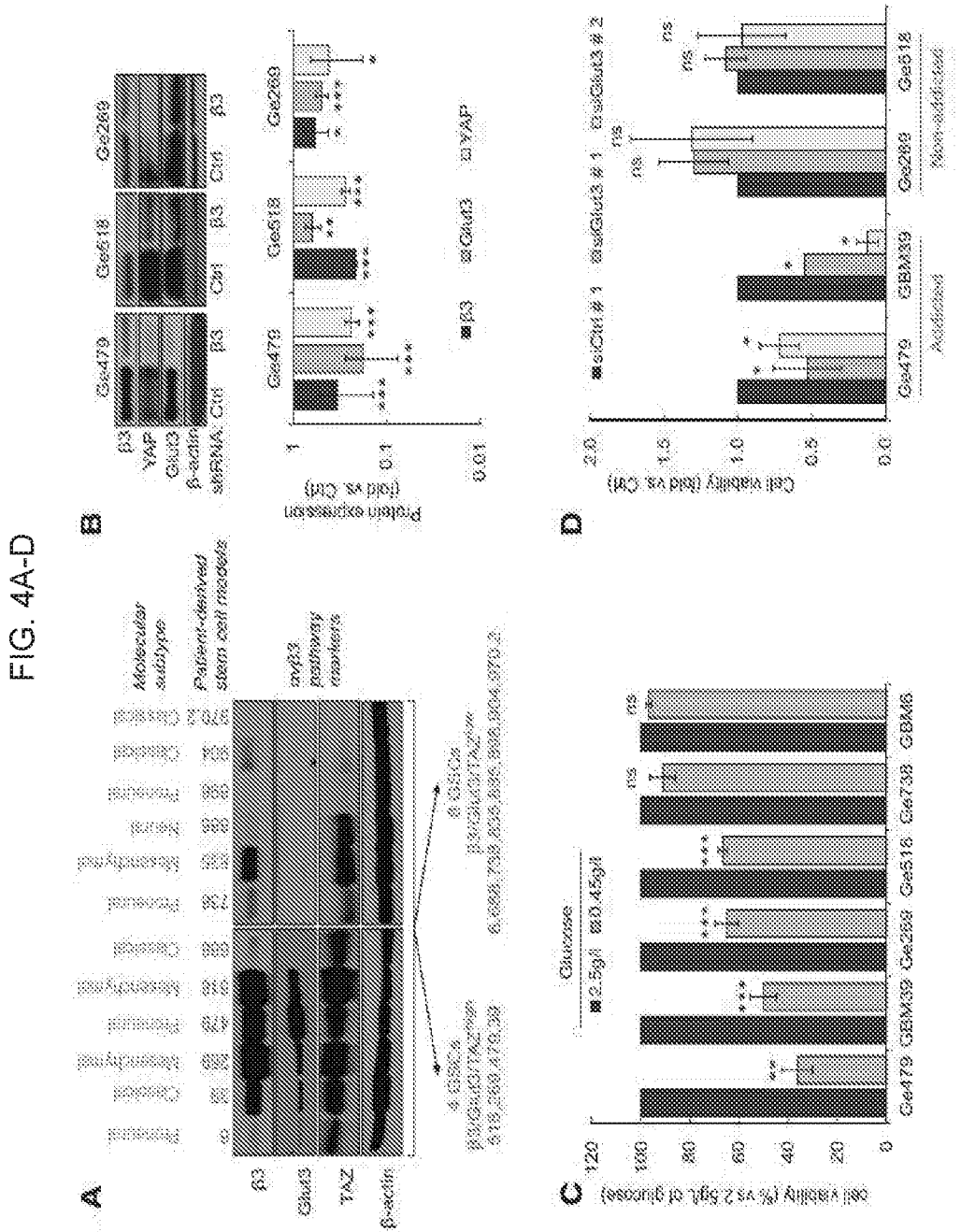
A
Molecular subtype
Patient-derived stem cell models
αvβ3 pathway markers
β3
Glut3
TAZ
β-actin
B
Ge479
Ge518
Ge269
siRNA: Ctrl β3 Ctrl β3 Ctrl β3
β3
YAP
Glut3
β-actin
Protein expression (fold vs. Ctrl)
Ctrl
β3
Glut3
YAP
C
Glucose
2.5g/l
0.45g/l
Cell viability (% vs 2.5g/L of glucose)
Ge479 GBM39 Ge269 Ge518 Ge738 GBM8
D
siCtrl # 1
siGlut3 # 1
siGlut3 # 2
Cell viability (fold vs. Ctrl)
Additives
Non-additives

FIG. 4E

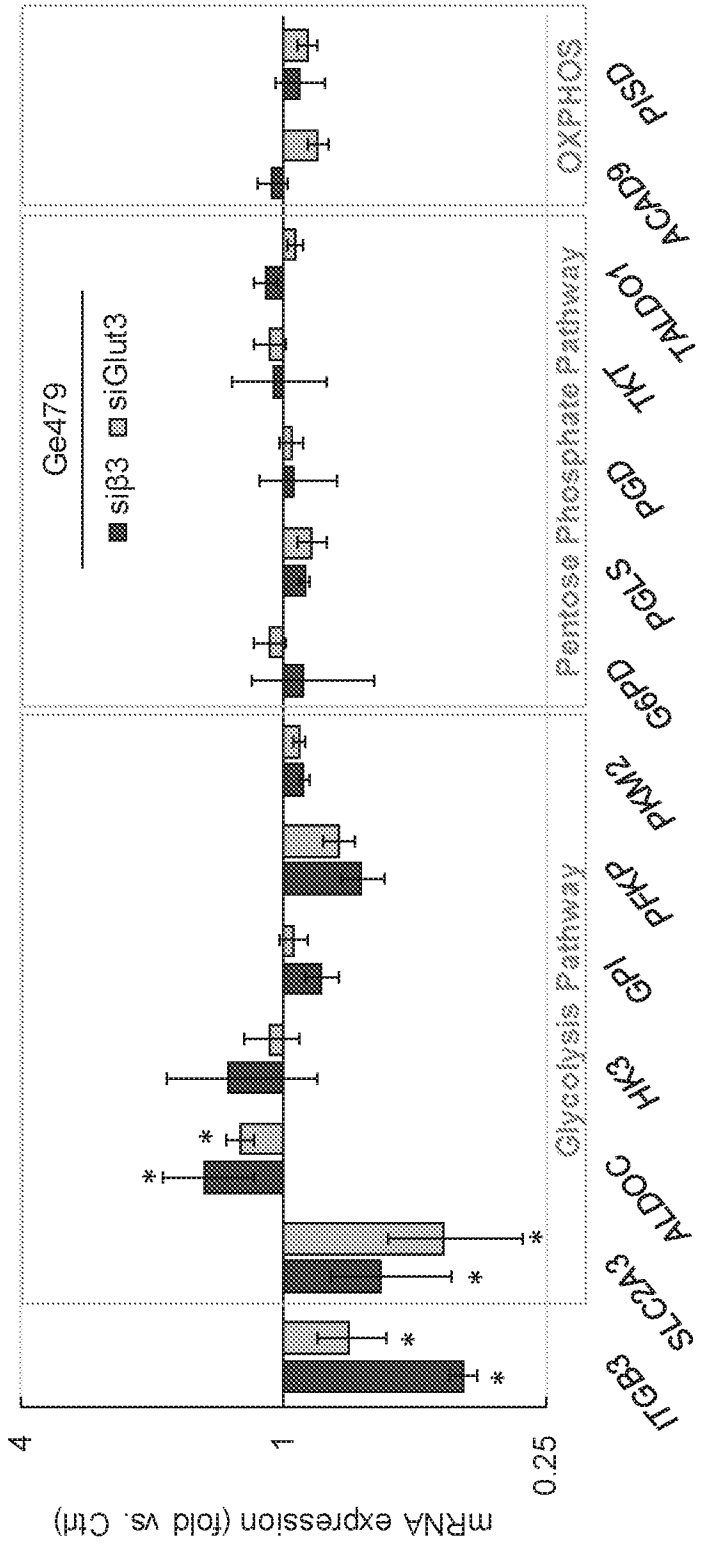
E
mRNA expression (fold vs. Ctrl)
4
1
0.25
Ge479
siβ3
siGlut3
Glycolysis Pathway
Pentose Phosphate Pathway
OXPHOS
ITGB3
SLC2A3
ALDOC
HK3
GPI
PFKP
PKM2
G6PD
PGLS
PGD
TKT
TALDO1
ACAD9
PISD

FIG. 5A-C

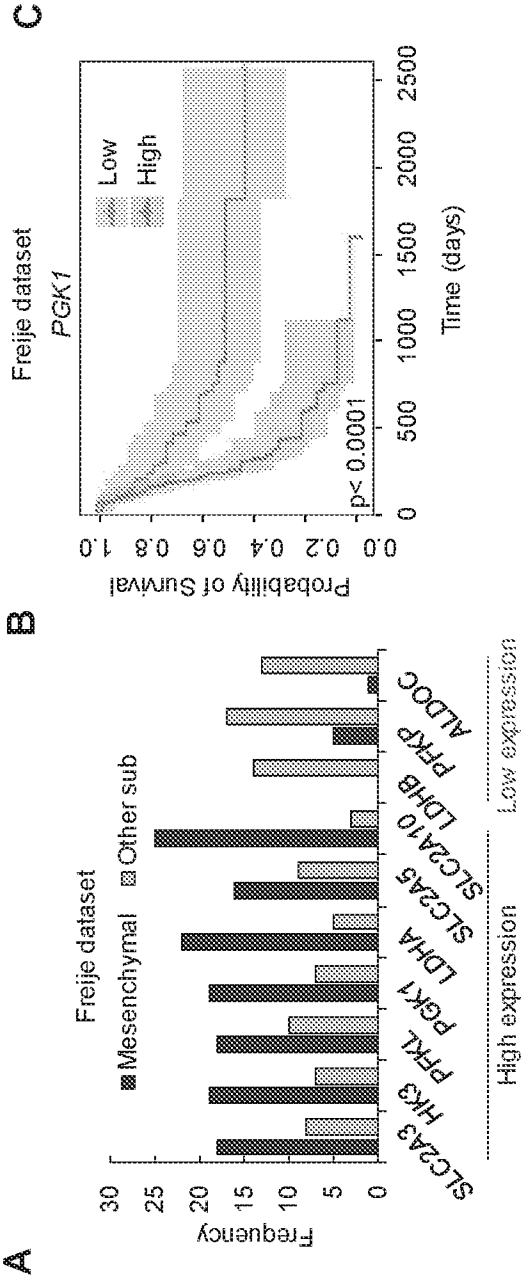
A
Freije dataset
Mesenchymal
Other sub
Frequency
30
25
20
15
10
5
0
SLC2A3
HK3
PFKL
PGK1
LDHA
SLC2A5
SLC2A10
LDHB
PFKP
ALDOC
High expression
Low expression
B
Freije dataset
PGK1
Low
High
p< 0.0001
Probability of Survival
1.0
0.8
0.6
0.4
0.2
0.0
0
500
1000
1500
2000
2500
Time (days)
C
Freije dataset
Mesenchymal
Other sub
Frequency
20
15
10
5
0
ITGB3
SLC2A3
WWTR1
YAP

FIG. 5D

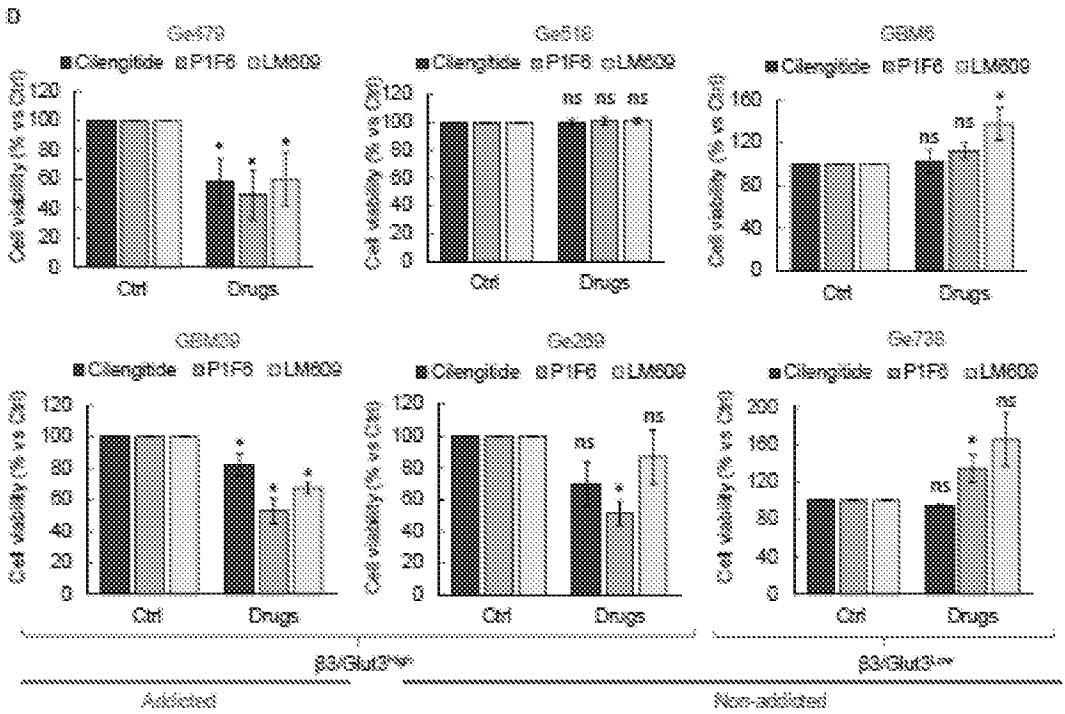
D
Ge479
Ge618
GBM6
GBM39
Ge280
Ge738
Cilengitide
P1F6
LM609
Cell viability (% vs Ctrl)
Ctrl
Drugs
ns
β3/Glut3^low
β3/Glut3^low
Addicted
Non-addicted

FIG. 5E

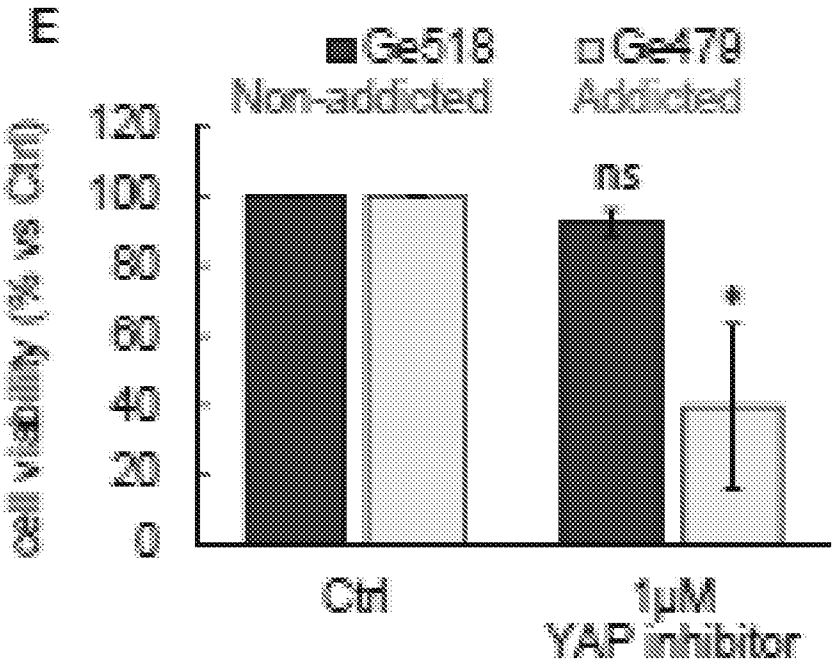
E
Ge518
Ge479
Non-addicted
Addicted
cell viability (% vs Ctrl)
120
100
80
60
40
20
0
ns
*
Ctrl
1μM
YAP inhibitor

FIG. 5F

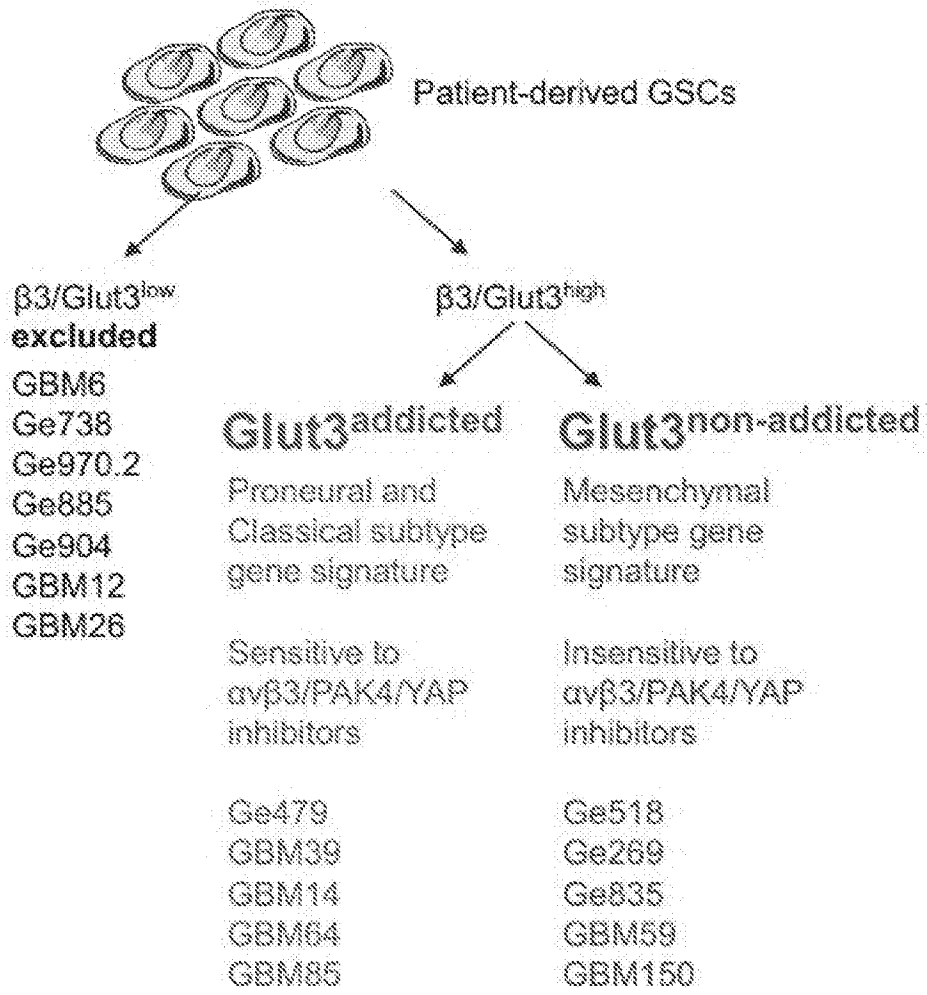
Patient-derived GSCs
β3/Glut3low
excluded
GBM6
Ge738
Ge970.2
Ge885
Ge904
GBM12
GBM26
β3/Glut3high
Glut3addicted
Proneural and Classical subtype gene signature
Sensitive to αvβ3/PAK4/YAP inhibitors
Ge479
GBM39
GBM14
GBM64
GBM85
Glut3non-addicted
Mesenchymal subtype gene signature
Insensitive to αvβ3/PAK4/YAP inhibitors
Ge518
Ge269
Ge835
GBM59
GBM150

FIG. 5G

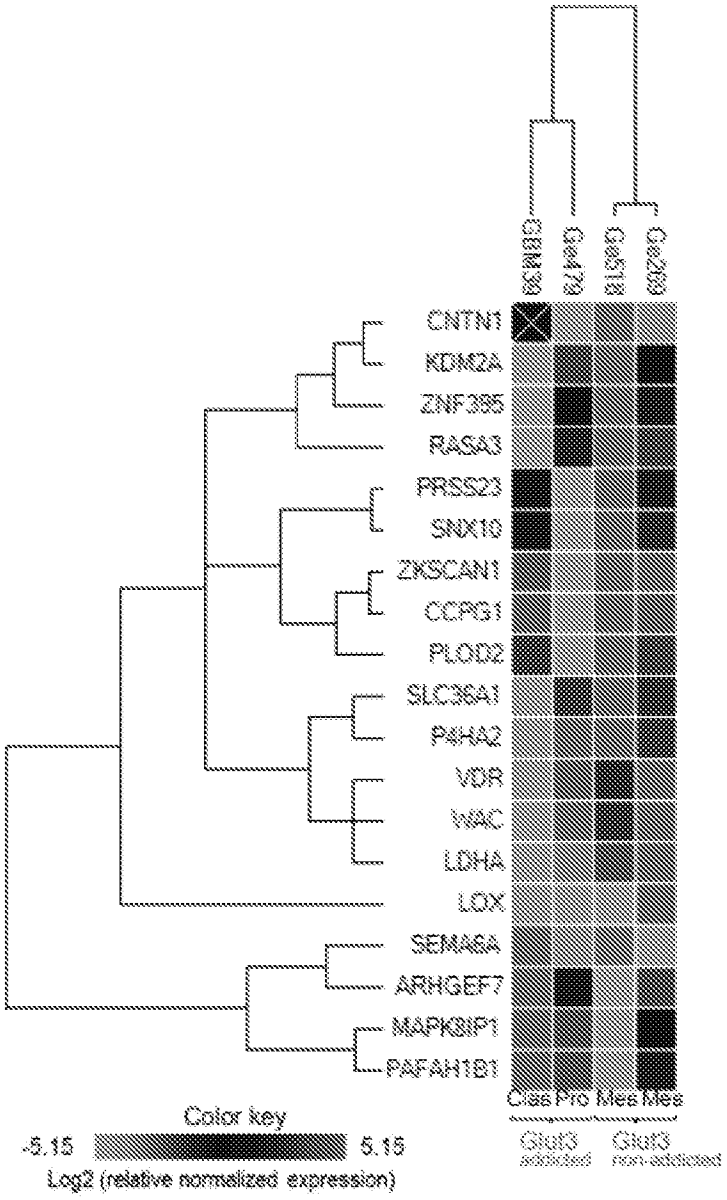
GBM39
Ge479
Ge518
Ge269
CNTN1
KDM2A
ZNF385
RASA3
PRSS23
SNX10
ZKSCAN1
CCPG1
PLOD2
SLC38A1
P4HA2
VDR
WAC
LDHA
LOX
SEMA6A
ARHGEF7
MAPK8IP1
PAFAH1B1
Class Pro Mes Mes
Glut3 addicted
Glut3 non-addicted
Color key
-5.15
5.15
Log2 (relative normalized expression)

FIG. 5I

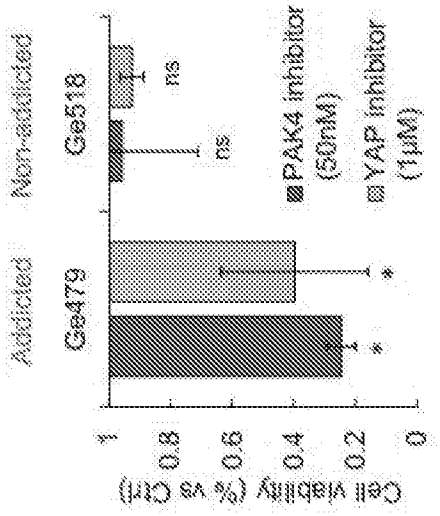
Addicted
Non-addicted
Ge479
Ge518
Cell viability (% vs Ctrl)
1
0.8
0.6
0.4
0.2
0
ns
*
PAK4 inhibitor (50nM)
YAP inhibitor (1μM)

FIG. 5H

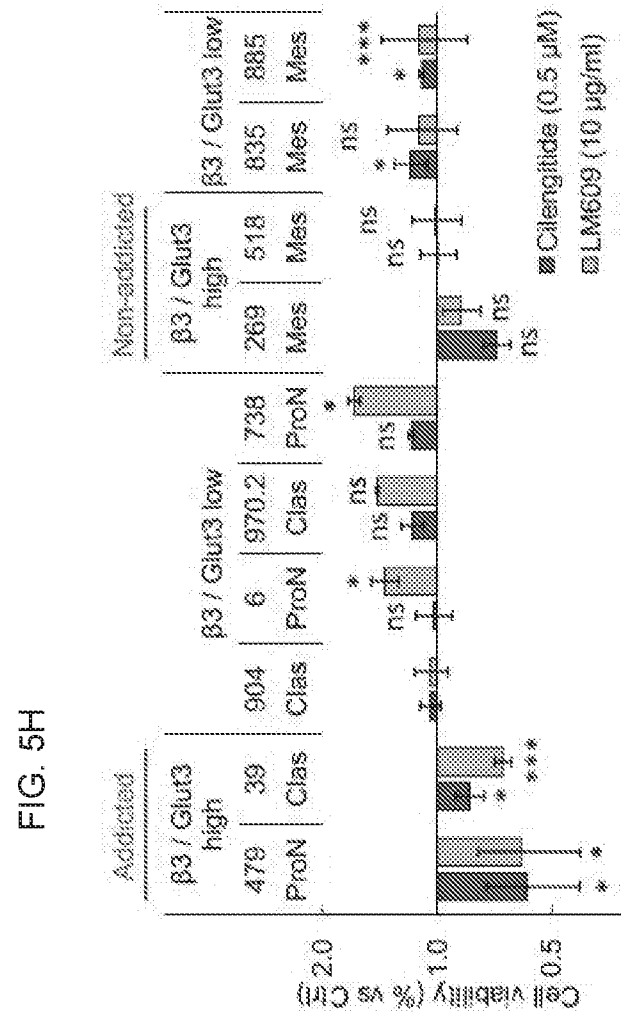
Addicted
Non-addicted
β3 / Glut3 high
β3 / Glut3 low
479 ProN
39 Clas
904 Clas
6 ProN
970.2 Clas
738 ProN
269 Mes
518 Mes
835 Mes
885 Mes
Cell viability (% vs Ctrl)
2.0
1.0
0.5
0.3
Cilengitide (0.5 μM)
LM609 (10 μg/ml)

FIG. 6

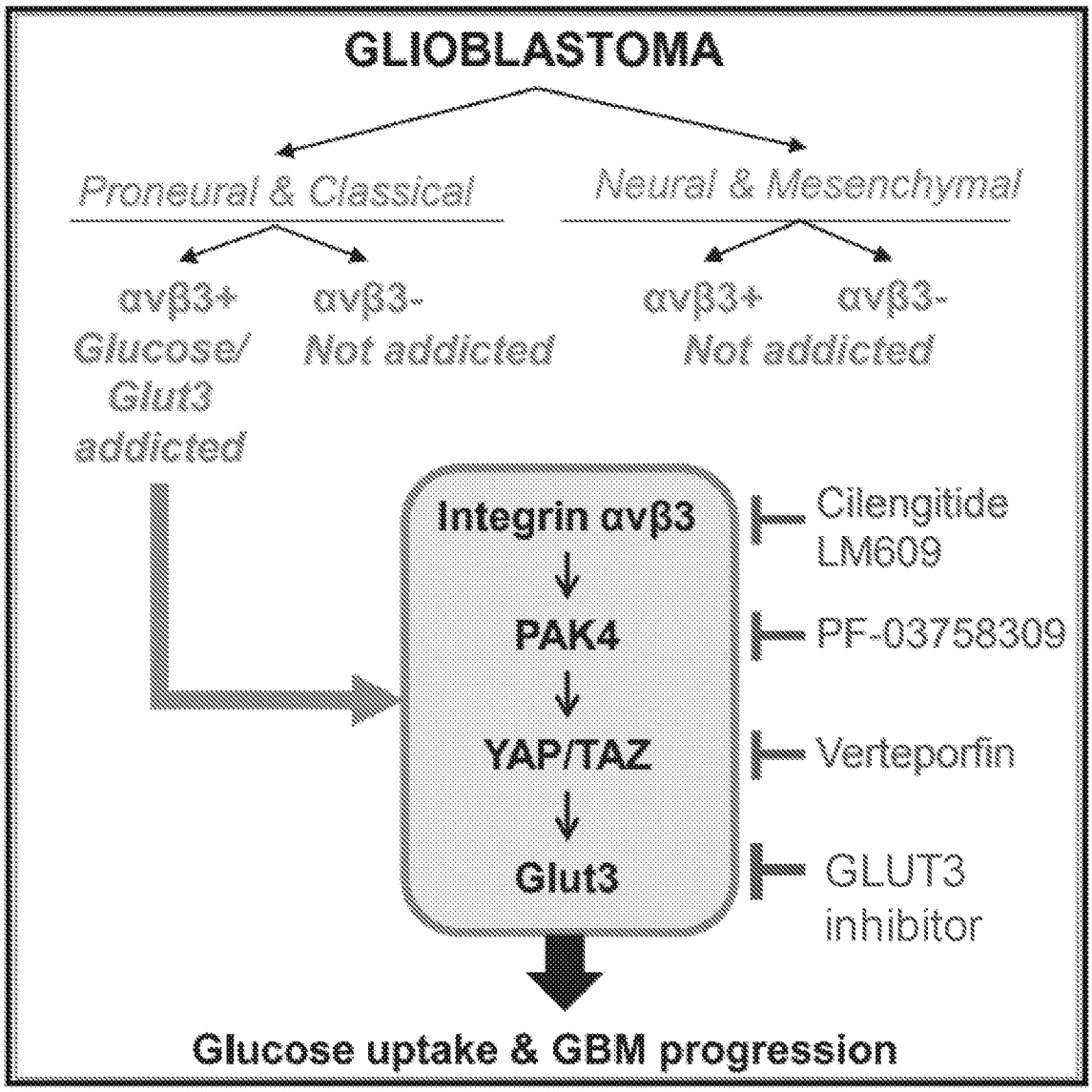
GLIOBLASTOMA
Proneural & Classical
Neural & Mesenchymal
αvβ3+
Glucose/
Glut3
addicted
αvβ3-
Not addicted
αvβ3+
Not addicted
αvβ3-
Integrin αvβ3
PAK4
YAP/TAZ
Glut3
Cilengitide
LM609
PF-03758309
Verteporfin
GLUT3
inhibitor
Glucose uptake & GBM progression

FIG. 7

	pValue		
Name	**Freije**	**Lee**	**TCGA***
ITGB1	0.48	0.11	< 0.001
ITGB2	0.59	0.54	0.51
ITGB3	0.03	0.01	0.008
ITGB4	0.06	0.13	0.58
ITGB5	0.61	0.05	0.36
ITGB6	0.15	0.13	0.99
ITGB7	0.84	0.84	0.004
ITGB8	0.62	0.86	< 0.001

*** TCGA GBM-LGG dataset**

FIG. 8A

Phillips dataset

Rank	Gene names	Rank	Gene names	Rank	Gene names	Rank	Gene names
1	*GPR176*	31	*RPS14*	61	*MMP14*	91	*SLC11A2*
2	*PI4K2A*	32	*MLPH*	62	*BACE2*	92	*SLC2A5*
3	*TRAF6*	33	*TNFRSF9*	63	*PHLDA1*	93	*ELK3*
4	*CCR2*	34	*MYD88*	64	*THAP7*	94	*ELAVL3*
5	*ZC3H12A*	35	*NOD2*	65	*RAB38*	95	*CDRT1*
6	*SLC2A3*	36	*COPS8*	66	*APOL6*	96	*FCGR2C*
7	*ICAM1*	37	*RNASE3*	67	*DOCK5*	97	*CACYBP*
8	*STK10*	38	*CASP5*	68	*LONRF3*	98	*MYOF*
9	*IL1B*	39	*ABL2*	69	*PDCD1LG2*	99	*FAM98A*
10	*ADAM17*	40	*CYP1A2*	70	*CHST4*	100	*ELOVL5*
11	*IL15RA*	41	*NRP2*	71	*IL1B*	101	*COL5A1*
12	*NFKB1*	42	*ICAM1*	72	*STK10*	102	*IL1RN*
13	*FPR2*	43	*ACPP*	73	*MMTR1*	103	*LPXN*
14	*BCL6*	44	*MTCP1*	74	*NEDD9*	104	*CCL13*
15	*SLC39A8*	45	*NPAS2*	75	*SPINT1*	105	*TP53I11*
16	*NRP2*	46	*STRN*	76	*MMP7*	106	*AKTIP*
17	*TLR8*	47	*SLC22A18AS*	77	*CCR4*	107	*MCTP2*
18	*LEF1*	48	*HSD3B2*	78	*NRP2*	108	*RBM19*
19	*CDK5RAP1*	49	*ITGA2B*	79	*GALNT4*	109	*STAT2*
20	*CYP2B6*	50	*PLA2G10*	80	*ENG*	110	*VDAC3*
21	*DEFB4A*	51	*RAC2*	81	*SNORA70*	111	*PGLYRP4*
22	*CYP2B7P*	52	*SLCO4C1*	82	*TNFRSF11A*	112	*MME*
23	*CSF1*	53	*SCGB1D1*	83	*SMG6*	113	*HOXB3*
24	*TTC21B*	54	*CALM1*	84	*SIGLEC9*	114	*CYLD*
25	*ADAM12*	55	*CHST3*	85	*CALM1*	115	*SGPL1*
26	*ADAM12*	56	*MPZL1*	86	*OSMR*	116	*SLC43A3*
27	*IL13RA1*	57	*HPS1*	87	*PML*	117	*DAB2*
28	*PHLDA1*	58	*SEL1L3*	88	*SAMD4A*	118	*ITGB1*
29	*CD44*	59	*DCBLD2*	89	*DST*	119	*CYP2A7P1*
30	*APAF1*	60	*HIST1H3E*	90	*PCDHB6*	120	*BAK1*

FIG. 8B

Sun dataset

Rank	Gene names	Rank	Gene names	Rank	Gene names	Rank	Gene names
1	*ITGB3*	31	*GNAQ*	61	*CHRNA9*	91	*CD44*
2	*RAB27A*	32	*STOX2*	62	*ACSS1*	92	*LOXL2*
3	*THBS1*	33	*CSMD1*	63	*MTA3*	93	*EMP1*
4	*ATP13A3*	34	*STOX2*	64	*SYT16*	94	*FBLIM1*
5	*ELK3*	35	*SH3BP2*	65	*RAB27A*	95	*TRAM2*
6	*USP32*	36	*IQGAP1*	66	*LYRM7*	96	*IRF1*
7	*ZBTB47*	37	*FCGR2C*	67	*FCGR2C*	97	*PGK1*
8	*CD44*	38	*FNDC3B*	68	*SLC2A3*	98	*USP32*
9	*PRSS23*	39	*TOM1L2*	69	*GRIA3*	99	*PATL1*
10	*SERPINE1*	40	*PPP2R1B*	70	*NAMPT*	100	*SRD5A1*
11	*ITGB3*	41	*TUBB6*	71	*WDFY3-AS2*	101	*WDR17*
12	*CA12*	42	*IDE*	72	*RABGAP1L*	102	*CD44*
13	*CD44*	43	*ITPRIPL2*	73	*TSPAN4*	103	*NRP2*
14	*CD44*	44	*PXN-AS1*	74	*TPM4*	104	*PGK1*
15	*RBM47*	45	*USP32P2*	75	*CLEC2B*	105	*SMURF1*
16	*LPP*	46	*ESYT2*	76	*MALT1*	106	*MAGI2*
17	*PPP1R3B*	47	*THBS1*	77	*SP1*	107	*SLC9A6*
18	*CD44*	48	*SHC1*	78	*RAB32*	108	*S100A11P1*
19	*EPM2A*	49	*IQGAP1*	79	*CFLAR*	109	*CACYBP*
20	*NRP2*	50	*PGK1*	80	*CADM2*	110	*MVP*
21	*MAPT*	51	*IL13RA1*	81	*CEP97*	111	*SRPX2*
22	*RALGPS1*	52	*ITPRIP*	82	*TAF9B*	112	*CYP46A1*
23	*ITGB3*	53	*CLASP2*	83	*STOX2*	113	*FNDC3B*
24	*CD44*	54	*MATR3*	84	*ACACA*	114	*OSMR*
25	*IL13RA1*	55	*CADM2*	85	*MACC1*	115	*LOXL1*
26	*RALGAPA1*	56	*PPP1R3B*	86	*APLP2*	116	*CAST*
27	*BACE2*	57	*ESYT2*	87	*SAT1*	117	*ANXA2P2*
28	*SLC22A17*	58	*MALT1*	88	*TMCO3*	118	*CAMSAP2*
29	*TMCO3*	59	*ZDHHC22*	89	*CNIH4*	119	*MUM1*
30	*NRP2*	60	*IRF1*	90	*NRXN1*	120	*SERTAD1*

FIG. 8C

Rank	Gene names	Rank	Gene names	Rank	Gene names	Rank	Gene names	Rank	Gene names	Rank	Gene names
1	THRA	31	SPATA2	61	ABAT	91	BHLHE40	121	CAMK2G	151	LIMCH1
2	ALDOC	32	SUSD4	62	CAMTA1	92	CYP46A1	122	OGFOD3	152	RAB6B
3	FXYD6	33	TCEAL2	63	BEX4	93	FAM127A	123	COL6A1	153	ARHGEF4
4	ITPR3	34	FAM192A	64	PIK3R1	94	ITGA4	124	ICAM1	154	LAMB1
5	FTO	35	RAB27A	65	MAPT	95	PAAF1	125	RBMS1	155	APC
6	NRXN1	36	ABHD10	66	FDFT1	96	DZIP3	126	NRP1	156	NFE2L3
7	ITGB3	37	GORASP1	67	TJP2	97	NRP2	127	GMFB	157	C1ORF61
8	CLASP2	38	C14ORF132	68	RUFY3	98	TRAPPC2L	128	CPD	158	LOX
9	AKTIP	39	NCOA1	69	NDUFS1	99	ERBB4	129	MYO18A	159	B3GAT1
10	WWTR1	40	KIF5C	70	HEXB	100	ADD3	130	ABAT	160	TSSC1
11	THRA	41	CLCN6	71	LAMC1	101	ANKRD46	131	LAMA4	161	NRXN1
12	SHC1	42	SERPINE1	72	GTDC1	102	NRP2	132	GNAZ	162	UGGT1
13	OMG	43	NDRG2	73	KDELR3	103	PFN2	133	KCNQ2	163	ICAM1
14	SVIL	44	TTYH1	74	ATP9A	104	BLCAP	134	ZNF189	164	SLC6A1
15	TSPYL4	45	ACO2	75	MAPT	105	NAP1L3	135	TUBB4A	165	SLC2A3
16	OSMR	46	DES1	76	SC5D	106	PKIA	136	KIF5C	166	HMGCS1
17	BCAT1	47	PMAIP1	77	SLC9A6	107	PFKM	137	CA12	167	CEP68
18	KIF1B	48	APBA2	78	ALDH5A1	108	TPM4	138	ATP8A1	168	BCR
19	CTNND2	49	ADGRB3	79	WEE1	109	NOL12	139	TMEM35B	169	EDEM1
20	TNFRSF10B	50	NCAN	80	SLC22A17	110	MAPT	140	RBMS1	170	ABHD6
21	IQGAP1	51	NRXN2	81	CTIF	111	COL6A1	141	ASRGL1	171	NGRN
22	GABARAPL2	52	SLC20A1	82	RTN3	112	FDFT1	142	PIK3R1	172	DOPEY1
23	IQGAP1	53	PRKACB	83	SDC1	113	MR1	143	MARCKSL1	173	NCOA1
24	NRXN2	54	NTM	84	ADAM22	114	HIP1R	144	THTPA	174	BEX1
25	WASF3	55	NUDT3	85	ADGRE5	115	N/A	145	ANXA2P2	175	APC
26	ITPR3	56	PLCB1	86	SCN3A	116	NCALD	146	CHSY1	176	RUNX1
27	FUT9	57	MMP14	87	PTBP2	117	KIF21B	147	COL6A1	177	KCNB1
28	SHC1	58	CLIP3	88	RAB27A	118	SEC24A	148	MAP1A	178	PPP2R2B
29	CLASP2	59	VMP1	89	TNFRSF12A	119	GDF15	149	WASF1	179	LOX
30	PEA15	60	ADD1	90	APBA2	120	GRIA2	150	ACACA	180	PHLPP1

FIG. 9

		Gene name		
		Glut3	ALDOC	PFKM
Dataset name	Freije	0.0016	0.022	0.00073
	TCGA	0.000000021	0.0037	0.47
	Lee	0.0196	0.12	0.56

FIG. 10

Family of genes/Pathway	Name	Sequence
Housekeeping genes	Cyclo FWD	CAGGTCCTGGCATCTTGTCC
	Cyclo REV	TTGCTGGTCTTGCCATTCCT
	Tuba2 FWD	AGGAGCTGGCAAGCATGTG
	Tuba2 REV	CGGTGCGAACTTCATCGAT
	ALAS1 FWD	CTCACCACACACCCCAGATG
	ALAS1 REV	AGTTCCAGCCCCACTTGCT
	EEF1A1 FWD	AGCAAAAATGACCCACCAATG
	EEF1A1 REV	GGCCTGGATGGTTCAGGATA
Glut transporters	SLC2A1 FWD	TATCGTCAACACGGCCTTCACT
	SLC2A1 REV	AACAGCTCCTCGGGTGTCTTAT
	SLC2A2 FWD	CAACCATTGGAGTTGGCGCTGT
	SLC2A2 REV	AGGTCCACAGAAGTCCGCAATG
	SLC2A3 FWD	TCCACGCTCATGACTGTTTC
	SLC2A3 REV	GCCTGGTCCAATTTCAAAGA
	SLC2A6 FWD	CGGAAGCTGAGCATCATGT
	SLC2A6 REV	GGGAGCAATCTCAGACACGTA
Integrins	ITGB3 FWD	GTGACCTGAAGGAGAATCTGC
	ITGB3 REV	TCACTCACTGGGAACTCGATG
Stem cells	CD133 FWD	ACTCCCATAAAGCTGGACCC
	CD133 REV	TCAATTTTGGATTCATATGCCTT
	Oct4 FWD	TCTCCCATGCATTCAAACTGAG
	Oct4 REV	CCTTTGTGTTCCCAATTCCTTC
	Nanog FWD	TCTCCCATGCATTCAAACTGAG
	Nanog REV	CCCACTTCTGCAGAGAATAGTG
Astrocytes	GFAP FWD	AAGAGATCCGCACGCAGTAT
	GFAP REV	AGGTCAAGGACTGCAACTGG
Neurons	Tubb3 FWD	CGGTGGTGGAACCCTACAAC
	Tubb3 REV	AGGTGGTGACTCCGCTCAT
YAP/TAZ	hYAP FWD	CCAAGGCTTGACCCTCGTTTTG
	hYAP REV	TCGCATCTGTTGCTGCTGGTTG
	hTAZ FWD	TCACCAACACCAGCAGCAGATG
	hTAZ REV	GCATTCTCTGAAGCCGCAGTTT
Mitochondrial oxidative phosphorylation	PISD FWD	CCACCGACTGGACTGTGTC
	PISD REV	CCGCTCGTTATGGCAGAAGA
	PISD REV	CCGATGGGCTAATCACGCTG
	ACAD9 FWD	AGTTCTTGGGACCCGTGGAA
	ACAD9 REV	GTCTTGAGTACATGGTGTTGGA
Glycolytic pathway	HK3 FWD	GGACAGGAGCACCCTCATTTC
	HK3 REV	CCTCCGAATGGCATCTCTCAG
	HK2 FWD	GAGCCACCACTCACCCTACT
	HK2 REV	CCAGGCATTCGGCAATGTG
	HK1 FWD	GCTCTCCGATGAAACTCTCATA
	HK1 REV	GGACCTTACGAATGTTGGCAA
	GPI FWD	CAAGGACCGCTTCAACCACTT
	GPI REV	CCAGGATGGGTGTGTTTGACC
	ALDOC FWD	ATGCCTCACTCGTACCCAG
	ALDOC REV	TTTCCACCCCAATTTGGCTCA
	PFKP FWD	GCATGGGTATCTACGTGGGG
	PFKP REV	CTCTGCGATGTTTGAGCCTC
	TPI1 FWD	CTCATCGGCACTCTGAACG
	TPI1 REV	GCGAAGTCGATATAGGCAGTAG
	Gapdh FWD	GCACAAGAGGAAGAGAGAGAC
	Gapdh REV	AGGGGAGATTCAGTGTGGTG
	PGK1 FWD	GAACAAGGTTAAAGCCGAGCC
	PGK1 REV	GTGGCAGATTGACTCCTACCA
	PKM2 FWD	ATGTCGAAGCCCCATAGTGAA
	PKM2 REV	TGGGTGGTGAATCAATGTCCA
	ENO1 FWD	GCCGTGAACGAGAAGTCCTG
	ENO1 REV	ACGCCTGAAGAGACTCGGT
	ALDOA FWD	ATGCCCTACCAATATCCAGCA
	ALDOA REV	GCTCCCAGTGGACTCATCTG
Pentose Phosphate Pathway	G6PD FWD	CGAGGCCGTCACCAAGAAC
	G6PD REV	GTAGTGGTCGATGCGGTAGA
	PGLS FWD	GGAGCCTCGTCTCGATGCTA
	PGLS REV	GAGAGAAGATGCGTCCGGT

FIG. 10 (continued)

	PDG FWD	ATGGCCCAAGCTGACATCG
	PGD REV	AAAGCCGTGGTCATTCATGTT
	TKT FWD	TCCACACCATGCGCTACAAG
	TKT REV	CAAGTCGGAGCTGATCTTCCT
	TALDO1 FWD	CTCACCCGTGAAGCGTCAG
	TALDO1 REV	GTTGGTGGTAGCATCCTGGG
	Name	Sequence
	SYT1 FWD	GTGAGCGAGAGTCACCATGAG
	SYT1 REV	CCCACGGTGGCAATGGAAT
	SYT5 FWD	AGACGCTGAACCCTCACTTTG
	SYT5 REV	CGAAGTCGTACACCGCCAT
	SLC12A5 FWD	TGCTCCTGTACGATGCTCAC
	SLC12A5 REV	GCTCCTGCAAAGGTAGTGC
	PACSIN1 FWD	GAACAGCAAGACGGAGCAATC
	PACSIN1 REV	GACCAGCCGCTTTTCCTCAA
	RGS4 FWD	ACATCGGCTAGGTTTCCTGC
	RGS4 REV	GTTGTGGGAAGAATTGTGTTCA
	MAL2 FWD	GTCCGTGACAGCGTTTTTCTT
	MAL2 REV	AATTGAGGCTGCTACGTTTATGT
	DLL3 FWD	CACTCCCGGATGCACTCAAC
	DLL3 REV	GATTCCAATCTACGGACGAGC
	DCX FWD	GACAGCCCACTCTTTTGAGC
	DCX REV	TGGGTTTCCCTTCATGACTC
	OLIG2 FWD	CAGAAGCGCTGATGGTCATA
	OLIG2 REV	TCGGCAGTTTTGGGTTATTC
	ERBB3 FWD	GGTGATGGGGAACCTTGAGAT
	ERBB3 REV	CTGTCACTTCTCGAATCCACTG
	PDGFRA FWD	TGGCAGTACCCCATGTCTGAA
	PDGFRA REV	CCAAGACCGTCACAAAAAGGC
	P2RX7 FWD	TATGAGACGAACAAAGTCACTC
	P2RX7 REV	GCAAAGCAAACGTAGGAAAAGA
	BMP2 FWD	ACTACCAGAAACGAGTGGGAA
	BMP2 REV	GCATCTGTTCTCGGAAAACCT
	SOX2-FWD	GGGAAATGGGAGGGGTGCAAA
	SOX-2-REV	TTGCGTGAGTGTGGATGGGATT
	CD44 FWD	AAGGTGGAGCAAACACAACC
	CD44 REV	AGCTTTTTCTTCTGCCCACA
	YKL40 FWD	TCAAGAACAGGAACCCCAAC.
	YKL40 REV	AAATTCGGCCTTCATTTCCT
	MET FWD	CCCCACCCTTTGTTCAG
	MET REV	TCAGCCTTGTCCCTCCT
	RelB FWD	TGAATGTGGTGAGGATCTGC
	RelB REV	CGCAGCTCTGATGTGTTTGT
	LGALS3 FWD	GTGAAGCCCAATGCAAACAGA
	LGALS3 REV	AGCGTGGGTTAAAGTGGAAGG
	LOX FWD	CCTACTACATCCAGGCGTCCA
	LOX REV	CATAATCTCTGACATCTGCCCCT
	THBS1 FWD	TGCTATCACAACGGAGTTCAGT
	THBS1 REV	GCAGGACACCTTTTTGCAGATG
	LAMB1 FWD	CACAAGCCCGAACCCTACTG
	LAMB1 REV	GACCACATTTTCAATGAGATGG
	DAB2 FWD	GTAGAAACAAGTGCAACCAATG
	DAB2 REV	GCCTTTGAACCTTGCTAAGAGA
	S100A4 FWD	GATGAGCAACTTGGACAGCAA
	S100A4 REV	CTGGGCTGCTTATCTGGGAAG
	COL1A2 FWD	GAGCGGTAACAAGGGTGAGC
	COL1A2 REV	CTTCCCCATTAGGGCCTCTC
	MMP9 FWD	TGTACCGCTATGGTTACACTCG
	MMP9 REV	GGCAGGGACAGTTGCTTCT
	VEGFA FWD	AGGGCAGAATCATCACGAAGT
	VEGFA REV	AGGGTCTCGATTGGATGGCA
	IGFBP2 FWD	GACAATGGCGATGACCACTCA
	IGFBP2 REV	CAGCTCCTTCATACCCGACTT
	Gli2 FWD	CTGCCTCCGAGAAGCAAGAAG
	Gli2 REV	GCATGGAATGGTGGCAAGAG
	EGFR FWD	CAGCGCTACCTTGTCATTCA
	EGFR REV	AGCTTTGCAGCCCATTTCTA
	ACSBG1 FWD	ACACTGTGCATCGGATGTTCT

FIG. 10 (continued)

	ACSBG1 REV	AGGAGATGTGTTCCCACTTGT
	IGF2 FWD	GTGGCATCGTTGAGGAGTG
	IGF2 REV	CACGTCCCTCTCGGACTTG
	Nestin FWD	GGAAGAGAACCTGGGAAAGG
	Nestin REV	CTTGGTCCTTCTCCACCGTA
	shh FWD	CTCGCTGCTGGTATGCTCG
	shh REV	ATCGCTCGGAGTTTCTGGAGA
	Notch3 FWD	CGTGGCTTCTTTCTACTGTGC
	Notch3 REV	CGTTCACCGGATTTGTGTCAC
	GAS1 FWD	ATGCCGCACCGTCATTGAG
	GAS1 REV	TCATCGTAGTAGTCGTCCAGG
	MCM2 FWD	CCGTGACCTTCCACCATTTGA
	MCM2 REV	GGTAGTCCCTTTCCATGCCAT
	CENPF FWD	CTCTCCCGTCAACAGCGTTC
	CENPF REV	GTTGTGCATATTCTTGGCTTGC
	TOP2A FWD	TTAATGCTGCGGACAACAAACA
	TOP2A REV	CGACCACCTGTCACTTTCTTTT
	KCNF1 FWD	GCCAGCGACGACATAGAGATA
	KCNF1 REV	CCAGCCAAGCAGTTGATGAG

FIG. 11

Glut3 non-addicted signature

1	MAFF	76	MBD4
2	SYNM	77	IL15R
3	MRC1	78	NUCB2
4	SLC9A3	79	GRK5
5	TAGLN	80	CLRN3
6	SERPINE1	81	NTAN1
7	LGR	82	PPP1R15A
8	CYP1B1	83	MGAT2
9	MAFF	84	FAM162A
10	CXCL8	85	ARF1
11	CAV1	86	PARVB
12	TNFS1	87	COPB1
13	GOS2	88	PGS
14	DMN2	89	NUP98
15	KCTD10	90	UNK2
16	ANXA2	91	CAPZA1
17	IL1R1	92	LGALS8
18	DYNL13	93	ETF1
19	IL1R2	94	SHD1
20	CCN	95	BNIP3L
21	SYNM	96	GNA15
22	TNR1	97	MBD4
23	CAV2	98	ARPC2
24	PLOD2	99	CCQ10B
25	ACSL1	100	ATP13A3
26	SNX10	101	FYCO1
27	BHLHE40	102	SEC1M1
28	TNFAIP3	103	HCC3
29	IL1R2	104	MARE
30	PCSK1	105	YDH
31	ARHGAP29	106	SEPHS2
32	ACTN1	107	SLC26A1
33	PRSS23	108	GTPDN1
34	KNL2	109	CARS
35	RGS2	110	SRPR8
36	TPM1	111	SEC31A
37	RASL3	112	GTPBP2
38	PLAU	113	KRR1A
39	CEBPB	114	SLC19A6
40	MPP1	115	XDH
41	SYNPO	116	MAMBA
42	NCRNA1	117	EXT2
43	SLC9A1B	118	PIGB
44	SQRL	119	DNAJC28-GNG10
45	LDHA	120	STX4
46	HRH1	121	MED8
47	MICAL2	122	AP3S1
48	ANGPTL4	123	YIPF1
49	HTATIP2	124	ACBD3
50	OSBPL10	125	SERTAD3
51	MAP2K6	126	SRP54
52	CPD	127	ITPKC
53	MPP1	128	TBC1D8B
54	KNNYN	129	SPG21A
55	MMP1	130	IRAK3
56	HIST1H2AC	131	VPS37C
57	SEMO2	132	CRET1
58	TGM2	133	WDR54
59	FTH1	134	TMED2
60	ERBIP2	135	KIF10B
61	SEC23A	136	CCPG1
62	UAP1	137	IRGK3
63	ZNF395	138	CHMP4A
64	SLC2A14	139	FTH1P5
65	POLR1D	140	TASP1
66	RBPMS	141	MAPK13
67	RGS1	142	SUN1
68	GSTO1	143	NFE2L3
69	STBD1		
70	SAT1		
71	PPCS		
72	SPAG9		
73	RASD1A		
74	CD55		
75	TPGS2		

Glut3 addicted signature

1	KDR52	76	GLYR1
2	SCAM	77	ANAPC5
3	CLIC2	78	ANP32A
4	PCDHGA4	79	SRSF6A
5	IGL3	80	GTF2I
6	PCDHGB3	81	SRPK2
7	ADGRG1	82	HSP90AB1
8	KCNN3	83	CRSP1
9	FNK1	84	KLHL32
10	PSAT1	85	TC4F1P1
11	IGV	86	SLC19A6
12	PHGDH	87	HSAFX
13	MMP2	88	PPP6R1
14	STX1	89	PAT21
15	ZEB1	90	KRR1B
16	CNTN1	91	TBC1D5
17	MAP4K4P1	92	NAB1
18	PPAN-P1	93	DSCR2
19	ZBTB18	94	GTF2I2
20	MARCKS	95	PRKAB1
21	TAF9B	96	DTX3
22	PLXNB1	97	HMGB1P1
23	SLUD2	98	NPPL3
24	SPAG9	99	ARHGAP39
25	GPSM2	100	CBX5
26	HACD3	101	RELCH
27	SPTBN1	102	GDAP1
28	RAC21	103	TDRKH2
29	NREP	104	KCTD18
30	WNK	105	PAT21
31	ANKFY1	106	KNS2
32	KCNJ10	107	SKSCAM1
33	SNX9	108	AKAP1
34	PEA15	109	KCTD20
35	EPN01	110	ZNF516
36	GPSM3	111	PEX1
37	SPTBN1	112	NCAM1
38	MCM3	113	GRIDEPL1
39	PTPN11	114	GNAQ
40	MPK2	115	HDAC8
41	TSPAN3	116	KMT2A
42	ZNF711	117	MATR3
43	HMGCS1	118	ZCWH2
44	FBXW11	119	POLDIP3
45	ANP32A	120	CDC5L
46	PAT21	121	GNL3
47	FOXO3/FOXO3	122	WIP11
48	RPS3	123	CDYL
49	PLXNC2	124	CDK17
50	PTK2	125	ABI2
51	ARHGEF4	126	RXRB
52	MYO9	127	CEP68
53	HDAFV	128	RGS12
54	TNPO	129	DCAMD
55	TJP1	130	ABI2
56	TNK2	131	PIK3R3
57	ARHGEF7	132	KMT2A
58	SRGN	133	RPS3
59	QKI	134	CDYL
60	PRKDC	135	CASKIN2
61	AEDI	136	SKP2
62	DST	137	DSTYK
63	PDP1	138	ATP5S
64	ZMYND11	139	4F1DV
65	USP34	140	KLHL12
66	SPN2	141	LGR5
67	RBM8A	142	NTATSF1
68	APC	143	ZNF213
69	HP1BP3	144	LLGL1
70	CAMSAP2	145	GTF2IRD2
71	KIDINS220	146	HMGB1P8
72	PAPOLB1	147	MKP
73	RBM8A	148	HMGB1P4
74	XPO7	149	LDAH
75	CCDC88A	150	SHMT2

FIG. 12A

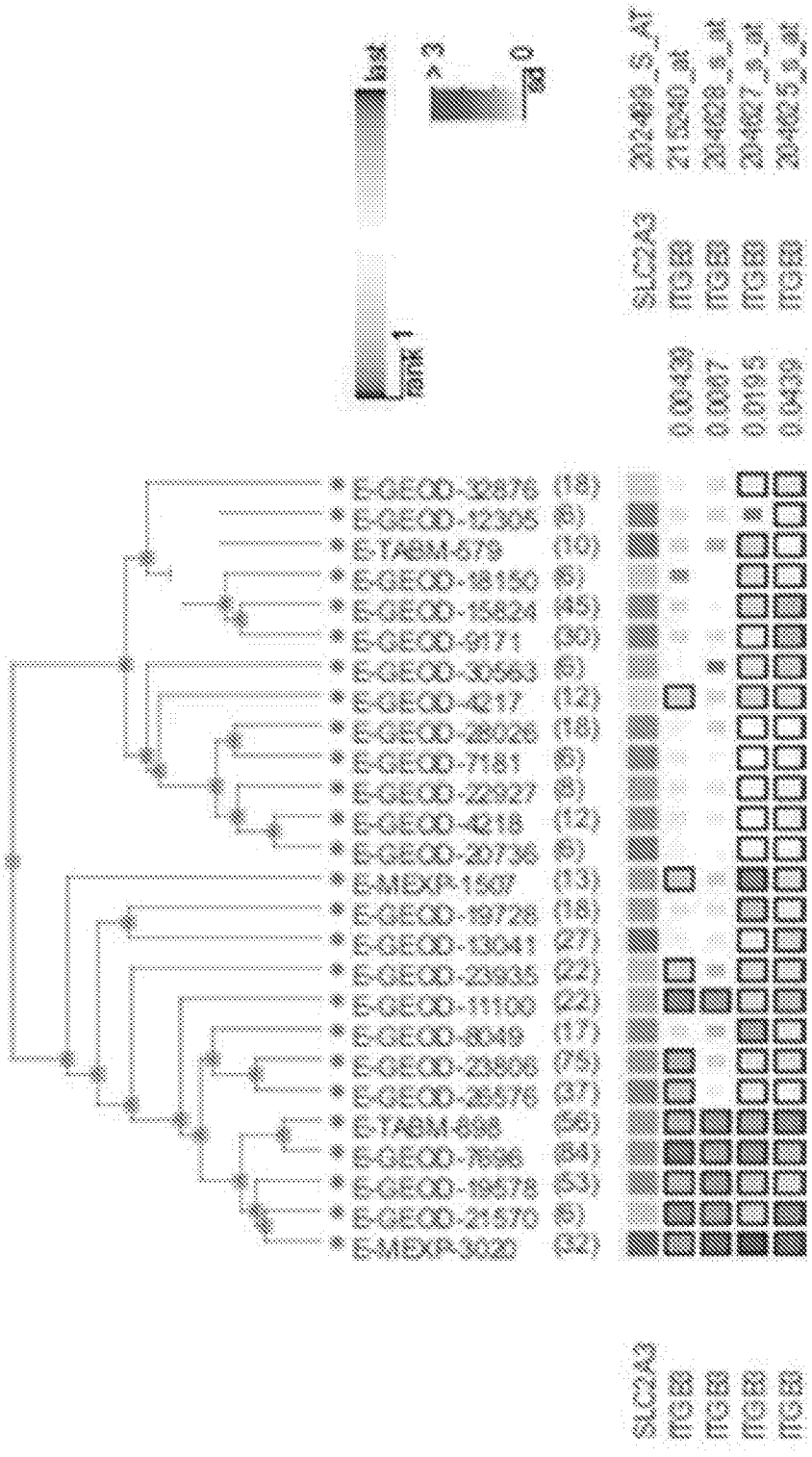
SLC2A3
ITGB3
ITGB3
ITGB3
ITGB3
E-GEOD-32676 (18)
E-GEOD-12305 (8)
E-TABM-479 (10)
E-GEOD-18150 (8)
E-GEOD-15824 (25)
E-GEOD-9171 (30)
E-GEOD-30563 (8)
E-GEOD-4217 (12)
E-GEOD-28026 (18)
E-GEOD-7181 (8)
E-GEOD-22027 (8)
E-GEOD-4218 (12)
E-GEOD-20736 (8)
E-MEXP-1507 (13)
E-GEOD-19728 (18)
E-GEOD-13041 (27)
E-GEOD-29935 (22)
E-GEOD-11100 (22)
E-GEOD-8049 (17)
E-GEOD-23606 (75)
E-GEOD-25576 (37)
E-TABM-698 (24)
E-GEOD-7696 (23)
E-GEOD-19678 (13)
E-GEOD-21570 (8)
E-MEXP-3020 (12)
SLC2A3
202460_s_AT
215240_at
204028_s_at
204027_s_at
204025_s_at
0.00439
0.0007
0.0195
0.0439
high
low
x 3
0

FIG. 12B

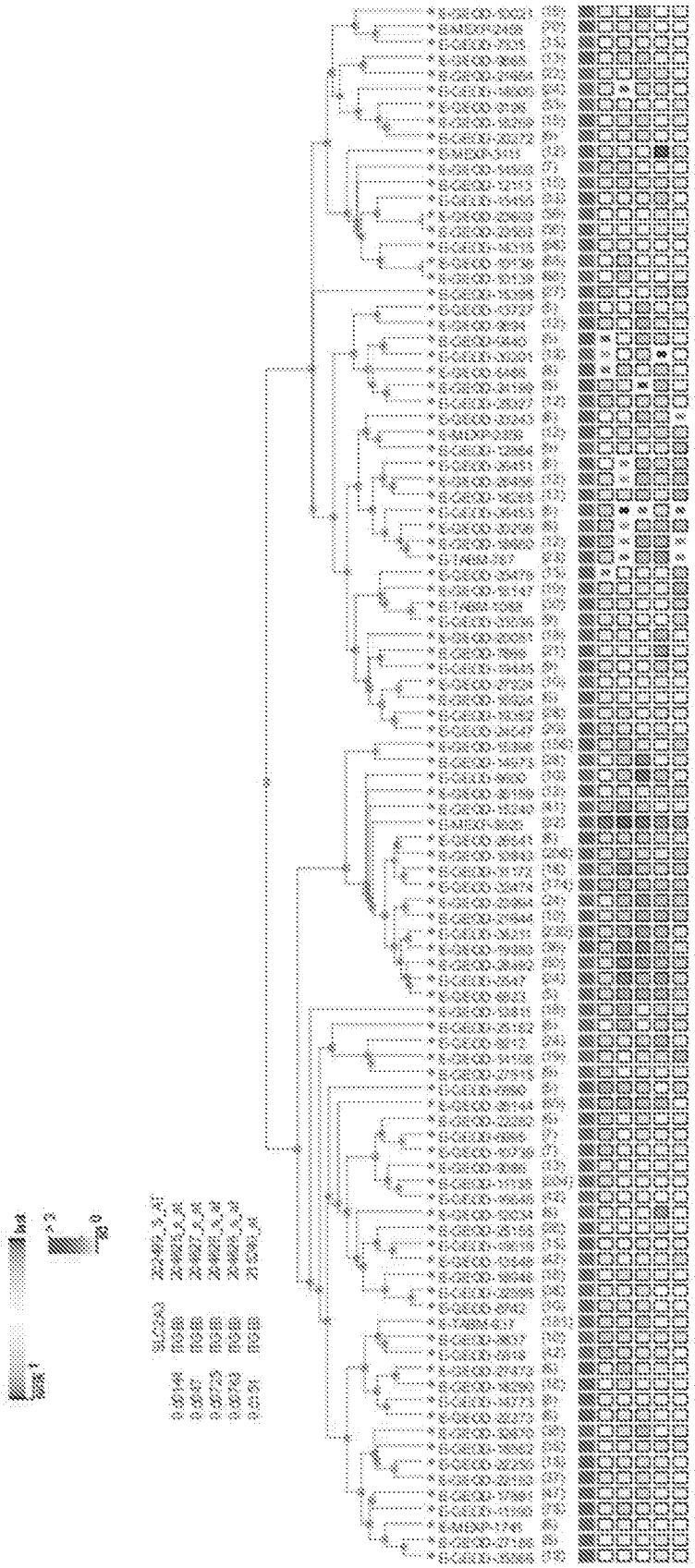

FIG. 13A-B

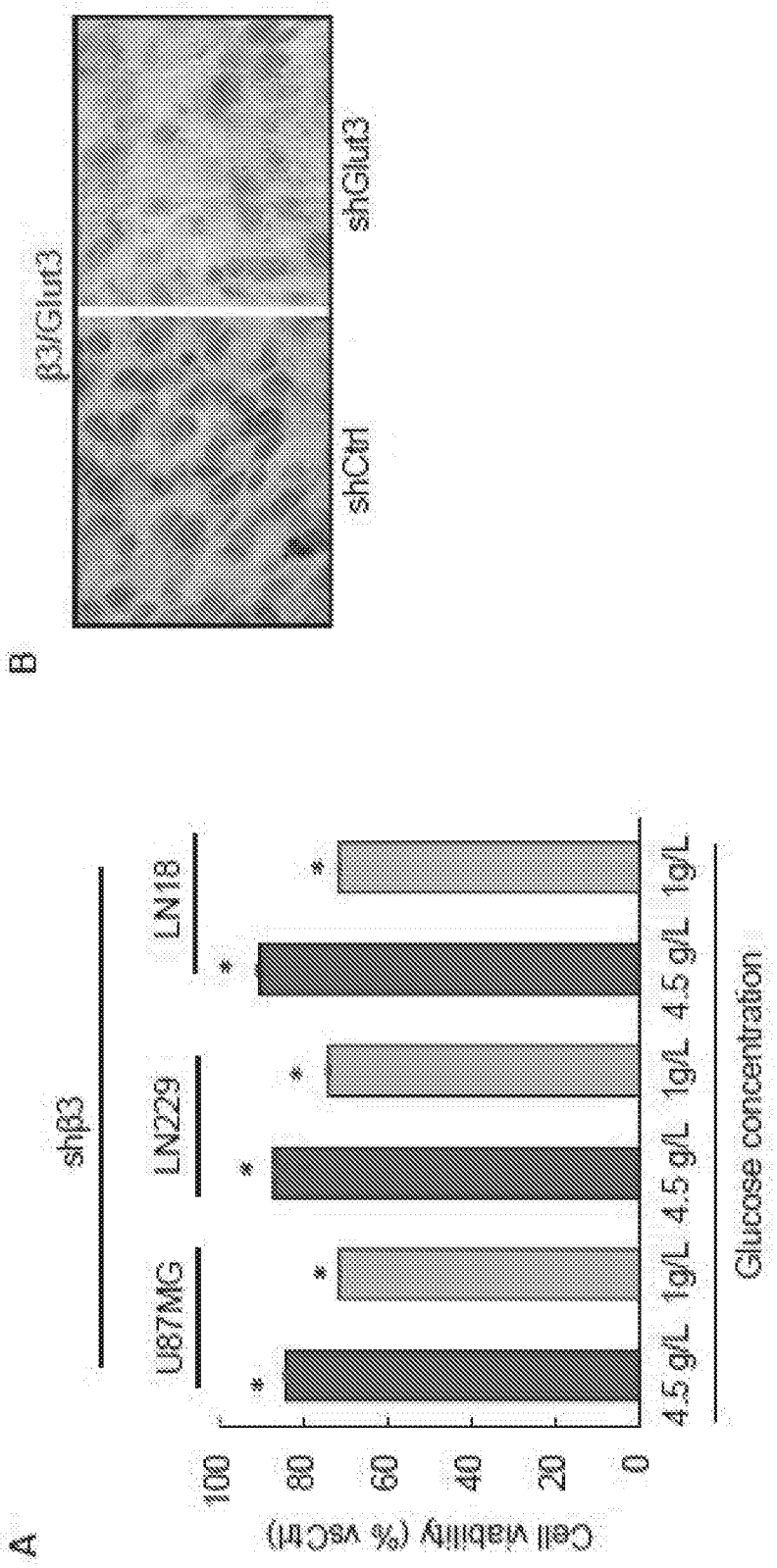
A
shβ3
U87MG
LN229
LN18
Cell viability (% vsCtrl)
100
80
60
40
20
0
4.5 g/L
1g/L
4.5 g/L
1g/L
4.5 g/L
1g/L
Glucose concentration
B
β3/Glut3
shGlut3
shCtrl

FIG. 13C-D

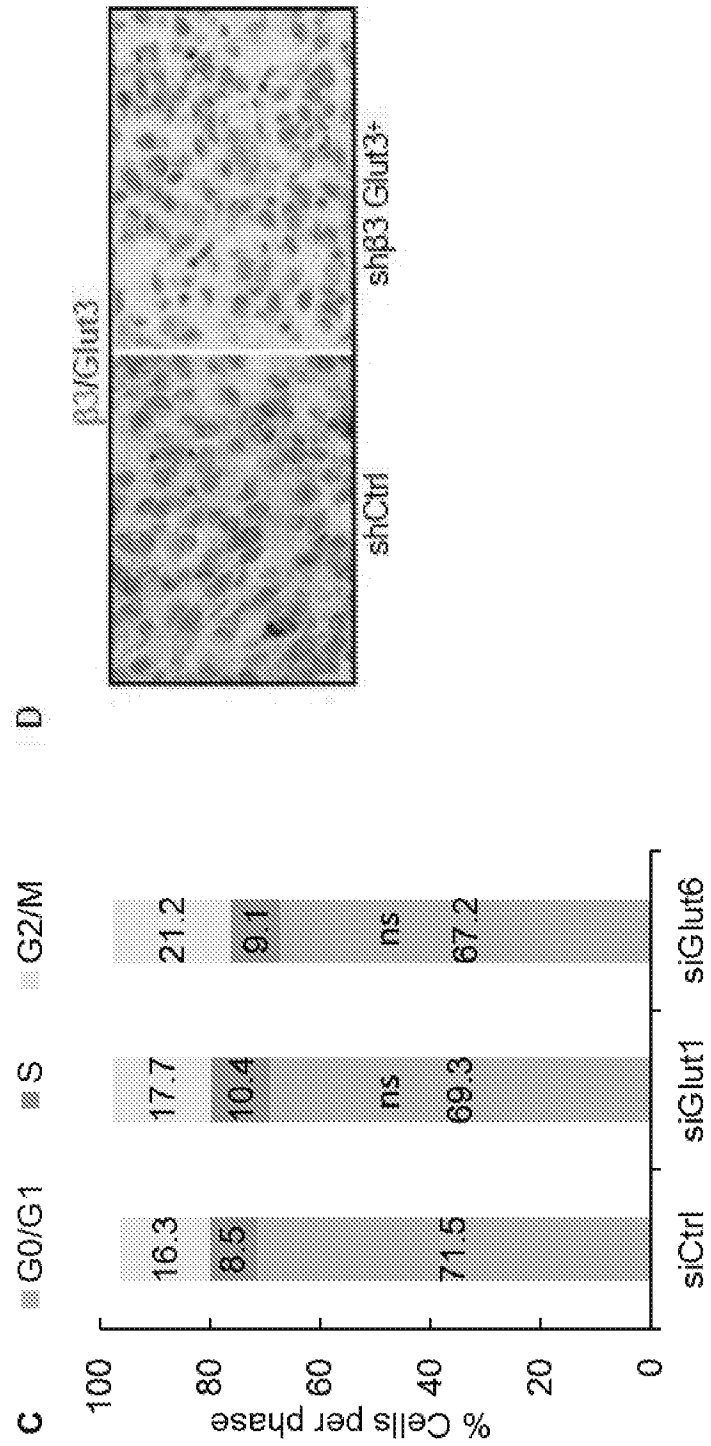
C
G0/G1
S
G2/M
% Cells per phase
100
80
60
40
20
0
16.3
8.5
17.7
10.4
21.2
9.1
71.5
69.3
ns
ns
67.2
siCtrl
siGlut1
siGlut6
D
β3Glut3
shCtrl
shβ3 Glut3+

FIG. 13E-G

FIG. 13E

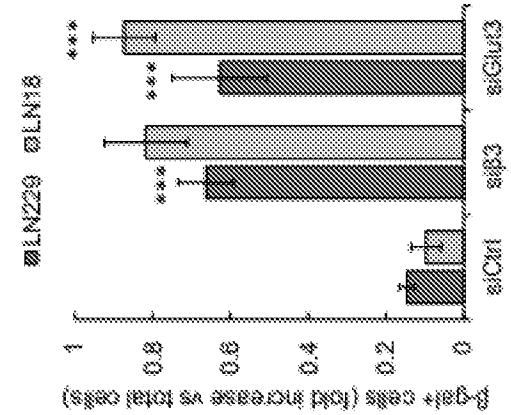

FIG. 13F

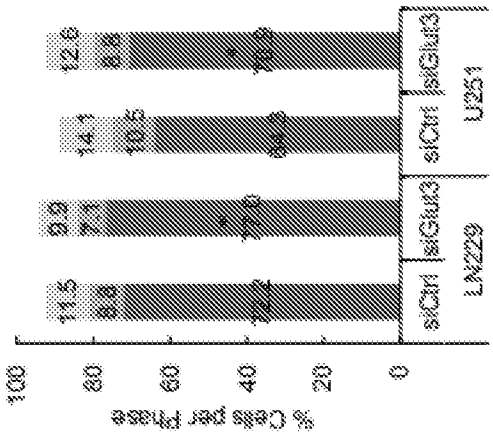

FIG. 13G

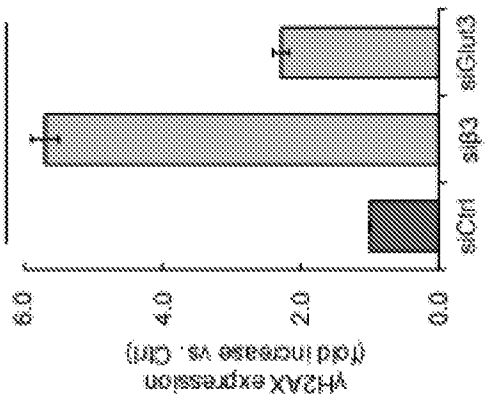

FIG. 13H

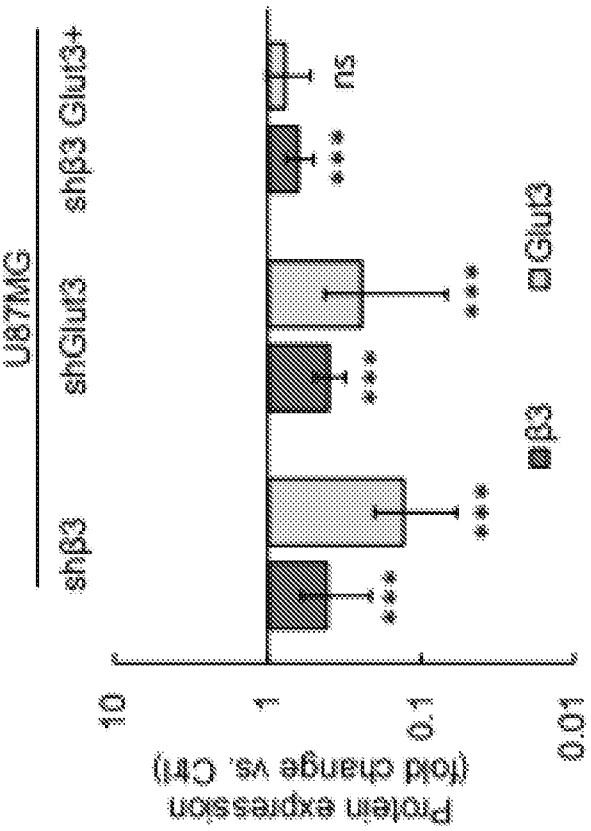
U87MG
shβ3
shGlut3
shβ3 Glut3+
Protein expression
(fold change vs. Ctrl)
10
1
0.1
0.01
***
***
***
***
***
ns
β3
Glut3

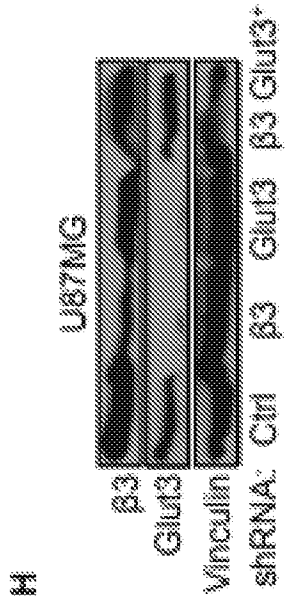
H
U87MG
β3
Glut3
Vinculin
shRNA: Ctrl β3 Glut3 β3 Glut3+

FIG. 14A-C

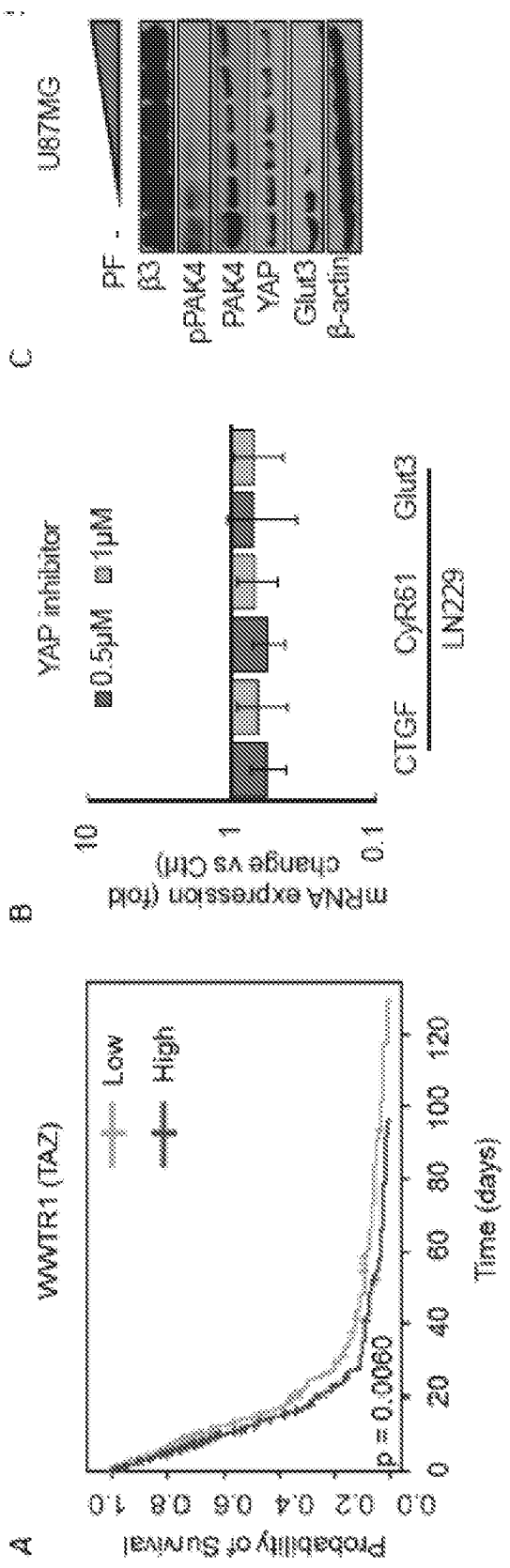
A
WWTR1 (TAZ)
Low
High
p = 0.0060
Probability of Survival
0.0 0.2 0.4 0.6 0.8 1.0
0 20 40 60 80 100 120
Time (days)
B
YAP inhibitor
0.5μM 1μM
mRNA expression (fold change vs Ctrl)
10
1
0.1
CTGF CYR61 Glut3
LN229
C
U87MG
PF -
β3
pPAK4
PAK4
YAP
Glut3
β-actin

FIG. 14D

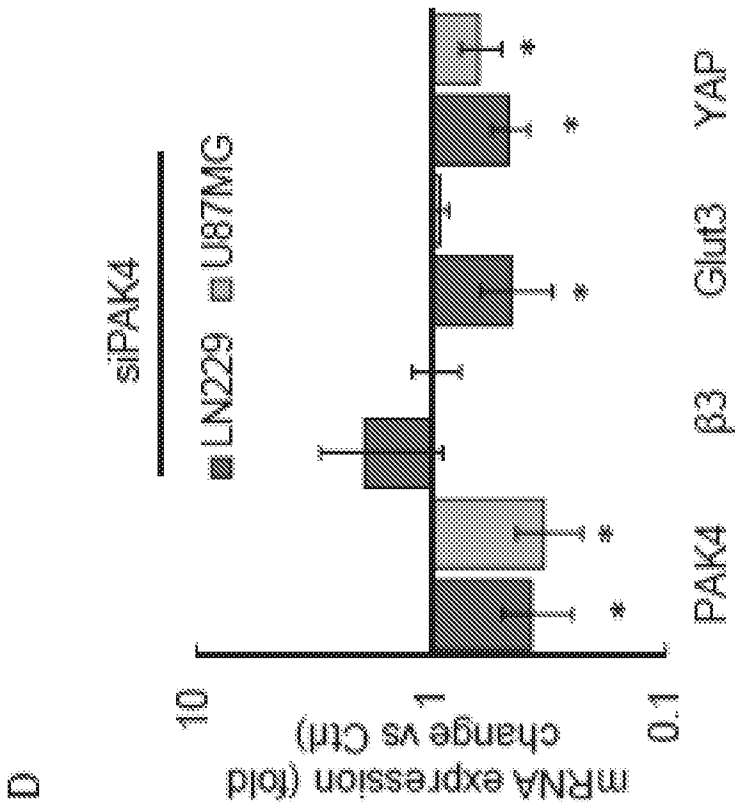
D
mRNA expression (fold change vs Ctrl)
10
1
0.1
siPAK4
LN229
U87MG
PAK4
β3
Glut3
YAP
*

FIG. 14E

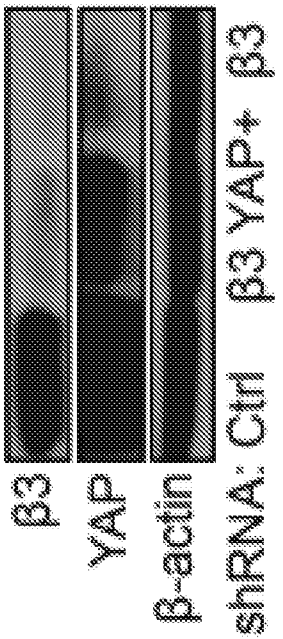

FIG. 14F

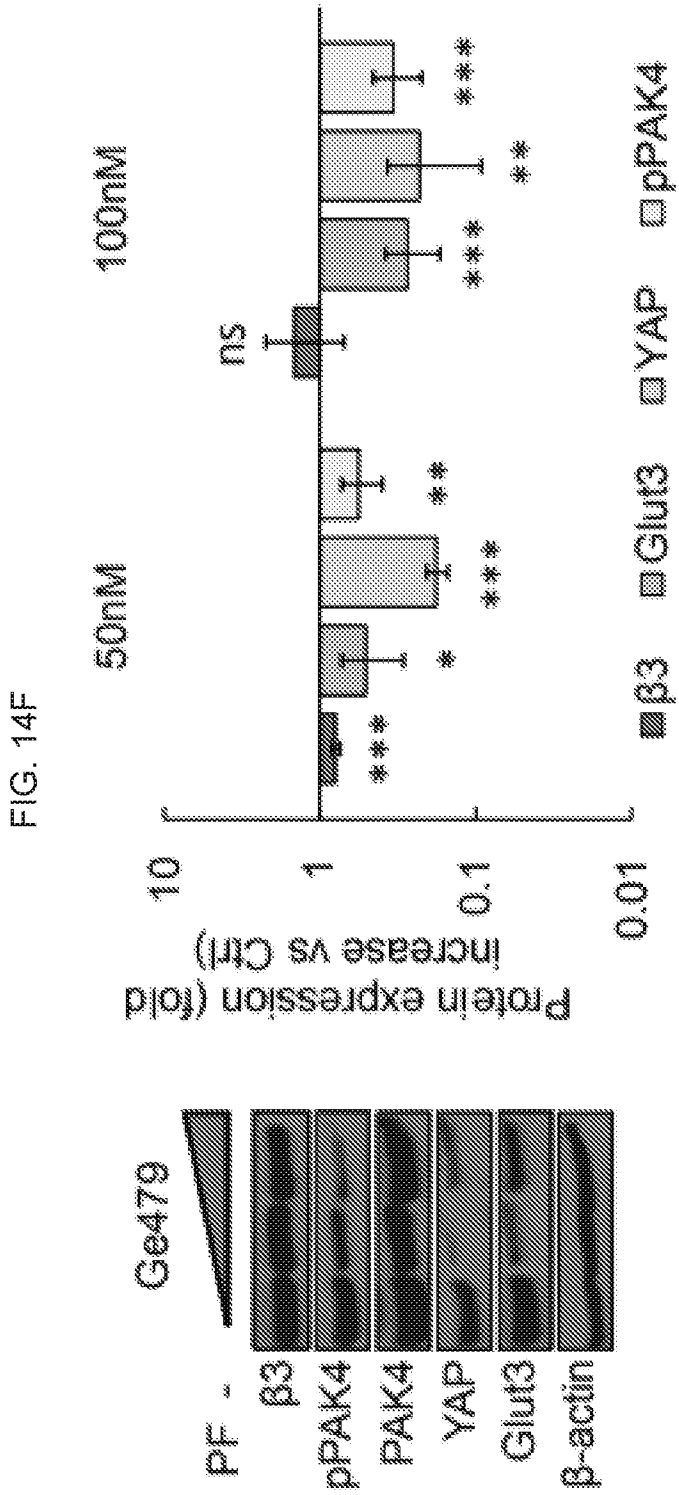
Protein expression (fold increase vs Ctrl)
10
1
0.1
0.01
50nM
100nM
ns
***
**
*
***
***
**
***
β3
Glut3
YAP
pPAK4
Ge479
PF -
β3
pPAK4
PAK4
YAP
Glut3
β-actin

FIG. 14G

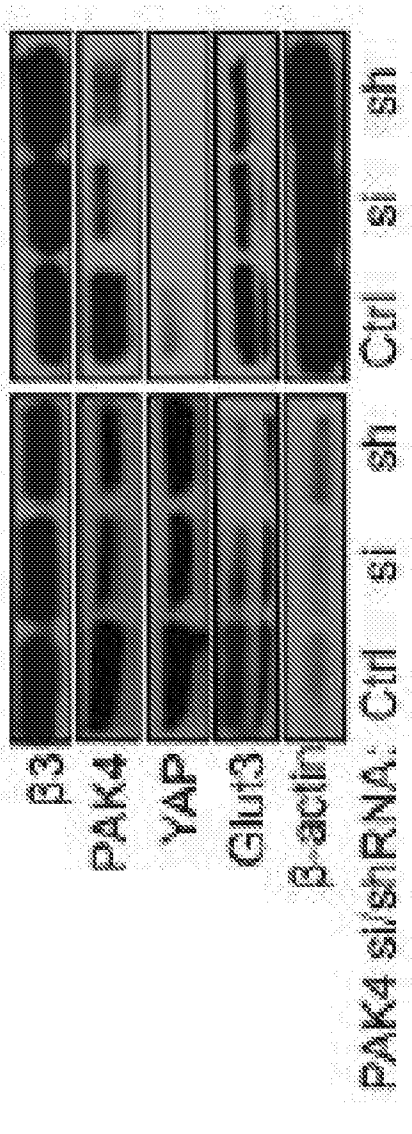
U87MG
LN229
β3
PAK4
YAP
Glut3
β-actin
PAK4 si/shRNA: Ctrl si sh Ctrl si sh

FIG. 15A-B

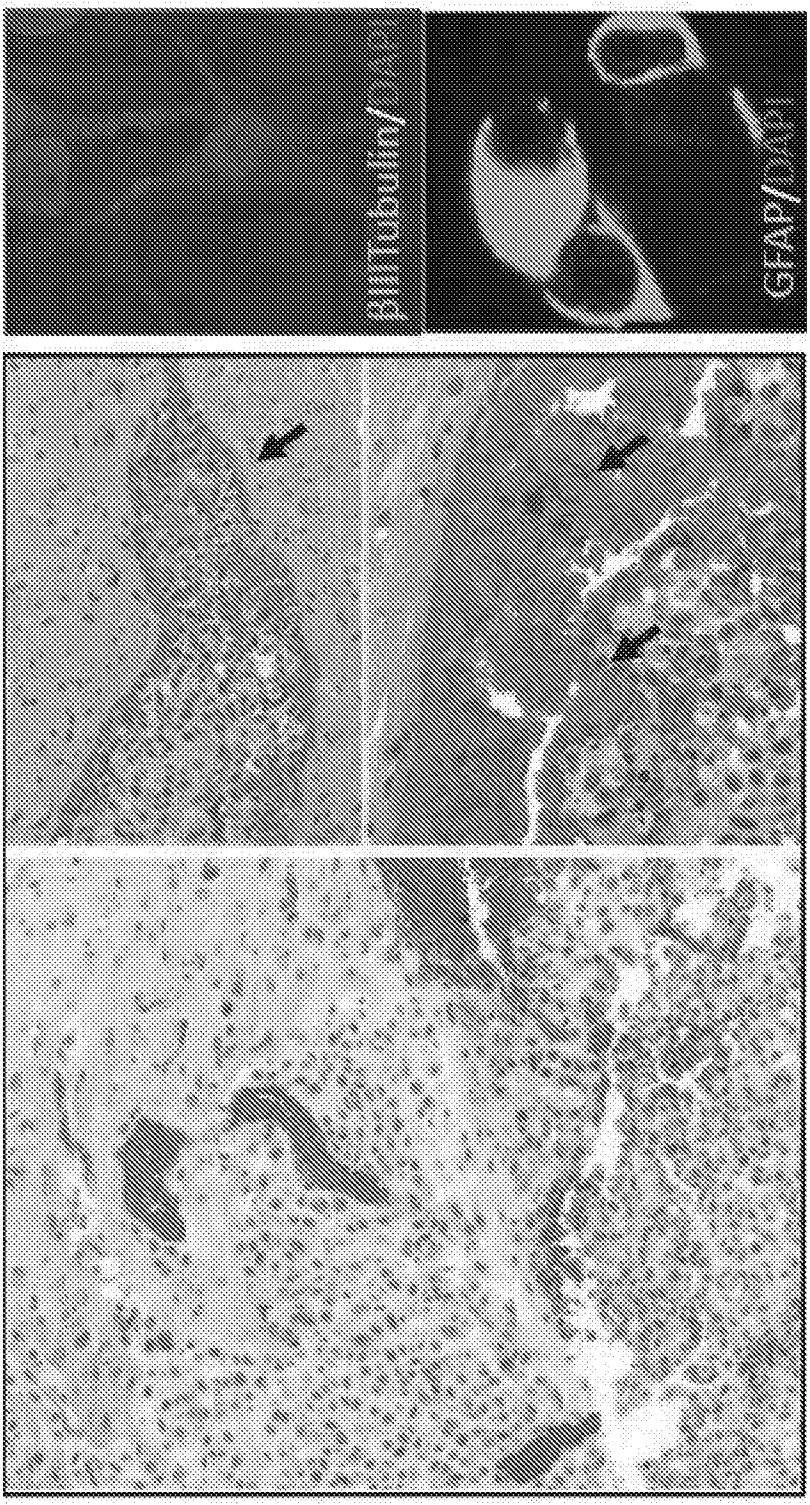

FIG. 15C-E

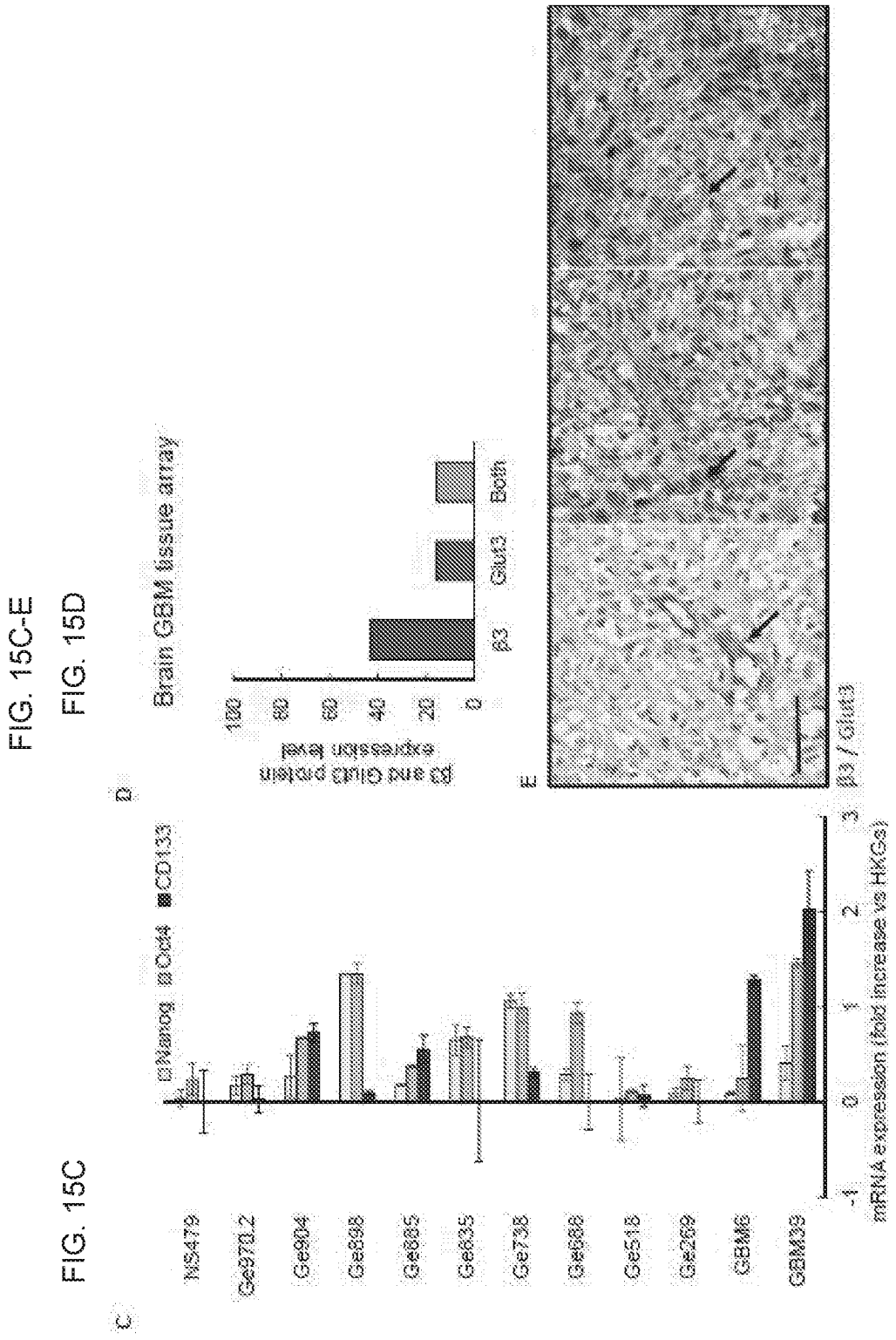

FIG. 15C

FIG. 15D

FIG. 15F-H

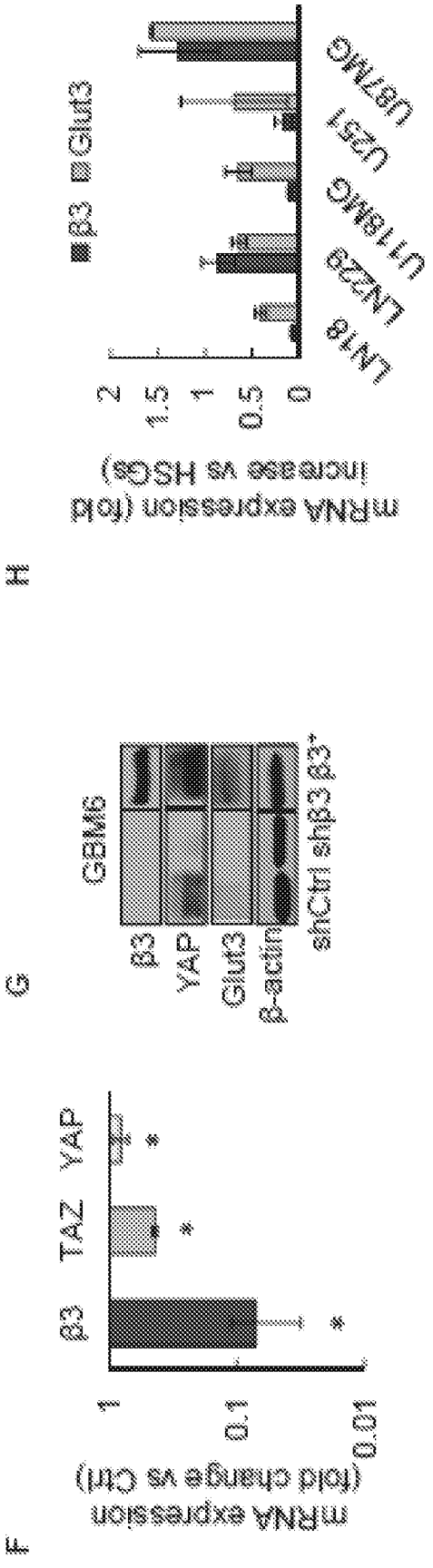
F
mRNA expression
(fold change vs Ctrl)
1
0.1
0.01
β3
TAZ
YAP
*
*
*
G
GBM6
β3
YAP
Glut3
β-actin
shCtrl
shβ3 β3+
H
mRNA expression (fold
increase vs HSCs)
2
1.5
1
0.5
0
β3
Glut3
LN18
LN229
U118MG
U251
U87MG

FIG. 15J

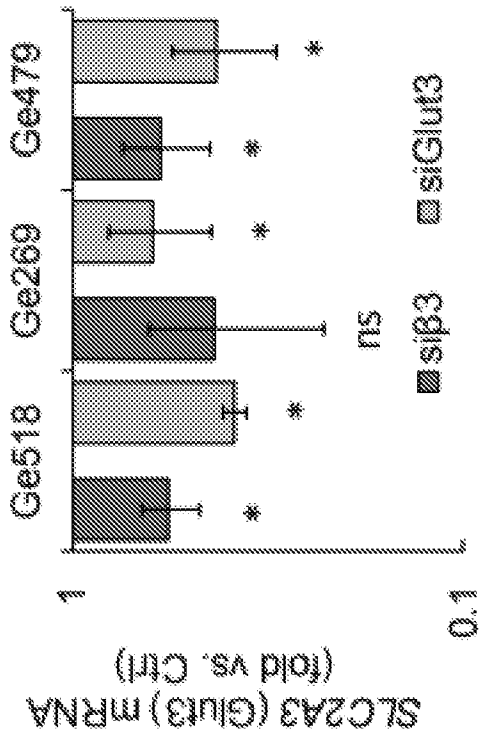

FIG. 15I

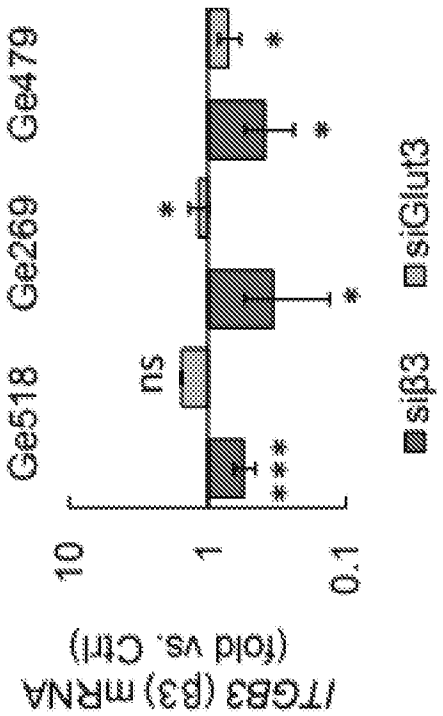

FIG. 16A-C

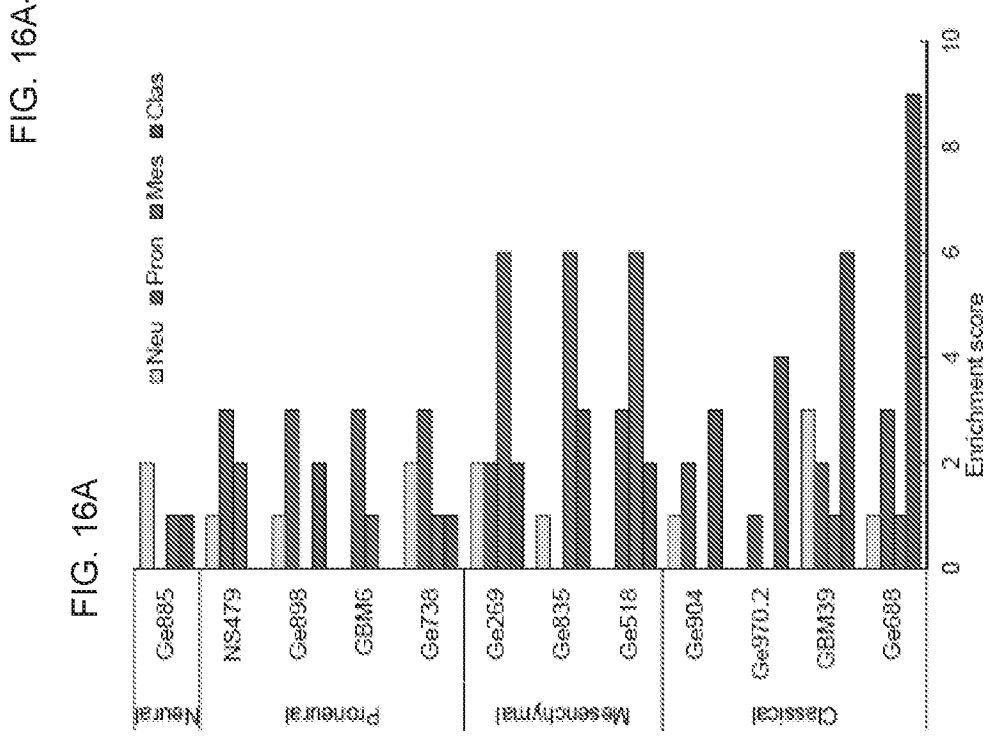
FIG. 16A
Neu
Pron
Mes
Clas
Neural
Ge885
Proneural
NS479
Ge838
GBM6
Ge738
Mesenchymal
Ge269
Ge835
Ge518
Classical
Ge504
Ge970.2
GBM39
Ge683
0
2
4
6
8
10
Enrichment score
FIG. 16B
Mesenchymal
Other sub
Relative frequency
20
15
10
5
0
HK2
ENO1
PFKM
GAPDH
ALDOA
C
PFKL
Low
High
p = 0.041
Probability of Survival
0.0
0.2
0.4
0.6
0.8
1.0
0
500
1000
1500
2000
2500
Time (days)

FIG. 16D-F

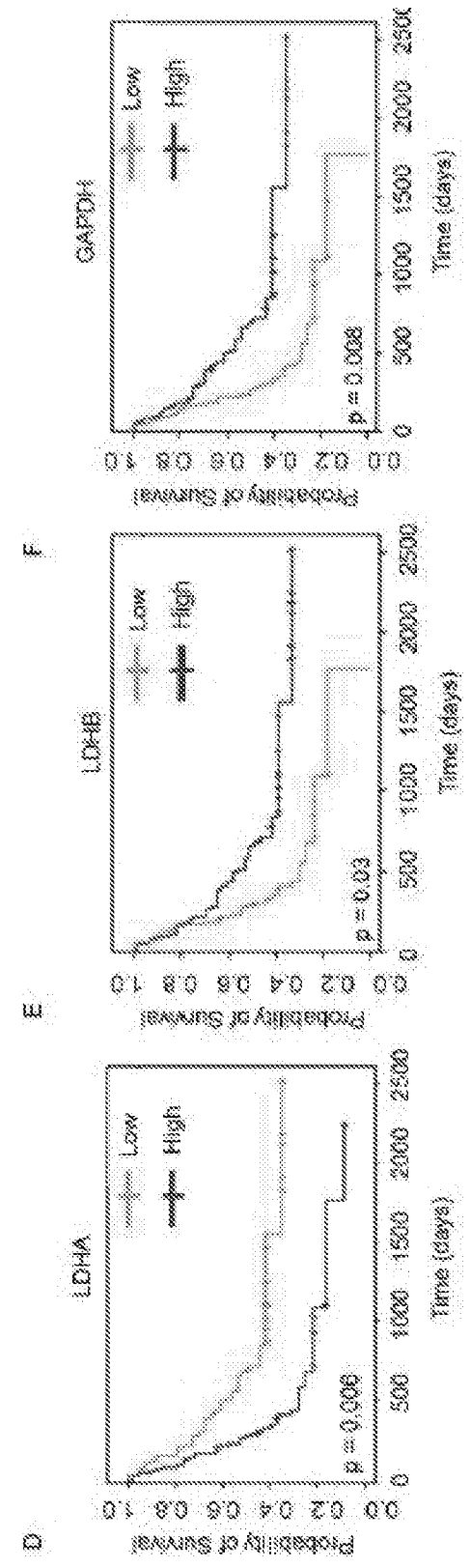
D
LDHA
Low
High
p = 0.008
Probability of Survival
Time (days)
E
LDHB
Low
High
p = 0.03
Probability of Survival
Time (days)
F
GAPDH
Low
High
p = 0.008
Probability of Survival
Time (days)

FIG. 17A-B

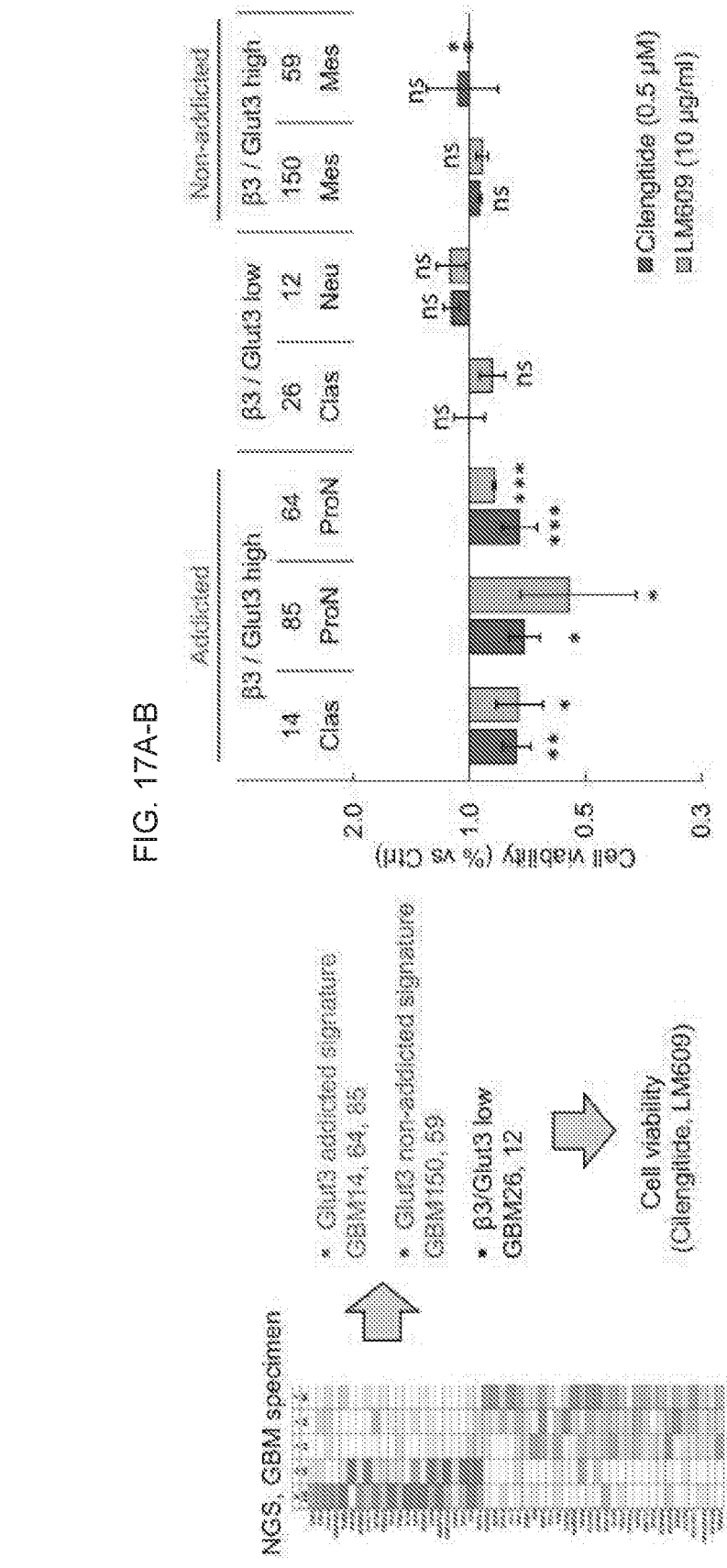

Table depicted in schematic is shown in Figure 18

FIG. 18

	Mes GBM150	Mes GBM59	Clas GBM14	ProN GBM64	ProN GBM85
	Glut3 non-addicted signature				
CAV1	162	44	1	4	1
CAV2	14	4	0	6	1
TAGLN	4	1	1	2	1
SERPINE1	241	4	1	2	0
THBS1	46	8	0	0	16
P4HA2	3	47	0	0	1
AHNAK2	15	4	0	0	0
DYNLT3	24	48	6	5	13
ACTA2	5	1	1	3	1
PRSS23	5	4	0	1	2
FHL2	41	8	0	5	0
TPM1	13	8	9	6	4
FLAU	156	18	3	1	1
UPP1	17	12	0	4	1
NDRG1	31	3	2	1	5
LDHA	137	222	48	45	30
ANGPTL4	19	16	2	0	0
MIR22HG	7	13	1	1	1
VMP1	18	25	11	11	8
PGK1	100	173	35	24	29
TPI1	315	303	148	84	89
GSTO1	46	76	17	24	9
	Glut3 addicted signature				
NDRG2	6	0	11	15	78
BCAN	1	1	60	170	744
OLIG2	73	1	6	142	107
DLL3	0	0	0	16	66
FHL1	13	24	27	44	49
PSAT1	26	14	2	75	66
ID4	47	13	137	18	62
MAP2	11	9	53	127	78
ETV1	15	16	29	8	39
ZEB1	23	22	55	35	7
CNTN1	1	9	0	66	21
MARCKS	72	49	82	150	126
TAF9B	7	28	22	11	25
PLXNB1	7	1	17	23	44
GPSM2	7	16	14	14	27
KCNJ10	28	0	23	22	22
DHX9	35	35	80	53	67
PEA15	113	34	133	143	126
PTPN11	15	18	43	39	19
HIPK2	4	4	21	27	25
ZNF711	3	1	11	20	36
MYO5	4	4	8	3	9
SEMA6A	2	3	6	6	14
POU3F3	23	7	58	32	13
GNG4	0	0	3	54	22
DGCR2	9	13	14	25	13
ARHGEF7	3	3	6	13	28
ARHGAP35	10	4	13	12	16
PIP4K2B	19	13	37	36	25
PRKDC	11	11	32	20	26

FIG. 19

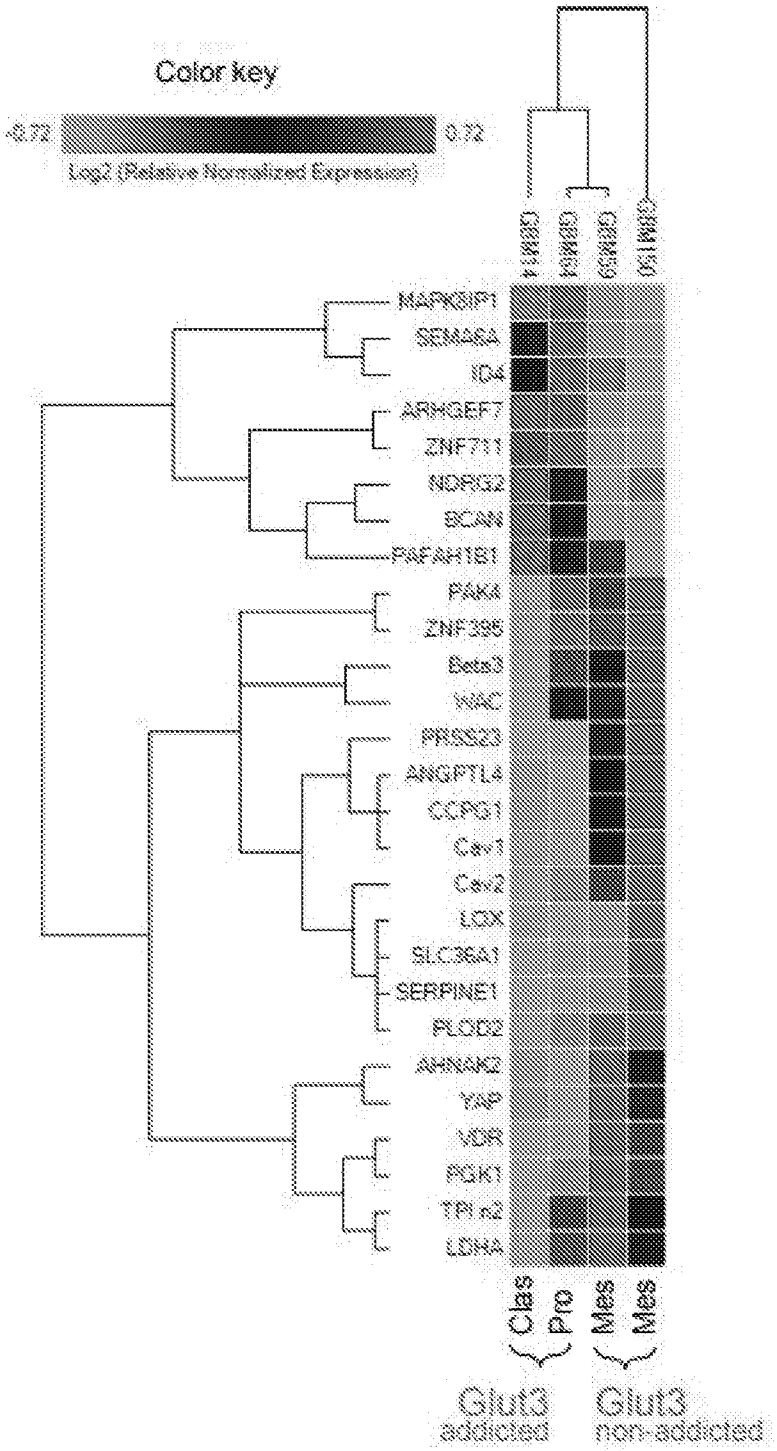
Color key
-0.72
0.72
Log2 (Relative Normalized Expression)
GBM14
GBM43
GBM59
GBM150
MAPKAPK5
SEMA5A
ID4
ARHGEF7
ZNF711
NDRG2
SCAI
PAFAH1B1
PAK4
ZNF395
Beta3
WAC
PRSS23
ANGPTL4
CCPG1
Cav1
Cav2
LOX
SLC39A1
SERPINE1
PLOD2
AHNAK2
YAP
VDR
PGK1
TPI1
LDHA
Clas
Pro
Mes
Mes
Glut3
addicted
Glut3
non-addicted

FIG. 20B

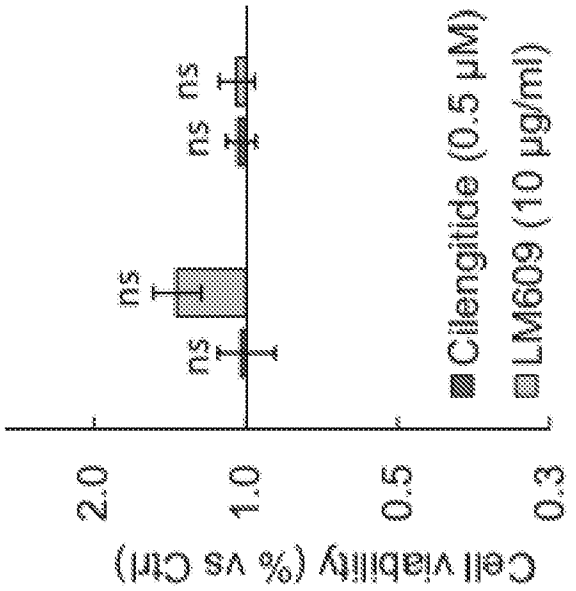

FIG. 20A

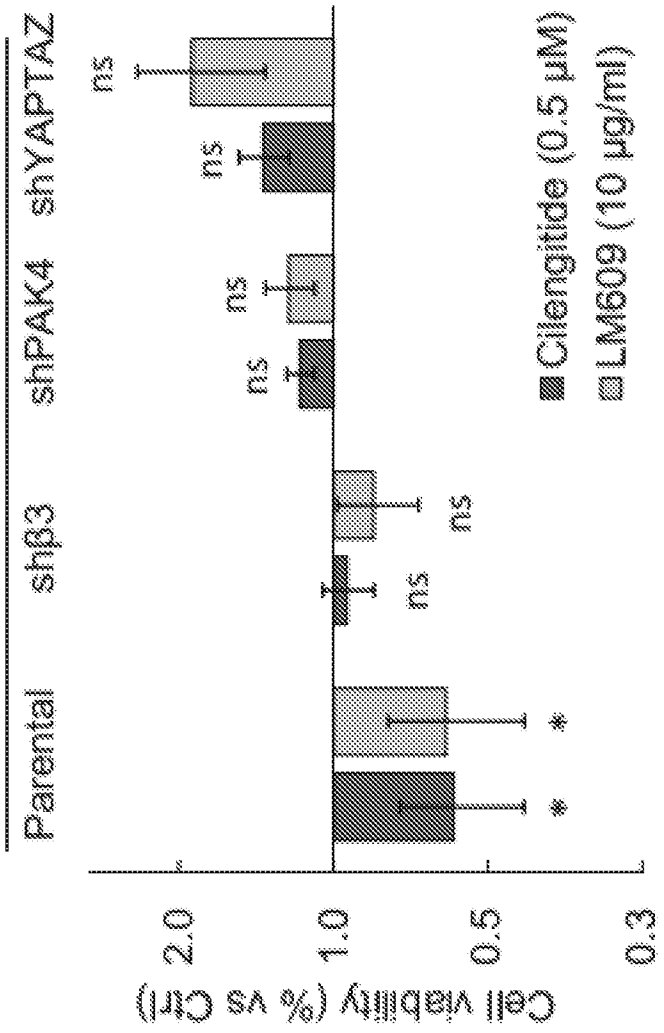

FIG. 21

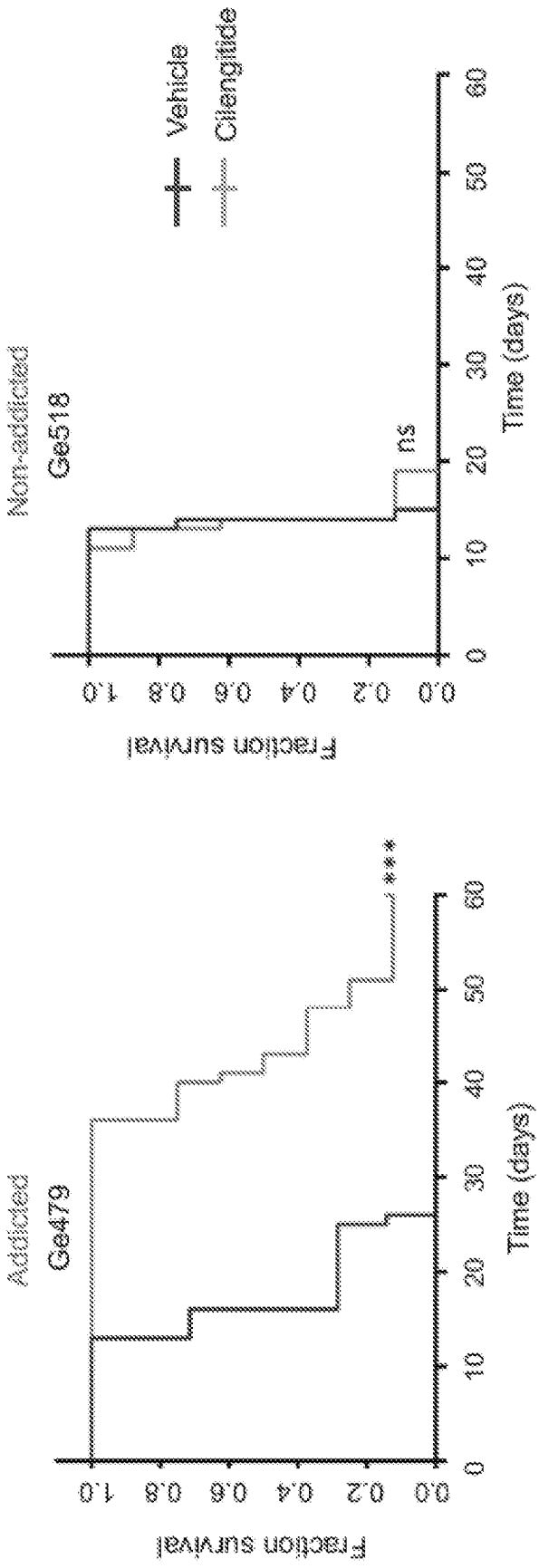
Addicted
Ge479
Fraction survival
0.0
0.2
0.4
0.6
0.8
1.0
0
10
20
30
40
50
60
Time (days)
***
Non-addicted
Ge518
Fraction survival
0.0
0.2
0.4
0.6
0.8
1.0
0
10
20
30
40
50
60
Time (days)
ns
Vehicle
Cilengitide

FIG. 22

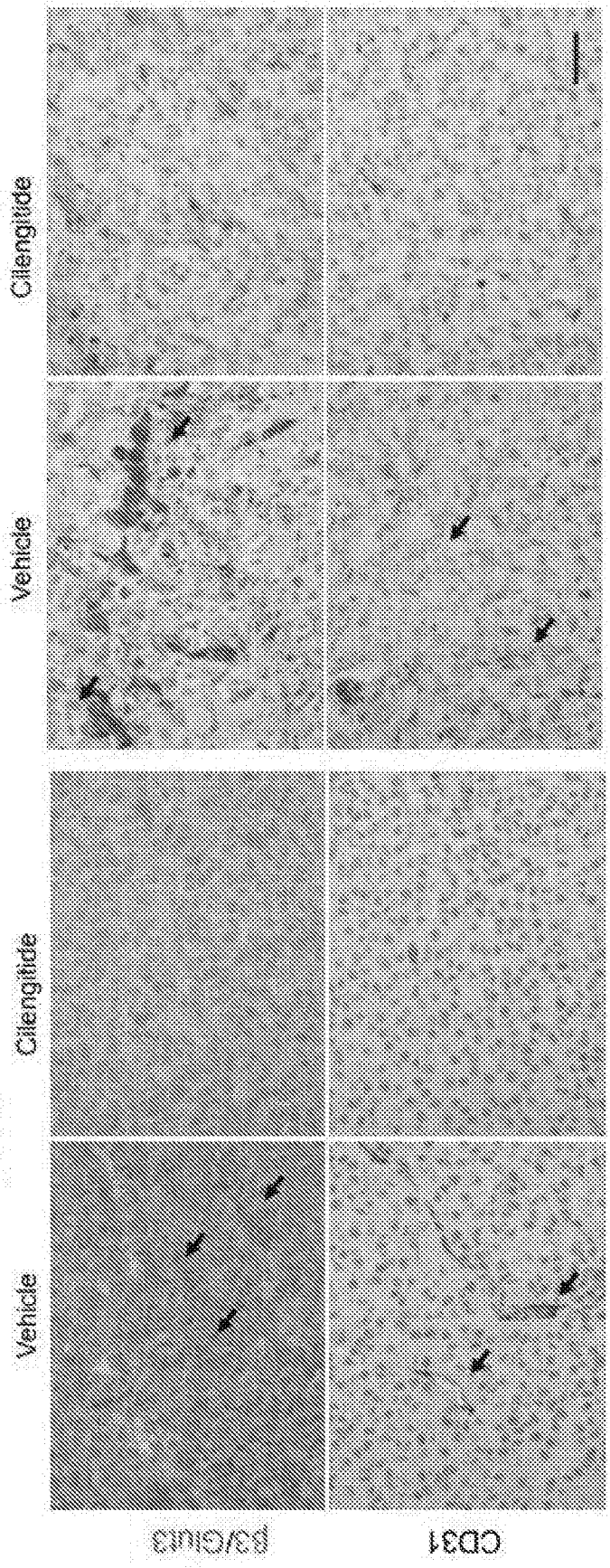
Ge518
Ge479
Vehicle
Cilengitide
Vehicle
Cilengitide
p3/Glut3
CD31

FIG. 23

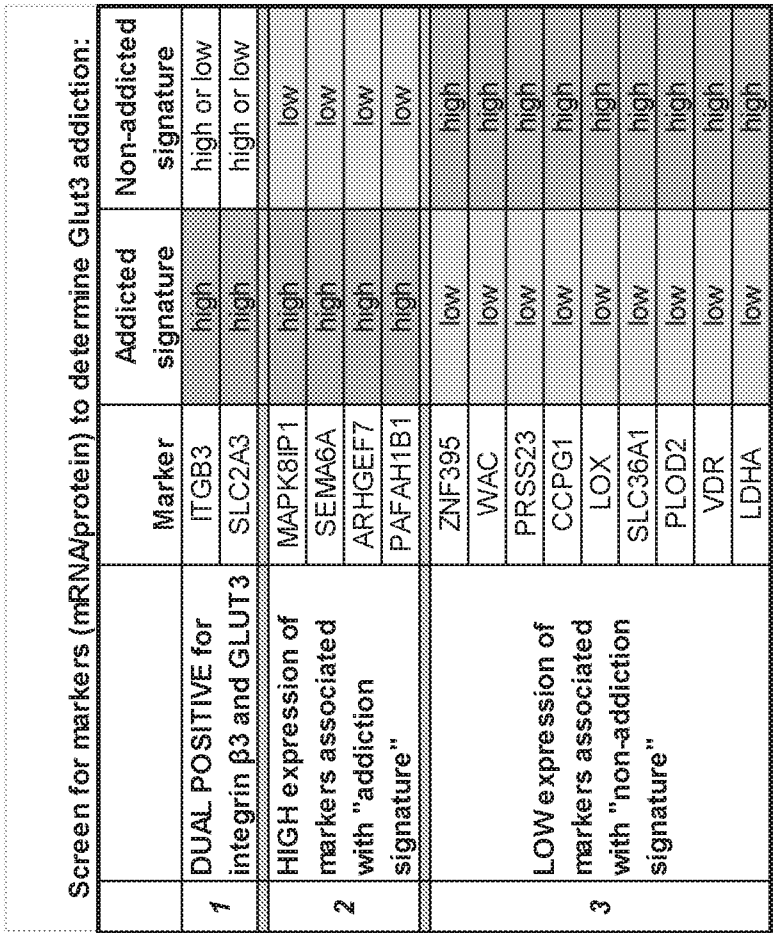

Screen for markers (mRNA/protein) to determine Glut3 addiction:

		Marker	Addicted signature	Non-addicted signature
1	DUAL POSITIVE for integrin β3 and GLUT3	ITGB3	high	high or low
		SLC2A3	high	high or low
2	HIGH expression of markers associated with "addiction signature"	MAPK8IP1	high	low
		SEMA6A	high	low
		ARHGEF7	high	low
		PAFAH1B1	high	low
3	LOW expression of markers associated with "non-addiction signature"	ZNF395	low	high
		WAC	low	high
		PRSS23	low	high
		CCPG1	low	high
		LOX	low	high
		SLC36A1	low	high
		PLOD2	low	high
		VDR	low	high
		LDHA	low	high

INTERNATIONAL SEARCH REPORT

International application No.
PCT/US 18/37595

A. CLASSIFICATION OF SUBJECT MATTER

IPC(8) - G01N 33/574; C12N 5/074, 5/09; C07K 11/02, 14/705; A61K 38/00 (2018.01)
CPC - C12N 5/0693, 5/0693, 5/0623, 5/0622, G01N 33/574, 2333/70557, 2800/52, 2400/00; C07K 14/705; A61K 38/00, 2039/5158

According to International Patent Classification (IPC) or to both national classification and IPC

B. FIELDS SEARCHED

Minimum documentation searched (classification system followed by classification symbols)

See Search History Document

Documentation searched other than minimum documentation to the extent that such documents are included in the fields searched

See Search History Document

Electronic data base consulted during the international search (name of data base and, where practicable, search terms used)

See Search History Document

C. DOCUMENTS CONSIDERED TO BE RELEVANT

Category*	Citation of document, with indication, where appropriate, of the relevant passages	Relevant to claim No.
Y	Franovic et al. Glioblastomas require integrin .alpha.v.beta.3/PAK4 signaling to escape senescence. Cancer Res. 1 November 2015, Vol 75, No 21, Pages 4466-4473. Especially pg 4466 col 1 para 2, pg 4467 col 2 para 1, pg 4467 col 2 para 3, pg 4470 col 2 para 2.	1-4
Y	Flavahan et al. Brain tumor initiating cells adapt to restricted nutrition through preferential glucose uptake. Nat Neurosci. October 2013, Vol 16, No 10, Pages 1373-1382. Especially abstract, pg 1373 col 1 para 1, pg 1374 col 2 para 2.	1-4
Y	Stoica et al. Identification of cancer stem cells in dog glioblastoma. Vet Pathol. May 2009, Vol 46, No 3, Pages 391-406. Especially abstract, pg 398 col 2 para 4.	1-4
X,P	Cosset et al. Glut3 Addiction Is a Druggable Vulnerability for a Molecularly Defined Subpopulation of Glioblastoma. Cancer Cell. ePub 30 November 2017, Vol 32, No 6, Pages 856 -868. Especially entire article.	1-4

☐ Further documents are listed in the continuation of Box C. ☐ See patent family annex.

* Special categories of cited documents:

"A" document defining the general state of the art which is not considered to be of particular relevance

"E" earlier application or patent but published on or after the international filing date

"L" document which may throw doubts on priority claim(s) or which is cited to establish the publication date of another citation or other special reason (as specified)

"O" document referring to an oral disclosure, use, exhibition or other means

"P" document published prior to the international filing date but later than the priority date claimed

"T" later document published after the international filing date or priority date and not in conflict with the application but cited to understand the principle or theory underlying the invention

"X" document of particular relevance; the claimed invention cannot be considered novel or cannot be considered to involve an inventive step when the document is taken alone

"Y" document of particular relevance; the claimed invention cannot be considered to involve an inventive step when the document is combined with one or more other such documents, such combination being obvious to a person skilled in the art

"&" document member of the same patent family

Date of the actual completion of the international search	Date of mailing of the international search report
4 September 2018	01 OCT 2018
Name and mailing address of the ISA/US Mail Stop PCT, Attn: ISA/US, Commissioner for Patents P.O. Box 1450, Alexandria, Virginia 22313-1450 Facsimile No. 571-273-8300	Authorized officer: Lee W. Young PCT Helpdesk: 571-272-4300 PCT OSP: 571-272-7774

Form PCT/ISA/210 (second sheet) (January 2015)

INTERNATIONAL SEARCH REPORT

International application No.
PCT/US 18/37595

Box No. I Nucleotide and/or amino acid sequence(s) (Continuation of item 1.c of the first sheet)

1. With regard to any nucleotide and/or amino acid sequence disclosed in the international application, the international search was carried out on the basis of a sequence listing:

   a. ☐ forming part of the international application as filed:

      ☐ in the form of an Annex C/ST.25 text file.

      ☐ on paper or in the form of an image file.

   b. ☐ furnished together with the international application under PCT Rule 13*ter*.1(a) for the purposes of international search only in the form of an Annex C/ST.25 text file.

   c. ☐ furnished subsequent to the international filing date for the purposes of international search only:

      ☐ in the form of an Annex C/ST.25 text file (Rule 13*ter*.1(a)).

      ☐ on paper or in the form of an image file (Rule 13*ter*.1(b) and Administrative Instructions, Section 713).

2. ☐ In addition, in the case that more than one version or copy of a sequence listing has been filed or furnished, the required statements that the information in the subsequent or additional copies is identical to that forming part of the application as filed or does not go beyond the application as filed, as appropriate, were furnished.

3. Additional comments:
ISA/225 mailed on 28 June 2018. No approved electronic sequence listing was submitted in response to the ISA/225.

INTERNATIONAL SEARCH REPORT

International application No.
PCT/US 18/37595

Box No. II Observations where certain claims were found unsearchable (Continuation of item 2 of first sheet)

This international search report has not been established in respect of certain claims under Article 17(2)(a) for the following reasons:

1. ☐ Claims Nos.:
because they relate to subject matter not required to be searched by this Authority, namely:

2. ☐ Claims Nos.:
because they relate to parts of the international application that do not comply with the prescribed requirements to such an extent that no meaningful international search can be carried out, specifically:

3. ☒ Claims Nos.: 5-9
because they are dependent claims and are not drafted in accordance with the second and third sentences of Rule 6.4(a).

Box No. III Observations where unity of invention is lacking (Continuation of item 3 of first sheet)

This International Searching Authority found multiple inventions in this international application, as follows:

1. ☐ As all required additional search fees were timely paid by the applicant, this international search report covers all searchable claims.

2. ☐ As all searchable claims could be searched without effort justifying additional fees, this Authority did not invite payment of additional fees.

3. ☐ As only some of the required additional search fees were timely paid by the applicant, this international search report covers only those claims for which fees were paid, specifically claims Nos.:

4. ☐ No required additional search fees were timely paid by the applicant. Consequently, this international search report is restricted to the invention first mentioned in the claims; it is covered by claims Nos.:

Remark on Protest

☐ The additional search fees were accompanied by the applicant's protest and, where applicable, the payment of a protest fee.

☐ The additional search fees were accompanied by the applicant's protest but the applicable protest fee was not paid within the time limit specified in the invitation.

☐ No protest accompanied the payment of additional search fees.